AD-A131 167 INVESTIGATION OF WAVE ROTOR TURBOFANS FOR CRUISE MISSILE ENGINES VOLUME 1.. (U) MATHEMATICAL SCIENCES NORTHWEST INC BELLEVUE WA R TAUSSIG ET AL. APR 83 MSNW-13.213.01.70-VOL-1 N00140-82-C-9729 F/G 21/5 1/2 NL

UNCLASSIFIED

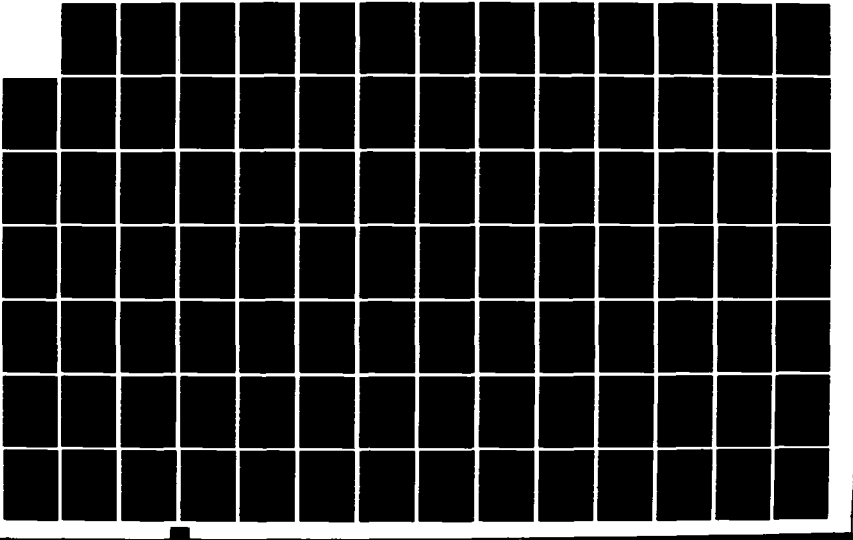

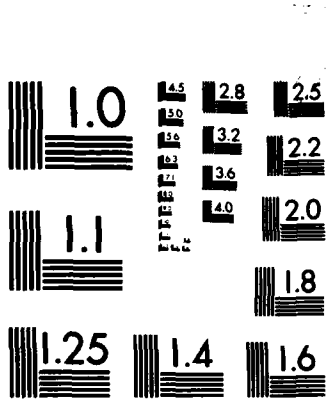

MICROCOPY RESOLUTION TEST CHART
NATIONAL BUREAU OF STANDARDS-1963-A

(12)

MSNW

Investigation of Wave Rotor Turbofans for Cruise Missile Engines Final Report

Volume 1

Sponsored by
DEFENSE ADVANCED RESEARCH PROJECTS AGENCY (DOD) DARPA Order No. 4361

Prepared by
MATHEMATICAL SCIENCES NORTHWEST, INC.

April 1983

MSNW 13.213.01.70

INVESTIGATION OF WAVE ROTOR TURBOFANS FOR CRUISE MISSILE ENGINES

F I N A L R E P O R T

V O L U M E 1

Prepared By

R. Taussig
P. Cassady
J. Zumdieck
W. Thayer
E. Klosterman
R. Milroy
R. Klug

W. Christiansen (Consultant)
G. Oates (Consultant)

Mathematical Sciences Northwest, Inc.
2755 Northup Way
Bellevue, Washington 98004
(206)827-0460

Sponsored By

Defense Advanced Research Projects Agency (DOD)
DARPA Order No. 4361

Issued By

U.S. Navy, Naval Air Propulsion Center
Contract No. N00140-82-C-9729

Effective Date of Contract: 11 June 1982

Contract Expiration Date: 11 June 1983

CONTENTS

The Appendixes to this report are bound separately as Volume 2.

TABLES

FIGURES

ABSTRACT

Wave rotors have been investigated as a technology for improving the performance of small turbofan engines in the 600 to 1000 lb. thrust class. This report summarizes the results of an eight-month study to analyze wave rotor performance for different configurations and to determine its sensitivity to operating and design parameters. Engine cycle calculations were also performed in order to estimate engine performance improvements and sensitivity to the wave rotor component. Wave rotor/turbines and pressure exchanger wave rotors both have been evaluated. In each case, experimental data exists which confirms predicted wave rotor performance over a wide range of operating conditions.

Wave rotor work transfer efficiencies ranging from 65 percent to 75 percent appear feasible for small wave rotors which process from 5 to 10 lb/s inflow air. The work transfer efficiency is equivalent to the product of a compressor efficiency times a turbine efficiency. In the small turbofan application, the wave rotor acts as a high pressure topping cycle with peak cycle temperatures in the range of 2500 to 3500 F. Under these conditions, the thrust-specific fuel consumption of a wave rotor turbofan engine will be 25 to 30 percent lower than existing turbofan engines of the same size.

The highest risk areas concern the ability to construct a high temperature wave rotor which can operate well, both on and off-design, with limited leakage and acceptable cyclic fatigue stresses. Computational codes used in the present analysis also need to be validated over a larger range than possible with current data by measurements from a carefully instrumented, high temperature wave rotor test. The study concludes with recommendations for a conceptual engine design evaluation to select the best wave rotor configuration, the construction and testing of a hot wave rotor meeting these specifications, and validation of the predictions of the wave rotor design codes through detailed performance measurements of the hot rotor.

EXECUTIVE SUMMARY

Wave rotors have been investigated as a technology for improving the performance of small turbofan engines in the 600 to 1000 lb. thrust class. Detailed cycle calculations show that a wave rotor pressure exchanger will serve as an efficient topping cycle for present turbofans and will reduce their thrust-specific fuel consumption by as much as 25 to 30 percent. This would allow a significant extension in the range of small subsonic aircraft flying at sea level conditions. No new materials development for rotating components would be required for these improvements.

The purpose of this study was to analyze the performance of the wave rotor component for several different configurations and to determine the sensitivity of that performance to operating and design parameters. Engine cycle calculations were performed in order to estimate the improvement in engine performance due to the wave rotor and to determine the sensitivity of the engine performance to the wave rotor component. Both on and off-design engine performance was studied. The wave rotor configurations included those which simply compress the inlet air an additional amount to a higher overall pressure ratio (pressure exchangers) and those which also produce output shaft power suitable for driving the lower stage compressor (wave rotor/turbine).

The advantages of wave rotors for advanced turbofans are

- Low thrust-specific fuel consumption
- Low rotor wall temperatures
- Low rotor tip speeds
- High component efficiency for small rotors
- Wide range of operating conditions

These attributes are associated with the cold intake air cycling onto the rotor with each revolution and an unsteady wave compression process which

is not subject to the same aerodynamic losses as conventional turbomachinery. The analytic tools for incorporating these features into a high efficiency device have only been refined to the point of usefulness in the past few years. Specifically, a detailed flow model for an efficient wave rotor has been developed and validated by experimental data, and modern computational techniques have turned this model into a practical design tool for optimizing the performance of wave rotors.

An unsteady one-dimensional flow code (FLOW) was used to evaluate the performance of the wave rotor component. FLOW was developed under previous DOE contract efforts and was modified during this study to include the effects of finite tube wall thickness, pressure recovery losses due to partially open tubes, impulsive loading of the rotor blades, and reactive forces due to a change in blade angle. The FLOW code has been verified by experimental data taken on the MSNW wave rotor facility at lower pressure and temperature. The data included both end wall and on-rotor pressure measurements which display the detailed behavior of the wave and flow processes on the rotor. Agreement between the code and the experimental data was good and was used to partially optimize the operation of the test rotor. The code relies on the use of the Flux-Corrected Transport (FCT) finite difference scheme called SHASTA, which integrates the Euler equations of fluid motion. Pipe flow terms have been appended to the momentum and energy equations to include the effects of wall friction and heat transfer.

Engine cycle calculations were carried out for turbofan engines which include the wave rotor as a topping cycle. The pressure exchanger version of the wave rotor pressurizes the inlet air to its peak value. The wave rotor/turbine version extracts additional work in the form of shaft output power and also compresses the input air. The actual wave rotor designs can vary considerably across this continuum of engines. The wave rotor compression and expansion efficiencies have been taken as variable parameters in order to assess the sensitivity of the engine performance to

the wave rotor component. The range of wave rotor efficiencies used in the cycle analysis is centered on values taken from the FLOW code.

Figure 1 illustrates the thrust-specific fuel consumption (TSFC) for several interesting engine diameters and, more generally, as a function of the specific thrust of the engine (abscissa). The net coordinates are the bypass ratio and the fan compression ratio. As the bypass ratio increases along a line of constant fan pressure ratio, the output thrust of the engine will increase and the efficiency of the engine will increase so that the TSFC will decrease until a minimum is reached, as shown in Figure 1. Further increases in the bypass ratio requires the gas flow through the core engine to expand down too far for its contribution to the thrust to be useful, and the TSFC will rise. There is also a maximum bypass ratio beyond which the core engine no longer has sufficient flow through it to provide the work needed to drive the fan. The minima values of TSFC are shown in Figure 1 as the small squares lying on lines of constant fan pressure ratio. One may conclude from these results that:

(a) Low values of TSFC are available in small wave rotor turbofans; on the order of 0.65 to 0.76 lb(m)/(hr.lb(f)) depending on the engine diameter at the 600 lb(f) thrust level.

(b) Fan pressure ratios are within reasonable bounds for these engine sizes, but the bypass ratios appear to be high, ranging from 5 to 11, respectively, for the 12 inch and 16 inch diameter engines for minimum TSFC designs.

(c) The core engines at the minima of TSFC in Figure 1 are constant at approximately 5 inches in diameter and process on the order of 5 to 6 lbm/sec for the 600 lb(f) thrust engines.

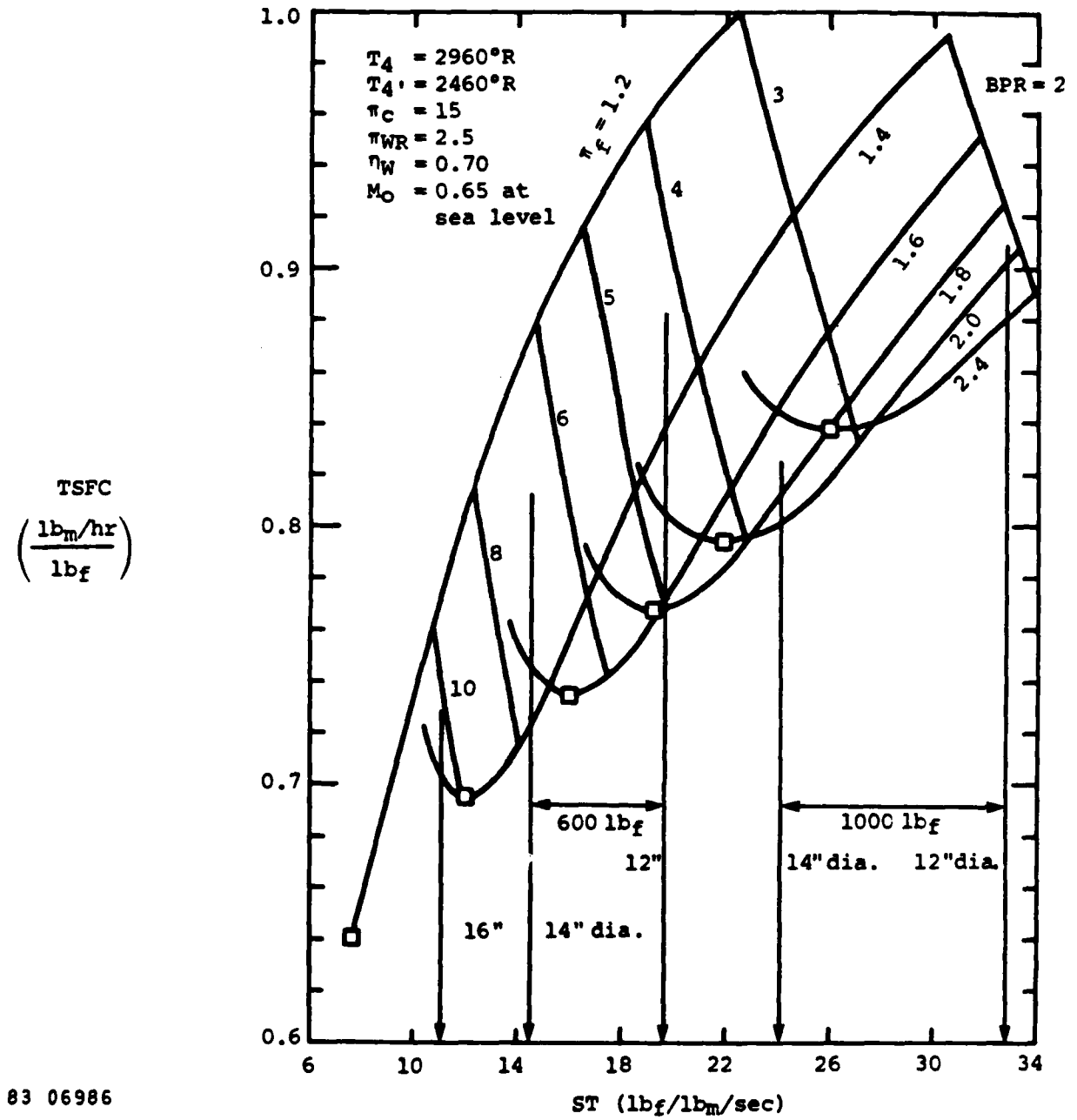

Figure 1. Thrust Specific Fuel Consumption (TSFC) vs. Specific Thrust (ST) for various Bypass Ratios (BPR) and Fan Pressure Ratios (π_f): No nozzle or diffuser losses.

(d) The minimum TSFC values are attainable with maximum turbine inlet temperatures of 2000 F; the wave rotor effectively protects the turbine from combustion temperatures in the range of 2500 to 3500°F.

(e) While a wave rotor work transfer efficiency (= compression efficiency x expansion efficiency) of 70% has been assumed for the results in Figure 1, these values of TSFC are not particularly sensitive to the wave rotor efficiency. Changing the rotor component efficiency from 70% to 80% decreased the TSFC only .013 points (i.e., from .758 to .745 for the 12 inch engine at a fan pressure ratio of 1.9).

Figure 2 shows the variation in the work transfer efficiency of a pressure exchanger wave rotor as a function of design and flow parameters normalized to a reference design. The reference case, while not optimized, represents a viable design with a work transfer efficiency of 70% for an inlet air flow of 5.3 lb/sec (2400 g/sec) and a combustion temperature of 3500°F. The rotor length and diameter are 5.6 inches (14.3 cm) and 5.8 inches (14.8 cm), respectively. This design uses 26 tubes, each with a cross-sectional area of 0.29 in^2 (1.9 cm^2). The wall temperature is 1260°K (1810°F). At its tip speed of 500 ft/sec (15,240 cm/sec), existing refractory metals can be employed.

The most important off-design effects occur when the pressure at the rotor inlet port for the combustion gas is lower than the reference value. Under these conditions, the compressed air is not removed completely from the rotor by the time a tube passes by the exit port for this gas. Because of this poor scavenging, the combustion gas cannot expand fully on the rotor, and less work is transferred to the compressed air than is desired. At the other extreme, when the combustion gas

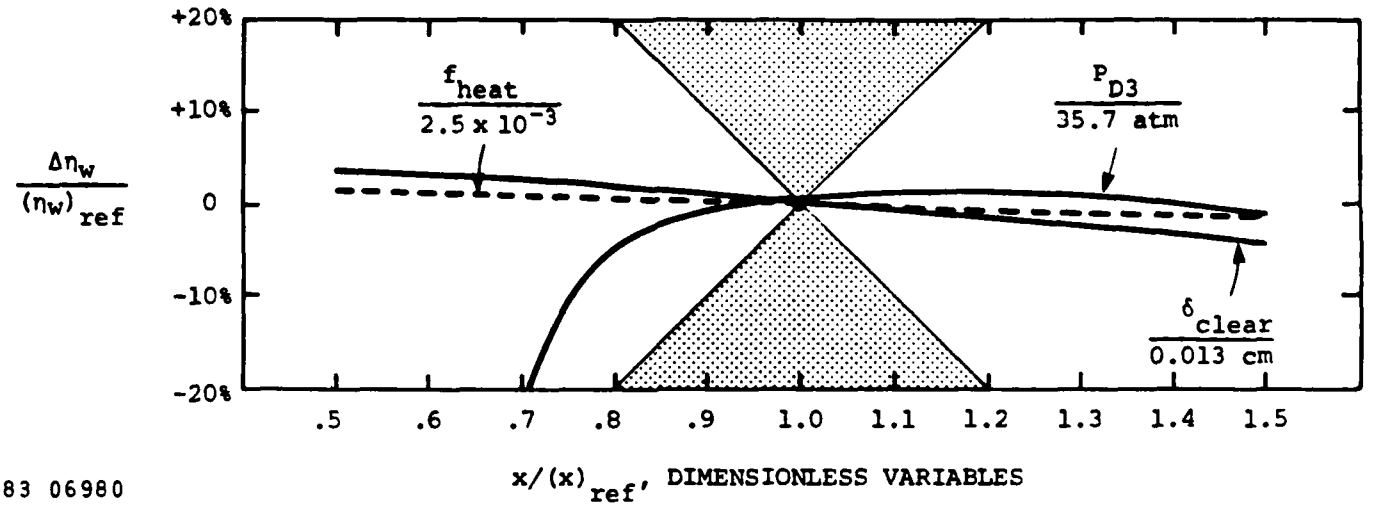

Figure 2. Sensitivity of Wave Rotor Work Transfer Efficiency η_w to:

Driver Gas Inlet Pressure, P_{D3}

Heat Transfer Coefficient, f_{heat}

Leakage (Clearance), δ_{clear}

Shaded regions indicate unacceptably high sensitivity.
(Reference case from Table 4-2)

pressure is higher than design, overscavenging occurs, which results in excess combustion gas escaping from the driven compressed air exit port. This has the immediate result of raising the work transfer efficiency at the expense of also raising the temperature of the gas mixture now exiting from the compressed air port. The temperature of the gas leaving the combustion gas exhaust ports is necessarily lower. The subsequent shift of outlet gas temperatures will have an effect on the overall engine cycle performance that must be accounted for. Generally, the most uniform wave rotor performance over a range of operating conditions is achieved for a rotor designed for slightly overscavenged conditions, a design strategy that is relatively easy to follow.

Similar variations in the work transfer efficiency occur when the heat transfer coefficient and the seal clearance controlling gas leakage are changed. Figure 2 shows the effects due to enhanced heat transfer. The reference value used for the heat transfer coefficient corresponds to the Reynolds number for the mean flow velocities in the tube. For slower velocities, the Reynolds number will also be smaller, implying a larger friction factor; however, the total heat transfer term also depends on the gas velocity to the first power, so that the variations in friction factor are countered by this velocity factor. At heat transfer levels smaller than the reference value, the effects of heat transfer are small compared to other losses related to leakage, pressure recovery, etc. Leakage, long recognized as a key problem for efficient wave rotor operation, has a slightly nonlinear effect on the work transfer efficiency in the vicinity of the reference case. At very low leakage levels, the work transfer efficiency tends asymptotically to 73% (i.e., $\Delta\eta/\eta_{Ref} \approx +4\%$ in Figure 2) and, at higher leakage levels, the efficiency declines towards 65%. At the reference conditions in Figure 2, leakage amounts to 5% of the total inlet air flow to the wave rotor. This corresponds to a 5 mil clearance with no special seals. Clearly, the leakage must be controlled, and the next series of rotor designs and tests must address this problem directly with a constructive solution. Similar tests must be carried out to determine the scavenge effectiveness and amount of heat transfer.

FLOW code calculations shown in Figure 3 are for off-design rotor operation corresponding to those flow conditions required by the upstream and downstream components of a wave rotor turbofan engine operating at part load. Several flow parameters are varied together in Figure 3 compared to the single variations shown in Figure 2. For example, if the engine is to fly at Mach 0.33 instead of 0.65, then the pressures, temperatures, and mass flows at the inlet and outlet ports to the wave rotor will also change in accordance with the overall engine requirements for half-speed operation. The dimensions and port locations of the wave rotor are held constant. However, the mode of operation of the wave rotor may be varied to compensate for the new flow conditions. For instance, the rotor tip speed may be increased in order to reduce the mass intake per cycle. A new wave pattern develops in the wave rotor and, depending on its design, it can accommodate well or poorly to such changes. The design techniques for producing a rotor which has relatively good performance over a wide operating range are understood in general at this point, but their application to particular designs is still somewhat of an art. The particular nine-port pressure exchanger chosen for the reference design shown in Figure 3 appears to have very stable off-design performance since the component efficiency varies at most by a few percent over quite a wide range of flight speeds. The rotor mass flow variations shown in Figure 3 also are accommodated to within a few percent over the same range by a linear variation of rotor tip speed with flight speed. A slightly nonlinear variation in rotor tip speed would reduce this mass flow defect to zero.

A risk evaluation was carried out to determine those technical areas of wave rotor design and operation which would have the greatest impact on turbofan performance measured in terms of TSFC. The cycle and rotor analysis typified by Figures 1 and 3 suggest that the turbofan TSFC is relatively insensitive to variations in the wave rotor efficiency. It has already been established by prior experiments that wave rotors will work over a wide range of operating conditions relevant to turbine engines. Peak cycle temperature and pressures are the strongest determining factors

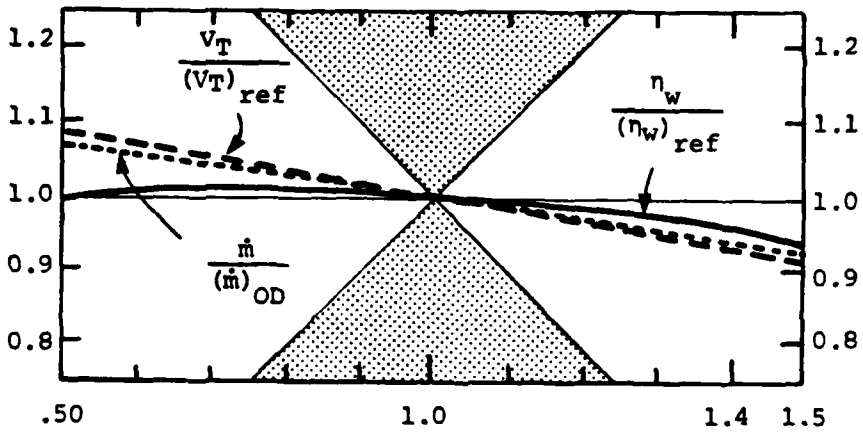

Figure 3. Off-Design Performance η_w of a wave rotor corresponding to off-design wave rotor turbofan engine operation at various flight speeds. The wave rotor tip speed V_T is varied as shown, relative to the reference value, to compensate for higher or lower mass flows. The actual wave rotor mass flow compared to the mass flow required by the off-design engine operation is indicated by $\dot{m}/(\dot{m})_{OD}$ for the particular V_T variations shown.

in the magnitude of improvement predicted for turbofan TSFC. The peak values attainable for these two variables are intimately connected with the rotor scavenge effectiveness, gas leakage, and on-rotor heat transfer. Figure 4 summarizes the impacts of peak temperature and pressure relative to the reference case, where the change in TSFC is given as a percentage difference relative to the reference case. The dashed and solid lines bracket the reference component efficiency of 70 percent. The possible increases in TSFC for higher temperature operation are most pronounced at higher pressures and for lower wave rotor component efficiencies. The fact that TSFC is scarcely affected by large deviations from predicted wave rotor efficiency indicates that this application of the wave rotor is particularly robust; that is, the risk is low to start with.

Recommendations for further research include, as the highest priority, a need to obtain experimental data from a carefully instrumented wave rotor test designed to demonstrate the predicted levels of performance at operating conditions appropriate to the small turbofan application. These tests should measure component efficiency and correlate those measurements with the amount of leakage, heat transfer, and other losses in the system. To insure the best choice of wave rotor design configuration for testing, a conceptual engine design evaluation should be carried out first, to address the questions of how to connect the wave rotor to adjacent components in the engine, to optimize its design, and to specify its major dimensions prior to carrying out a detailed design of the wave rotor test article. A companion effort should be devoted to improved models for pressure recovery losses in the manifold and heat transfer losses on the rotor. These models should be incorporated in the existing FLOW code and validated by wave rotor test data. The test results will establish the viability of wave rotor technology for high performance turbofan engines and will verify the design codes as valid tools for this application.

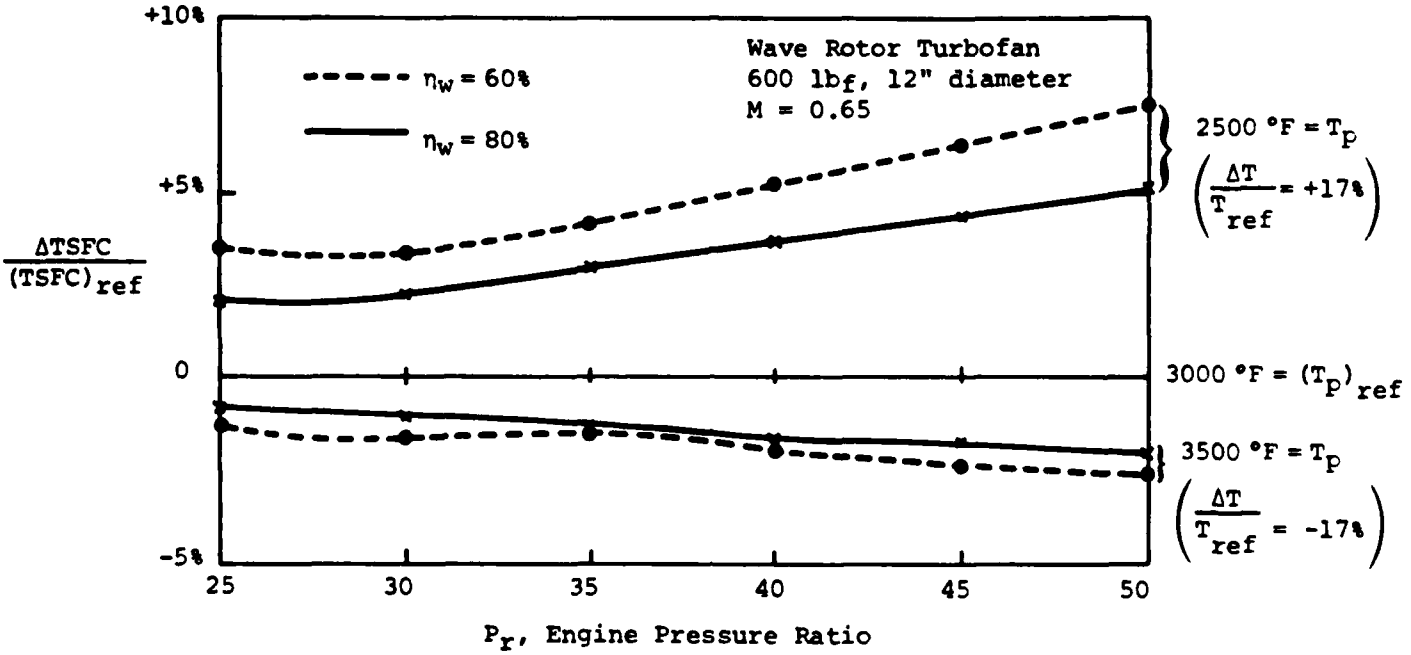

Figure 4. Percentage Variation in Thrust-Specific Fuel Consumption vs. Engine Pressure Ratio P_r for two values of work transfer efficiency η_w and two values of peak cycle temperature T_p (compared to the reference temperature of 3000 °F; data taken from Figure 2-2). The reference TSFC values for both $\eta_w = 60\%$ and 80% are plotted along the $\Delta TSFC = 0$ axis.

The next phase of research should be pursued in three consecutive stages: Stage 1 is a short effort consisting of the engine conceptual design evaluation, formation of an appropriate team to carry out the wave rotor design and tests, completion of the test program plans, and design of the test rotor; Stage 2 would demonstrate the test rotor operation and would include fabrication, assembly, and checkout of the rotor and its instrumentation; in Stage 3, detailed testing will complete the performance evaluation of the wave rotor and validation of the design codes.

Summarizing, the study covered a variety of wave rotor engine concepts from the viewpoint of cycle analysis and concluded that the potential for 25 to 30% reductions in the thrust-specific fuel consumption exists if the wave rotor efficiency lies in the range of 0.65 to 0.75. The FLOW code calculations project wave rotor efficiencies lying in that range for very plausible design and operating conditions. Part-load performance in the same range of efficiencies also appears to be quite possible.

From this analysis of the wave rotor, we conclude that this technology can reduce thrust-specific fuel consumption by a significant amount in small aircraft engines. The next steps are: To evaluate the best wave rotor design for testing; To carry out those tests to demonstrate its performance; and To validate the design codes used in predicting its performance.

Section 1
INTRODUCTION

This study analyzes wave rotor performance for turbofan engine applications and the sensitivity of that performance to rotor design and operating parameters. The study was completed over a six month period as the first phase of a more comprehensive program to evaluate the performance of wave rotor turbofan engines. The work has been divided into two main categories involving wave rotor component performance and the overall engine performance. Wave rotor performance is measured by two types of efficiency depending on whether the rotor simply transfers work of compression from one gas to another (e.g., a pressure exchanger wave rotor) or produces shaft power output (e.g., a wave rotor/turbine); these efficiencies are the work transfer efficiency and the shaft work efficiency, respectively.

The main thrust of the analysis was to compare preliminary estimates of wave rotor efficiency with more detailed calculations made with FLOW computer code. The preliminary estimates of efficiency were based on scaling arguments from existing experimental data on lower temperature wave rotors obtained at MSNW. These estimates included gas leakage and heat transfer losses and suggested that a wave rotor work transfer efficiency of 70 percent might be feasible if leakage and heat transfer could be restrained to proportional levels at higher temperatures and pressures. With improved sealing techniques and further design optimization, the work transfer efficiency could be projected to higher values. Even with a work transfer efficiency of 70 percent, these initial estimates indicated that a wave rotor turbofan fuel consumption value of 0.65-0.70 lbm/(lbf.hr) might be achieved in a small engine (e.g., 600 to 1000 lbf thrust) if the rotor could be operated at sufficiently high temperatures and pressures.

The Phase 1 research tasks consisted of:

1. **WAVE ROTOR ANALYSIS:** Evaluate wave rotor performance for on-design and off-design conditions. Model the work transfer and shaft power output for wave rotors. Compute gas stream properties including pressure, temperature, density, compression efficiency, expansion efficiency, velocity, and mass flow of the wave rotor as a function of design and operating conditions. The effects of heat transfer, viscosity, impedance mismatching, and gas leakage will be considered. Include at least one design with a re-entrant duct.

2. **PRELIMINARY WAVE ROTOR DESIGN:** Determine the size, shape, and speed of the wave rotor and rotor tubes appropriate to a turbofan propulsion system. Determine the manifold location and flow angles relative to the rotor face. Expand this preliminary design to include a range of possible designs corresponding to the wave rotor analysis.

3. **WAVE ROTOR TURBOFAN ENGINE PERFORMANCE AND SENSITIVITY:** Determine engine performance in terms of its thrust-specific fuel consumption for a range of pressure ratios, combustor temperatures, and other parameters corresponding to cruise missile propulsion conditions. Evaluate engine performance sensitivity to the wave rotor design and operating parameters.

4. **RISK EVALUATION:** Determine the technical risks in development of a wave rotor turbofan propulsion

system. Identify wave rotor features having a large impact on wave rotor turbofan engine performance. Wave rotor parameters will be varied over a reasonable range of values in order to bracket engine performance.

5. **RECOMMENDATIONS FOR FURTHER RESEARCH:** Analyze high risk areas to determine which of these can be resolved by relatively low cost analysis and/or experiments. Define and prioritize critical tests and analysis which reduce technical uncertainties and are prerequisite to an engine development program.

This report summarizes the results of these five tasks. During this research, a considerable amount of historical material on wave rotor development was also accumulated. A retrospective digest of that material is included as Appendix A because it lends further weight to the potential performance of wave rotors for aircraft engine application and highlights the problems that others have had in making these devices work efficiently. The bottom line from that review is that wave rotors have been run successfully in the past and that we should take advantage of those efforts by building on their successes.

The body of the report is organized so that the main implications of wave rotors for turbofan engines are discussed first. This motivates the more detailed study of the design and performance of wave rotors, which follows in subsequent sections. The evaluation of risk assumes that the primary risks are technical at this stage. Engine development is cast as later phases of an overall R & D program in order to proceed with greater certainty once the critical technical questions have been answered. An alternative would be a crash program where all tasks are taken in parallel and in which there are no particular funding limitations. The risk in this latter case would be a more complicated mix of technical and cost

factors; an additional effort is required to work out the details of a crash program.

The recommendations focus on essential experimental tests required to answer the most critical questions first. These are the verification of low leakage and the control of thermal/mechanical stresses in a high temperature wave rotor. A program directed toward this end should also include a selection of the best wave rotor for testing and analytic tasks to assist in the design and interpretation of the experimental results. In such a program, a hot stage wave rotor could be brought on-line and operated over a one-year period; an additional 8 to 10 months would be devoted to getting as much information as possible from the test rig, allowing for possible re-design to help optimize its performance.

Section 2

WAVE ROTOR TURBOFAN ENGINE PERFORMANCE AND SENSITIVITY

2.1 TECHNICAL BACKGROUND

Two basic wave rotor engine cycles have been considered: those which utilize the wave rotor to produce shaft work (wave rotor/turbines) and those which use the wave rotor to produce a high pressure hot gas (pressure exchange wave rotors). Both on- and off-design thermal cycle analyses have been carried out to determine the peak engine performance capabilities in terms of thrust-specific fuel consumption and the sensitivity of that performance to design and operating parameters, particularly to those parameters associated with the wave rotor component. This evaluation has focused on the performance of engines in the 600 to 1000 lb_f class for a range of pressure ratios from 20 to 50 and peak temperatures from 2500°F to 3500°F. More specific constraints on engine core size and bypass ratio are cited below. Typically, the engines are 12 to 18 inches in diameter with a core engine inlet diameter of 5 to 7 inches.

A relatively simple thermal cycle code has been used for this evaluation in order to keep the dependence of the results on wave rotor parameters as direct as possible. The cycle code calculates gas stream properties at each station in the engine, including pressure, temperature, and mass flow. The complete equations for the cycle code are summarized in Appendix B. Real gas effects include variations of the specific heat ratio γ with temperature and pressure and molecular weight at each flow station. A fuel having the heating value (i.e., 18,400 BTU/lb_m) and C/H mole fractions of JP4 are used throughout unless otherwise noted.

The cycle calculations suggest that a reference design wave rotor turbofan using a pressure exchange wave rotor may operate with a thrust-specific fuel consumption (TSFC) in the range of 0.65 to 0.75 for

reasonable bypass ratios (i.e., 5 to 8) and peak combustor (wave rotor inlet) temperatures of 2500 to 3500°F. The wave rotor efficiency, discussed in more detail in Section 4, has been varied from 0.60 to 0.80 to bracket the values obtained by detailed FLOW code calculations. Over this range of component efficiencies, the engine TSFC varies by only 5 percent (e.g., from 0.75 to 0.79 lb_m/lb_f hr for 2500°F peak temperatures).

The chief advantages of using a wave rotor are the increased cycle efficiency afforded by the automatic cooling of the wave rotor, and its high component efficiency in a small diameter, high pressure application. In particular, rotor wall temperatures do not exceed 1800°F for combustion temperatures reaching 3000°F. Additional cooling may be employed in a hybrid wave rotor/recuperator version of this engine, which will drop the rotor temperature to 1600°F or less. The exhaust from the rotor is also constrained to low temperatures so that the turbine inlet temperatures can be kept below 1900°F for an interesting class of wave rotor turbofan engines.

2.2 ENGINE CYCLE CONFIGURATIONS

The two primary engine configurations are shown in Figure 2-1, which illustrates the location of the wave rotor component relative to the rest of the engine and identifies the flow stations. A hybrid engine combining the attributes of each also exists but has not been evaluated within the scope of this study. The pressure exchanger wave rotor engine version illustrates the main flow paths for this type of engine. Partially compressed air enters the wave rotor at Station 3 from the compressor where it is compressed a factor of 2 to 3 more. The compressed air leaves the wave rotor at Station 3' and enters the combustor. Since only part of the fully heated air flow is needed to carry out compression work on the wave rotor, the rest of the air flow can be diverted at 4' to a turbine for work extraction. The diverted air flow should only be heated to the maximum feasible turbine inlet temperature; the peak cycle temperature can

(a)

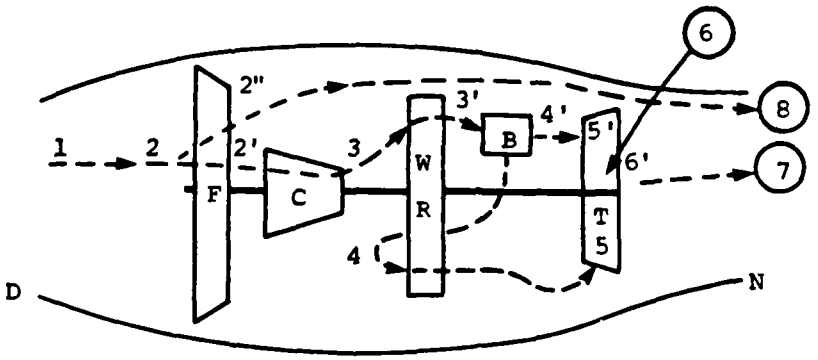

(b)

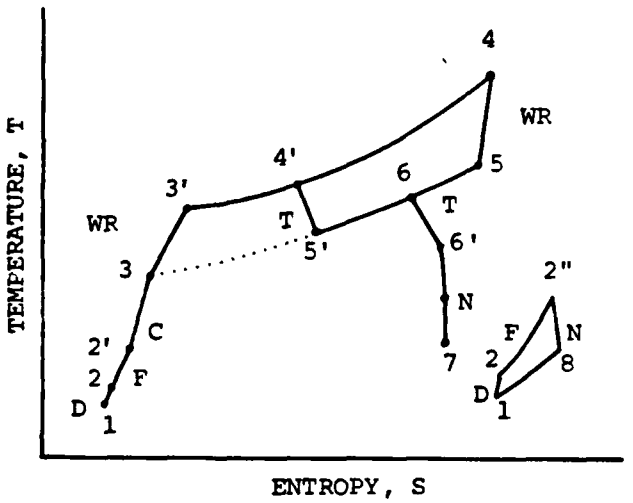

D = Diffuser
F = Fan
C = Compressor
WR = Wave Rotor
B = Burner
T = Turbine
N = Nozzle

(c) WAVE ROTOR/TURBINE

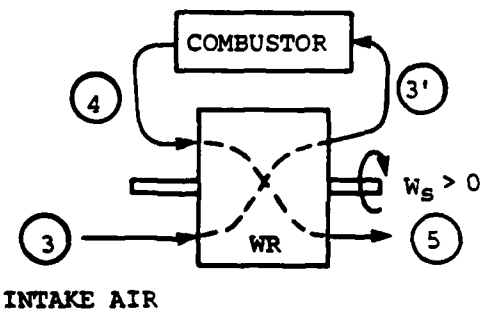

(d) WAVE ROTOR PRESSURE EXCHANGER

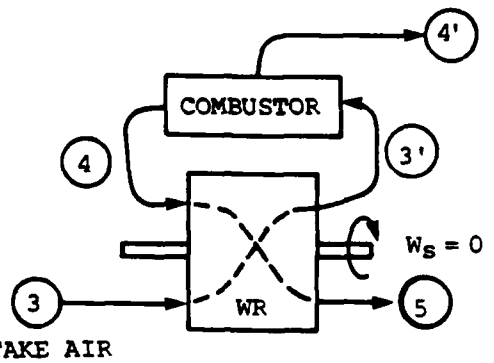

82 06910

Figure 2-1. (a) Wave Rotor Tubofan Engine Schematic [for (d)].
(b) Temperature-Entropy Diagram [for (d)].
(c) Wave Rotor/Turbine: Shaft Work Output ($W_s > 0$).
(d) Pressure Exchanger Wave Rotor: Compressed Gas Output (4'), no shaft work ($W_s = 0$).

be much higher than turbine inlet temperature because the wave rotor is more robust than the turbine and is an actively cooled component. The flow stream at peak cycle temperature re-enters the wave rotor at 4 where it compresses the incoming cold air by expanding against it before exhausting at 5 to the lower pressure turbine. The diverted flowstream passes through the high pressure turbine and expands to a pressure at 5' equal to the combustion gas pressure (at 5) where they are recombined (Station 6) before entering the low pressure turbine at a reasonable turbine inlet temperature. Some mixing losses occur at this stage in which the higher temperature gases lose some of their available work.

In the pressure exchange wave rotor engines, the wave rotor shaft is driven independently from the other components so that the shaft can be co-axial and in line with the other rotating components or it can be mounted transverse (i.e., at right angles to the turbine). The precise orientation does not influence the cycle calculations for the model used here. In an actual engine, the rotor placement will influence the duct lengths and the amount of duct turning and will have an effect on the cycle performance, which must be included in a more detailed evaluation.

The second primary engine configuration incorporates a wave rotor/turbine. The wave rotor/turbine engine differs in several important respects from the pressure exchange wave rotor engine. First, shaft work is extracted so that the wave rotor is integrally connected to the compressor. Therefore, the wave rotor tip speed must be chosen to match the compressor speed. Also, the exhaust gases from the combustor may be expanded through the wave rotor in several passes, requiring ducts to re-route partially expanded gases back onto the rotor for further expansion. The cycle calculation also differs since the principal output from the wave rotor is shaft work instead of available work of gas expansion.

2.3 THERMAL CYCLE CALCULATIONS

This analysis proceeds in the same manner as a conventional turbine engine cycle calculation. The pressure exchanger wave rotor can be considered as a compressor-turbine combination with compression (η_{CE}) and expansion (η_{TE}) efficiencies for each process. Since the work performed by the expanding combustion gases equals the work done to compress the incoming air, we can write that enthalpy balance as

$$\dot{m}_3[h_{(3')} - h_{(3)}] = \dot{m}_4[h_{(4)} - h_{(5)}]$$

where $h = c_p T$, $\dot{m}_4 = \dot{m}_{4'} - \dot{m}_5 + \dot{m}_f$ and $\dot{m}_{4'} = \dot{m}_f + \dot{m}_3$, and $\dot{m}_F$ is the fuel flow. A detailed consideration shows that the wave rotor work transfer efficiency $\eta_W = \eta_{TE}\eta_{CE}\, T_{3'}/T_{3',s}$ (e.g., see Section 4.4).

Calculations proceed as follows. Inputs include the flight Mach number and altitude, peak combustion temperature, and maximum inlet temperature to the high pressure turbine. Polytropic efficiencies are selected for the compressor, fan, and turbine components. A burner efficiency is also selected, and the values of η_{TE} and η_{CE} are chosen to be in the range of values computed from the flow code (as discussed in Section 4). A total engine thrust (e.g., 600 lb_f) and engine diameter (e.g., 12 inches) are selected in order to compute the required engine-specific thrust (i.e., ST in [lb_f/lbm·hr] of air). These values are then used to compute the optimum bypass ratio (see Appendix C) and fan pressure ratio that give the minimum TSFC. Alternatively, these parameters may be specified and the calculations provide the corresponding TSFC. The remainder of the cycle calculations provide the temperatures, pressures, and flow rates at each station.

2.4 ON-DESIGN CALCULATIONS

Results of on-design cycle calculations are shown in Figures 2-2 to 2-4. Figure 2-2 illustrates TSFC for several combustion temperatures as a function of the overall pressure ratio. The optimum bypass ratio and the inlet temperature to the low pressure turbine are shown as pairs of numbers at points along each curve. The low pressure turbine inlet temperature may be higher than high pressure turbine inlet temperature; realistic solutions would normally be constrained to the same temperature or lower. Figure 2-3 shows the sensitivity of the TSFC to wave rotor efficiency η_W for the engine pressure ratio 37.5 and peak temperature of 2500°F. The TSFC varies approximately 5 percent over the range of η_W values considered. The lack of TSFC sensitivity to η_W suggests that the wave rotor is a relatively low-risk approach to advanced turbofan engine development since its component efficiency is not very critical to the overall engine performance in this configuration.

Finally, we present in Figure 2-4 a combination of fan variables (bypass ratio and pressure ratio) which indicate the minimum locus of TSFC for several different engine diameters at 600 lb_f thrust. A substantial gain in TSFC is available if the engine diameter D_{eng} can increase from 12" to 14"; further improvement is possible if the engine is 16" in diameter, but at this size the bypass ratio is quite large. One would have to consider a geared fan or a derated fan efficiency if an engine of this size and bypass ratio is contemplated for 600 lb_f thrust. Figure 2-4 may also be used for any engine diameter or thrust by scaling the horizontal coordinates from

$$D = D_{eng}\left[\frac{1}{1 + .8889\ BPR}\right]^{1/2} \qquad [2\text{-}2]$$

$$\text{Specific Thrust} = \frac{4.73 \times \text{Thrust}\ [lb_f]}{[D_{eng}(in)]^2}$$

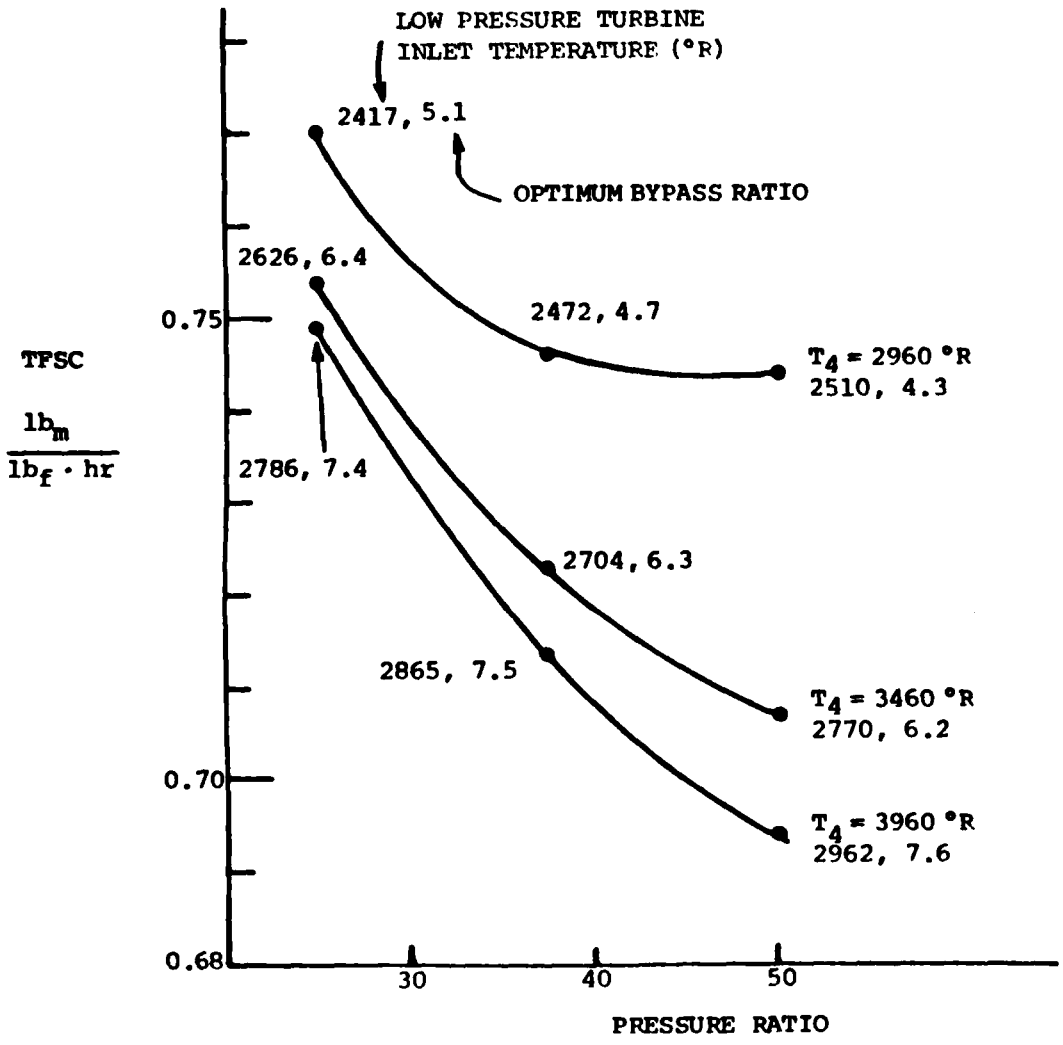

VARIATION OF TSFC WITH OVERALL PRESSURE RATIO

M_o = 0.65 at Sea Level

High P. Turbine Inlet Temperature = 2460 °R

No Nozzle, Diffuser Losses

Fan P.R. = 1.9

SPTH ≈ 20.6 lb_f/lb_m/sec
(12" dia engines @ 600 lb thrust)

Energy Exchanger PR = 2.5

POLYTROPIC
- Compressor Efficiencies, 89%
- High P Turbine Efficiency, 87.7%
- Final Turbine Efficiency, 85.5%
- Energy Exchanger Efficiencies, 89.5% Comp. 87.0% Exp.

82 06756

Figure 2-2. Variation of Thrust Specific Fuel Consumption (TSFC) with Pressure Ratio for Several Peak Cycle Temperatures T_4.

M = 0.65 at sea level
High P Turbine Inlet 2460 °R
Final Turbine Inlet 2470 °R
Peak Temperature 2960 °R
Fan P_r 1.9
SPTH 20.6 lb_f sec/lbm
(12" dia inlet, 600 lbj)

Compressor P_r = 15
Energy Exchanger P_r = 2.5
POLYTROPIC EFFICIENCIES:
Compressor 0.890
High P Turbine 0.877
Final Turbine 0.8555
Bypass Ratio 4.7
No Nozzle or Diffuser Losses

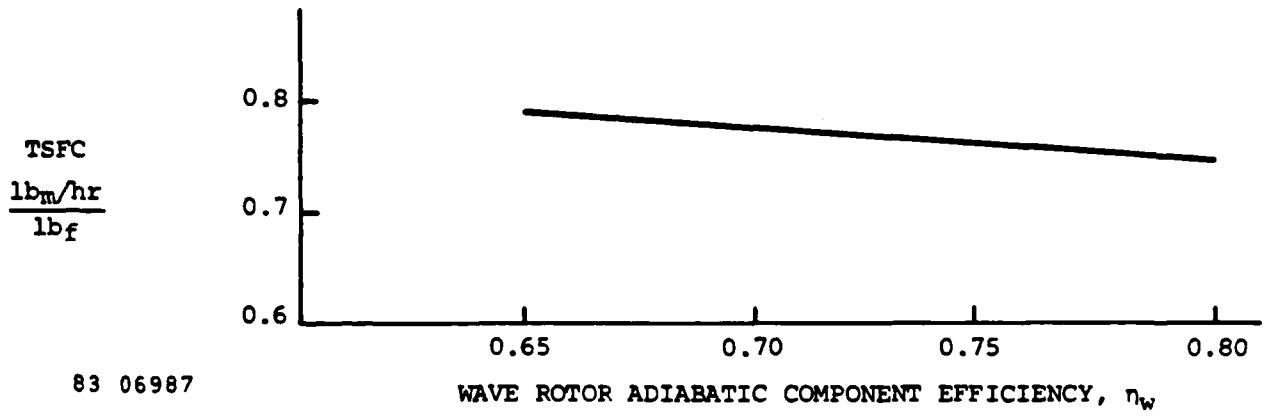

Figure 2-3. Effect of Wave Rotor Efficiency η_w on Thrust Specific Fuel Consumption (TSFC) at a particular peak pressure and temperature.

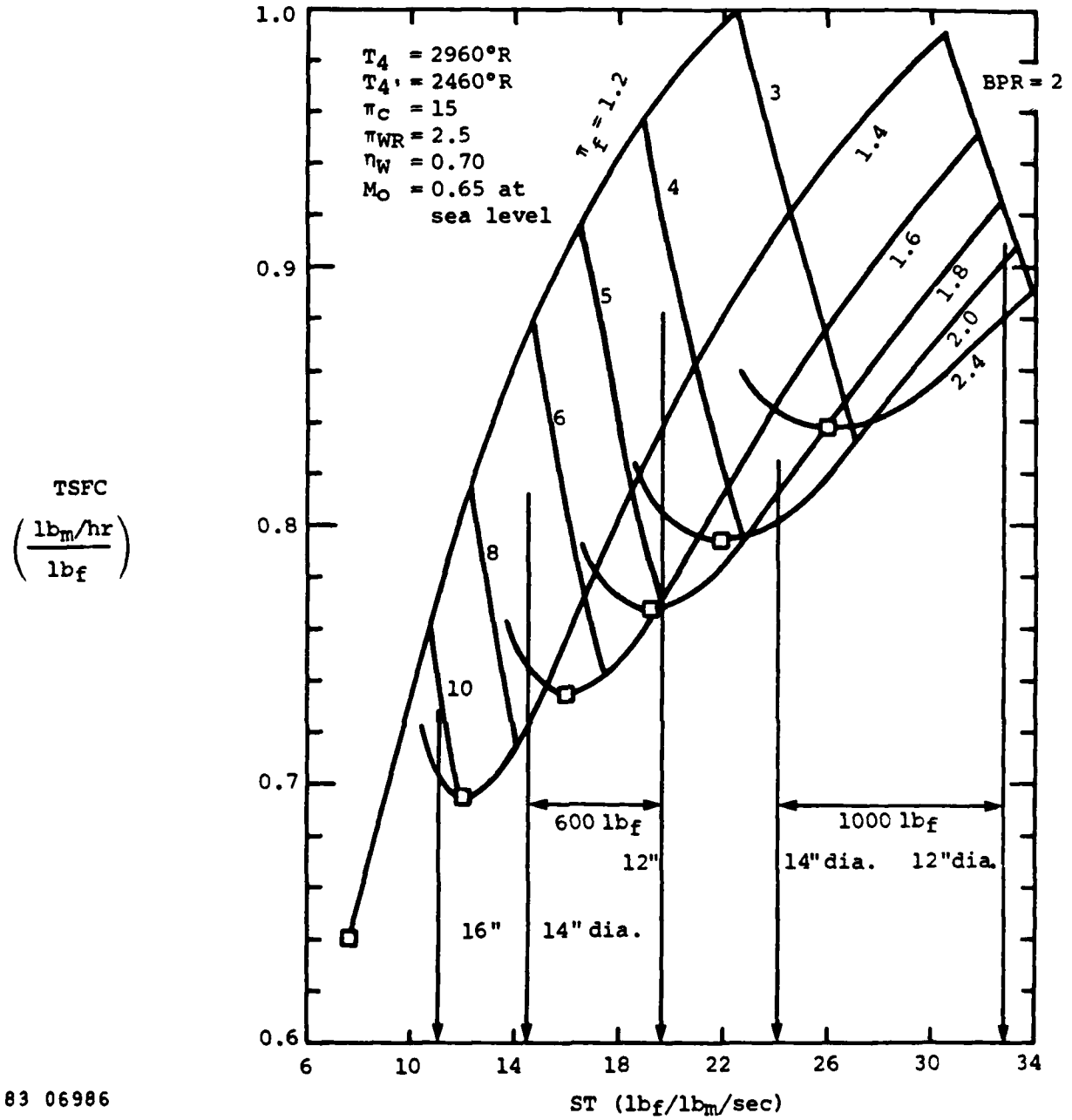

Figure 2-4. Thrust Specific Fuel Consumption (TSFC) vs. Specific Thrust (ST) for various Bypass Ratios (BPR) and Fan Pressure Ratios (π_f): No nozzle or diffuser losses.

where D is the core engine inlet diameter assuming a 1:3 hub-to-tip ratio and M_o = 0.65 at sea level. For the 600 lb_f examples, the minimum TSFC is achieved (see Figure 2-4) for essentially constant (5" diameter) core engine size at D_{eng} = 12", 14", and 18". That is, the bypass ratio corresponding to minimum TSFC increases just enough with engine size to eliminate any changes in the core engine diameter.

Rather little information is available on the component efficiencies of 5" diameter compressors and turbines using air and combustion gas. The most relevant recent literature comes from the development of the automotive gas turbine. Earlier data also exists for small rotating turbogenerator units developed for space. Each of these sources supports adiabatic turbine efficiencies on the order of 0.89 and adiabatic compressor efficiencies of 0.85. The fan efficiencies must be intuited by scaling down data from large engines. We have estimated η_{fan} as 0.885. A nominal combustion efficiency of 0.97 is assumed. Diffuser and nozzle efficiencies are taken equal to unity in order to give the uninstalled thrust-specific fuel consumption on a basis comparable to other engine studies.

2.5 Off-Design Engine Performance

An analysis of off-design engine performance was conducted to determine the inlet and outlet flow requirements for the wave rotor components. These requirements are used as input parameters for the off-design wave rotor flow code calculations in order to confirm the wave rotor component efficiencies used in the cycle calculations. The chief value of these results is to determine the sensitivity of part-load engine performance to the wave rotor component. A summary of the off-design engine cycle equations is presented in Appendix B.

An example of the results of off-design engine calculations are shown in Figure 2-5. These calculations allow one to examine off-design operation when the flight speed and altitude are varied. The off-design

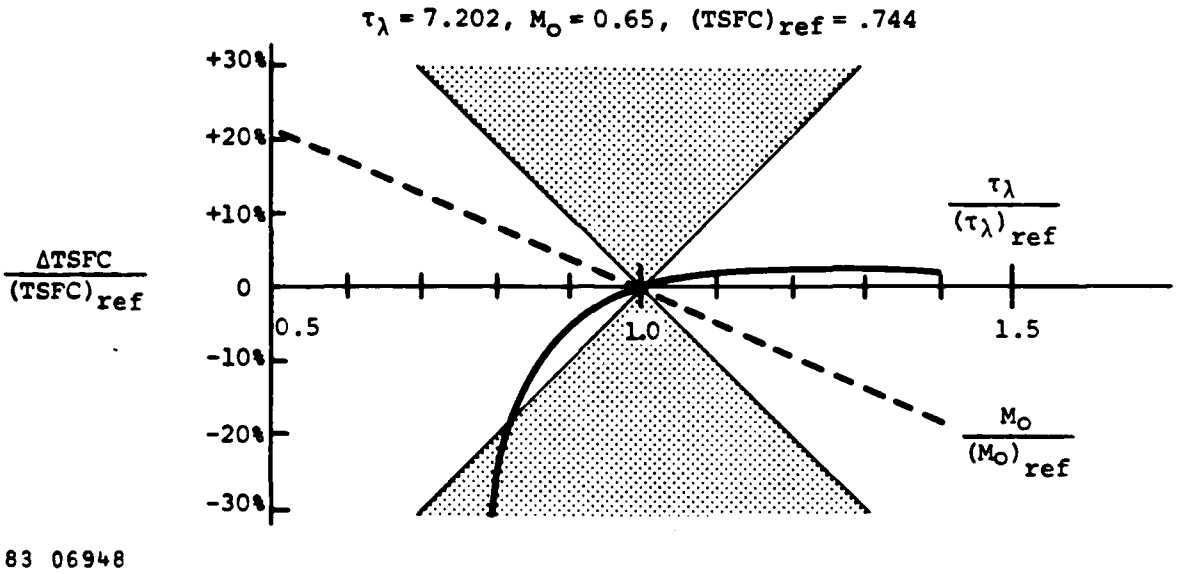

Figure 2-5. Off-Design Cycle Calculations for a Wave Rotor Turbofan Engine showing percentage changes in TSFC for variations in combustor temperature τ_λ, variations in flight speed M_o. Shaded regions indicate high sensitivity of TSFC to cycle or flight parameters.

model relates the manner in which parameters such as the mass flow through the engine, shaft rpm, and internal pressures and temperatures will change in concert with each other to maintain a self-consistent set of values representing actual engine operation at part load. The model predicts the changes in engine thrust level, fuel consumption rate, and flow properties at each station for the desired off-design conditions.

We have examined off-design operation with flight Mach numbers ranging from 50% to 140% of the reference value of 0.65 in order to include dash capability during a portion of the mission.

The horizontal axis of Figure 2-5 shows the fraction above or below the reference value (1.0) taken by the peak cycle temperature τ_λ and flight speed M_o. The vertical axis measures the fractional change in thrust-specific fuel consumption (TSFC) compared to $(TSFC)_{ref}$; positive values of this variable imply values of TSFC lower than the reference values.

For small variations (±10%) about the reference flight speed and peak cycle temperatures, the fractional change in TSFC is less than ±5%, implying local insensitivity to off-design performance.

For larger variations of τ_λ less than $(\tau_\lambda)_{ref}$ the TSFC deteriorates rapidly. However, very reasonable off-design performance persists for τ_λ 50% or higher than $(\tau_\lambda)_{ref}$, suggesting that the wave rotor turbofan engine might be very well suited for missions involving a high speed segment.

The fractional change in TSFC with flight speed is essentially linear, improving at slower speeds and deteriorating at higher speeds. In every case, the percent change in TSFC is less than the corresponding percent change in flight speed, implying that off-design performance is relatively insensitive to flight speed. A more complete analysis of airframe and mission conditions is required to carry out off-design engine calculations where flight speed and peak temperature vary together. We

may conclude that the wave rotor component preserves its advantages for good overall engine performance in both on- and off-design operation.

2.6 PERFORMANCE FOR A 600 LB THRUST ENGINE

On the basis of the results presented above, it is possible to select reference design conditions for a 600 lb_f thrust wave rotor turbofan engine. These two reference designs are preliminary involving just the first estimates of flow conditions, diameters, and performances calculated from the cycle codes and are not optimized to any extent. Additional analysis and design would be needed to arrive at optimized designs. As reference designs they serve as analytic benchmarks against which further improvements in design and performance can be measured. They do indicate the promising potential of the wave rotor approach to small turbofan engine performance. The 600 lb_f thrust engine has a TSFC = 0.776 for a 12" diameter engine; a 1000 lb_f thrust engine exhibits a TSFC of 0.89 for the same engine diameter. The design values for a 600 lb_f thrust engine are summarized in Table 2-1. Clearly, we can expect substantial improvement by moving to larger engine diameters (and correspondingly larger bypass ratios) as indicated in Figure 2-4. Further optimization would, therefore, also require a sharper definition of particular mission requirements in order to delineate such things as the maximum allowed engine diameter, bypass ratio, etc.

It is worthwhile noting from the reference designs that the combustor temperature (i.e., peak cycle temperature) is 2500°F (1647°K at station 4), but the turbine inlet temperatures are maintained at 2000°F. The wave rotor wall temperatures are also below 1500°F, so that ***no new materials development is required for this engine.***

As new high temperature materials do become available, the wave rotor will always be able to maintain a higher inlet temperature than turbines made of the same materials. Thus, the wave rotor will boost cycle

Table 2-1

Preliminary Reference Design Values for 600 lb_f Thrust Wave Rotor Turbofan Engines

Flow Stations*	T °K (°R)	P MPa (atm)	ṁ kg/sec (lb/sec)
FAN			
1	288 (519)	0.10 (1)	10.4 (22.9)
2	313 (563)	0.13 (1.326)	10.4 (22.9)
2"	384 (692)	0.26 (2.52)	10.4 (22.9)
8	384 (692)	0.10 (1)	10.4 (22.9)
CORE ENGINE			
2'	384 (692)	0.26 (2.52)	2.8 (6.2)
3	744 (1340)	2.02 (19.9)	2.8 (6.2)
3'	1017 (1831)	5.04 (49.7)	2.8 (6.2)
4	1647 (2965)	4.74 (46.8)	2.4 (5.2)
4'	1365 (2457)	4.88 (48.2)	0.4 (1.0)
5	1395 (2511)	1.89 (18.7)	2.4 (5.2)
5'	1129 (2032)	1.96 (19.3)	0.4 (1.0)
6	1364 (2455)	1.90 (18.8)	2.8 (6.2)
6'	799 (1439)	0.14 (1.40)	2.8 (6.2)
7	799 (1439)	0.10 (1.0)	2.8 (6.2)

* See Figure 2-1(b)

Thrust = 600 lb_f

Specific Thrust = 20.57

Engine Diameter = 11.75 inches

TSFC = 0.776 $lb_m/lb_f/hr$

Bypass Ratio = 4.68

Mach 0.65 at sea level

POLYTROPIC COMPONENT EFFICIENCIES:

$\epsilon_{nozzle} = \epsilon_{diffuser} = 1$

$\epsilon_C = 0.892$, $\epsilon_{HPT} = 0.877$, $\epsilon_{LPT} = 0.855$

$\epsilon_{CE} = 0.838$, $\epsilon_{TE} = 0.800$

performance for a given turbine materials technology and protect the turbines from excessive temperatures.

2.7 CONCLUSIONS

Performance calculations for the wave rotor turbofan based on a pressure exchange wave rotor indicate low (0.68 to 0.75) thrust-specific fuel consumption from on-design (e.g., full load TSFC = .776) conditions to off-design (50% flight speed TSFC = 0.621) conditions. These results are not very sensitive to the wave rotor component efficiency for the range of values of η_W predicted by more detailed flow code calculations. The corresponding engine designs suggest that this performance may be achieved for engines in the 600 lb to 1000 lb thrust categories (at 0.65 Mach number, sea level conditions) having entrance diameters of 12 inches to 14 inches, and bypass ratios of 4 up to 8; the core engine diameter (i.e., compressor inlet diameter) for these cases was nearly constant at 5 inches (e.g., for the 600 lb_f engine) assuming a 3:1 tip-to-hub ratio for the compressor.

Wave rotor wall temperatures and turbine gas inlet temperatures are maintained at or below 1950°F so that no new materials development would be required for such engines. A preliminary reference design at 600 lbs. thrust provides the basis for a more detailed evaluation in which specific design questions involving the integration of a wave rotor with the rest of the engine may be addressed.

Section 3
PRELIMINARY WAVE ROTOR DESIGN

3.1 SCOPE

Existing wave flow patterns have been used to establish preliminary wave rotor designs appropriate to a turbofan engine for cruise missile application. A reference case design has been developed for a wave rotor corresponding to a turbofan engine providing 600 lb(f) thrust at Mach 0.65 and sea level flight conditions. The reference case preliminary design has been expanded to include several other example designs which span the range of parameters considered in the wave rotor analysis task.

The wave rotor preliminary design emphasizes basic dimensions of the rotor (radius and length), number and shape of compression tubes, rotor tip speed, injection nozzle and exhaust manifold port placement, and flow angles relative to the rotor face. This design information is sufficient for carrying out FLOW code calculations to evaluate wave rotor performance. A much more detailed wave rotor design evaluation is required before any device of this sort is tested. Selection of a test design also requires an evaluation of conceptual engine designs in order to choose the most appropriate rotor configuration for testing. The preliminary design information developed here is intended primarily to allow the FLOW code calculations to be made, and as an approximate measure of the size and weight of the wave rotor component.

The basic design relations are discussed below and the preliminary wave rotor designs are derived from these relations. The results show that the wave rotor component is small (on the order of 3 to 6 inches in diameter and length) and lightweight. Despite its small size, the individual compression tubes can be relatively large in order to help reduce boundary layer losses. Compared to the high pressure stages of conventional axial flow compressors, the size of the wave rotor tubes is

relatively large. The losses in the wave rotor compression process are related to unsteady gasdynamic wave processes and nonuniform flow in the manifolds, as compared to axial flow compressor losses which are primarily aerodynamic (i.e., related to boundary layer separation and blade tip effects). As a result, the penalties for small wave rotor designs are not as severe as for more conventional turbo-compressor systems.

A second point in the wave rotor design concerns the effect of tip speed versus its capabilities to be efficient. Tip speed does not have a dominant effect on wave rotor efficiency. Unlike a turbine or compressor where tip speed must be matched aerodynamically to the gas flow in order to achieve good efficiencies, the wave rotor efficiency depends instead on the relation between the rotor period of revolution and an acoustic wave transit time within the rotor, which in turn depends on the length of the rotor. The longer the rotor, the lower the tip speed can be. Thus, the tip speed for a wave rotor can be relatively slow and still achieve good efficiency. The consequence of this feature is that the usual creep strength limits which apply to high temperature turbines are much less severe for wave rotors, allowing them to operate at higher metal temperatures. A more important concern for wave rotors is thermal cycling fatigue due to the heating and cooling of the tube walls with each cycle.

Specific effects, such as heat transfer and leakage, are design dependent and will help to determine such things as the number of tubes and tube size and shape for a given set of flow conditions. These effects are modeled analytically in this section to provide a way of estimating their magnitude and the equilibrium wall temperature of the rotor. Much of the design optimization can be carried out with these analytic models before invoking the FLOW code for more detailed results.

Re-entrant ducts are also discussed from a design point of view as a means for establishing the appropriate boundary conditions for the FLOW code. The details of these ducts are deferred to the future, when a conceptual engine design evaluation will be carried out.

3.2 ROTOR DESIGN RELATIONS AND SCALING

The basic dimensions of the wave rotor are determined by the mass flow through the system, the wave rotor pressure ratio (and, hence, the wave diagram), and the peak inlet gas temperature. Considerable design freedom exists regarding the shape and number of tubes, the length of the rotor, and the tip speed. These parameters are constrained largely by the material properties of the rotor, the degree of dimensional stability required, the collection efficiency, and any upper limits on wave rotor diameter - by the engine envelope within an airframe, for example. This section concentrates on modeling of the basic rotor wave processes and dimensions. The following section extends this analysis to heat transfer effects.

3.2.1 Analytic Approximations to the Wave Diagram

The fundamental flow pattern established within the wave rotor is called a wave diagram because the essential compression, expansion, and scavenging processes are caused by the propagation of unsteady gasdynamic waves along the length of each tube as the rotor spins past each of the inlet and exit ports of the device. The construction of an idealized wave diagram is the first step in the design of a wave rotor since the strength of each of the waves is related directly to the strength of the compression of expansion desired of the device and because the speed of these waves helps to determine the location and azimuthal extent of each of the ports supplying the gas to the rotor. Figure 3-1 shows a wave rotor with two complete compression and expansion cycles per revolution. It is possible to represent the wave processes occurring in the device, as shown schematically at the left in this figure. The dashed lines represent the location of wave fronts and the interface between the combustion gases and the intake air.

A basic precept for wave diagrams is the concept of periodic flow. After one revolution, the flow in a given tube must return to its original

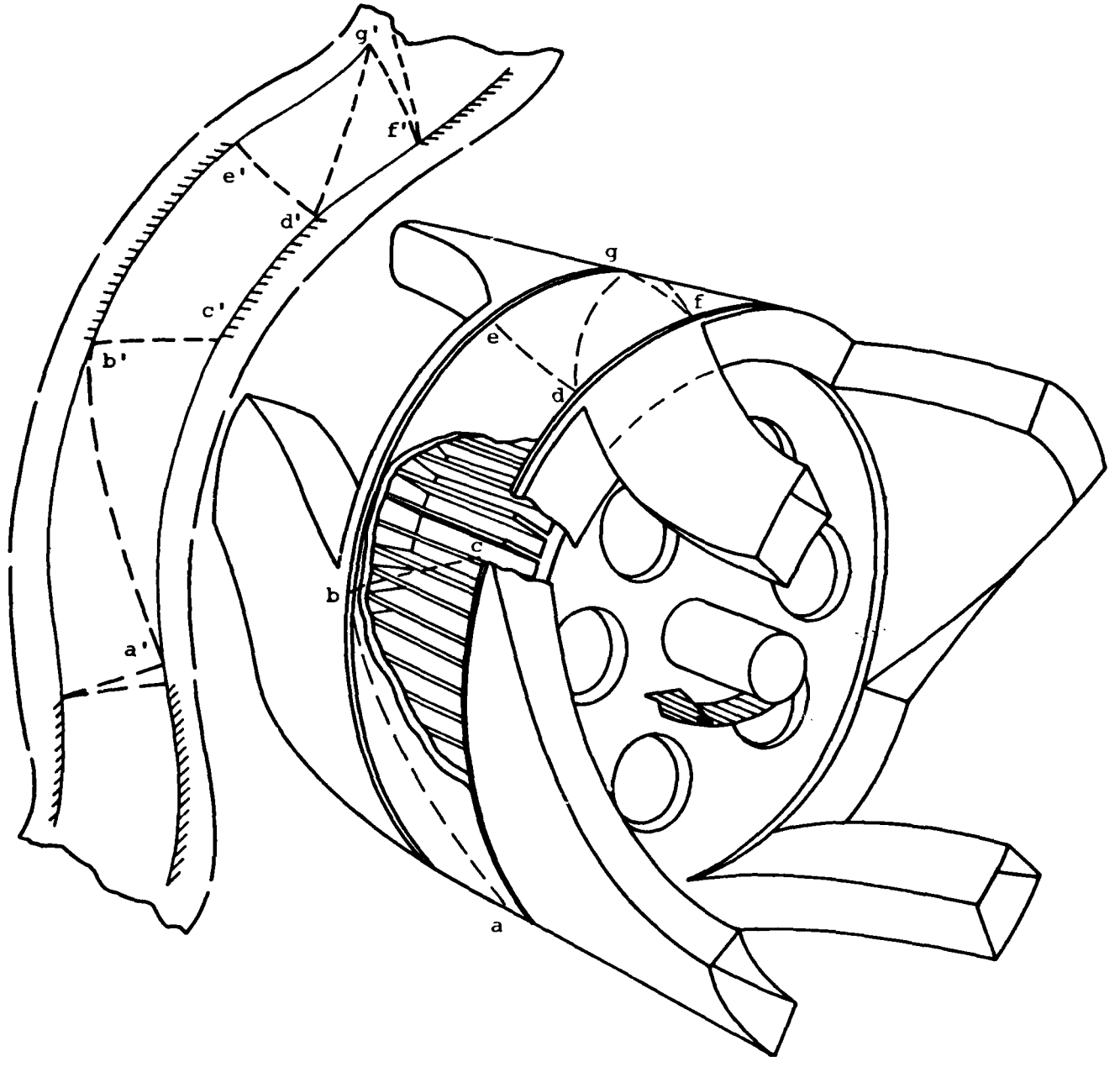

Figure 3-1. Superposition of Wave Diagram on Two Cycle Pressure Exchanger Wave Rotor Configuration

state at each point in the tube. This does not mean that the flow in the tube is uniform at this point, but it does imply that the flow is steady as observed from the stationary frame of the outside observer; in particular, the manifold or port flows are steady for a periodic wave system. A steady port flow device allows it to be mated to other steady flow devices, such as axial flow turbines or compressors, as an integrated component of an engine.

Complete periodicity is difficult to guarantee for wave diagrams in general since there may be a large number of internal reflected waves which are difficult to account for with an analytic scheme. The FLOW code does this automatically. Thus, an analytic approximation may be used to start the FLOW code calculation, and the code itself will compute a revised wave pattern which, after two to three cycles, converges to a new periodic pattern with all of the innumerable wave reflections included.

There are certain classes of wave diagrams that guarantee periodic behavior within the context of the analytic approximations to be discussed shortly. These wave diagrams make use of completely uniform manifold flows, no waves crossing any of the contact surfaces as they traverse the tubes, and wave management ports to cancel wave reflections at the ends of the tubes. It is useful to examine one of these manifestly periodic wave diagrams as an example because it represents probably one of the most efficient forms of the wave rotor pressure exchanger, and it allows us to give a particularly simple description of the work transfer efficiency of such a device.

Figure 3-2 shows this type of wave diagram for a pressure ratio 2.5 pressure exchanger wave rotor. Note that the driven gas (air) is compressed by two shock waves of equal strength and then exits from port d3 on the left. The hot high pressure driver gas (e.g., from the combustor) enters at port D3 on the right, compressing the driven gas already in the tube by sending the second shock wave across the tube. The gas interface or contact surface between these two gases is immediately

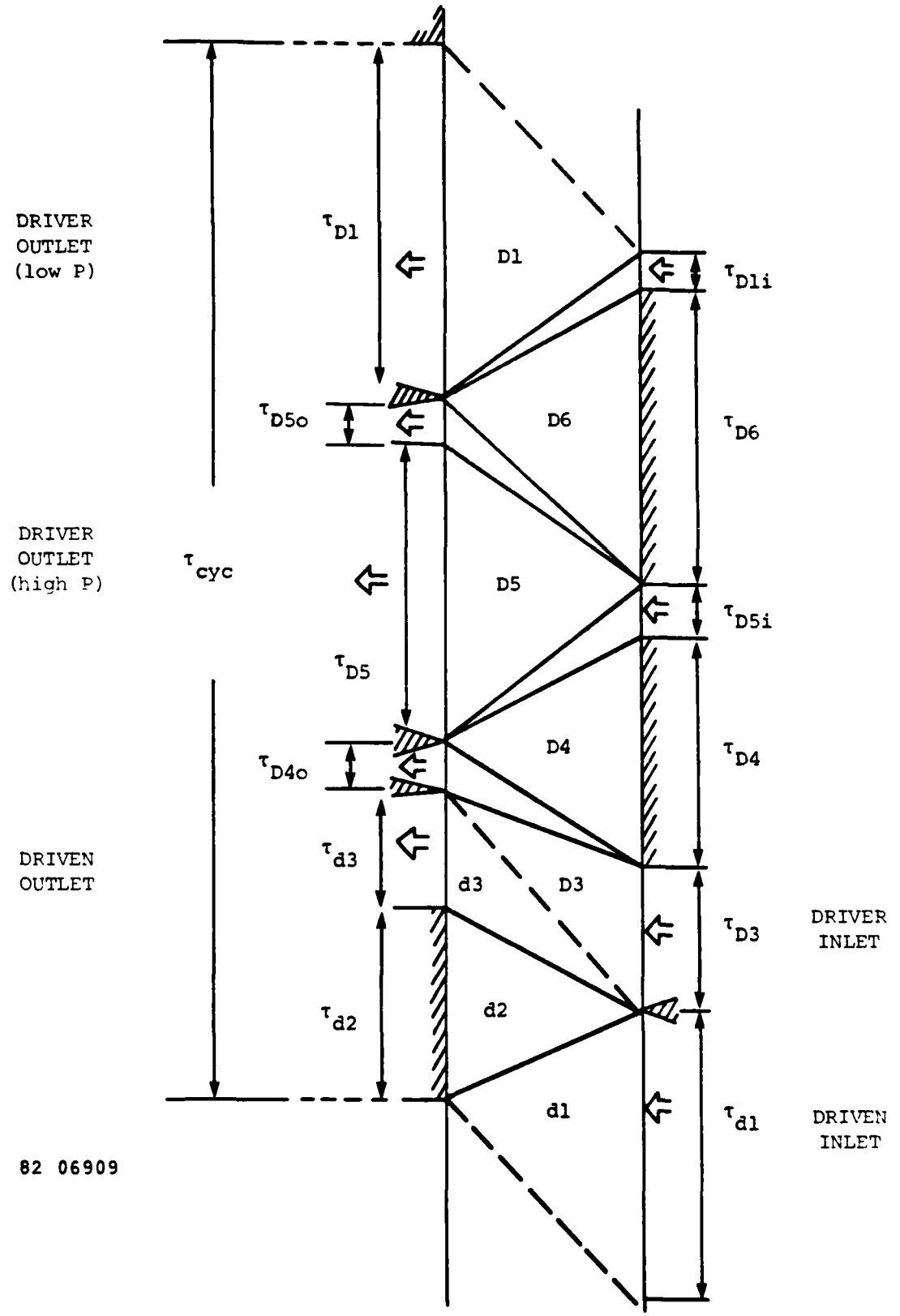

Figure 3-2. Ideal Wave Diagram for a Nine Port Pressure Exchanger Wave Rotor portraying the cycle time τ_{cyc}, identification of uniform flow regions, port and endwall times.

overtaken by the compression wave and travels at a slower speed across the tube. A wave management port is located at the trailing edge of the driven gas exit port d3 in order to slow the exiting gases to a zero velocity and to cancel the rarefaction wave (i.e., zero reflection) which accounts for this deceleration. The driver gas is subsequently scavenged from the tube in two separate ports, D5 and D1. Two ports are necessary if the final gas velocity in port D1 and pressure there are to match the incoming driven gas conditions at port d1. A careful consideration of the Riemann invariants associated with the unsteady expansion waves shown in Figure 3-2 attests to this fact and guarantees the periodicity of this system.

There are four wave management ports for this particular wave diagram. Each of these involves non-uniform flows, but generally the mass flows through these ports are so small that the port losses do not significantly affect the wave rotor efficiency. Their impact on suppression of reflected waves is considerable and represents their main benefits to device efficiency. The main inlet and outlet manifold flows are uniform since no waves from inside the device are incident on the ports. The equations used to construct the wave diagram of Figure 3-2 are given in Appendix D. These equations do allow the two gases represented here to have different specific heats and molecular weights. A modification of these equations also allows an analytic estimate of the heat transfer (see Section 3.3). The solution procedure is straightforward algebraic substitution; no iteration or convergence is required. Thus, the results are exact in this approximation.

A related but more complicated procedure has been used in the past for constructing wave diagrams in which internal wave reflections occur. This is an iterative technique in which one cycle is completed and then the initial parameters are adjusted to approximate the end of the first cycle; the next cycle is similarly constructed, and so on until the beginning and end of successive cycles agree well enough. This technique approximates the process followed with the FLOW code except that the FLOW

code is capable of following all of the waves whereas the analytic procedures simplify the process by following only a finite number of waves which represent the main gasdynamic process in progress. The most useful format for this technique has been described by Pearson in his chapter on wave engines in Horlock's text on advanced turbine engines. He uses three nomograms which relate the physical states of the gases on either side of a wave to the wave's position in the tube and to the characteristic velocities of the flow and small disturbances in the flow: the so-called state, position, and pole diagrams. The calculation includes the same Riemann invariants used in the pressure exchange calculation for the wave diagram shown in Figure 3-2. However, the technique can be refined considerably to include finite opening and closing of each tube, losses associated with angle of attack of flow entering the tubes, and the details of wave-wave and wave-contact surface interaction within the tubes as well as wave reflection at the tube ends. Figure 3-3 shows an example of a complex wave diagram constructed by Pearson using this technique for a wave rotor/turbine which produces shaft power output. In this example the manifold flows are not uniform. However, the wave diagram is periodic, and the gases are complete scavenged in one cycle. Later we shall see wave diagrams where incomplete scavenging occurs in one cycle so that a considerable amount of compression and expansion of gas entrained on the rotor from one cycle to the next occurs. This leads to an inefficient use of the wave rotor with an equivalent high back work ratio since the entrained gases are not available at the end of each cycle to perform external work. Further, the losses associated with these entrained gases must be kept to an absolute minimum in order to extract any useful work from the system.

3.2.2 Design Relations

The design process for a pressure exchanger wave rotor begins with an assumption of the kind of wave processes which will be used to expand or compress the working gases. For example, Figure 3-2 illustrates the wave processes chosen for a pressure exchange wave rotor having the maximum

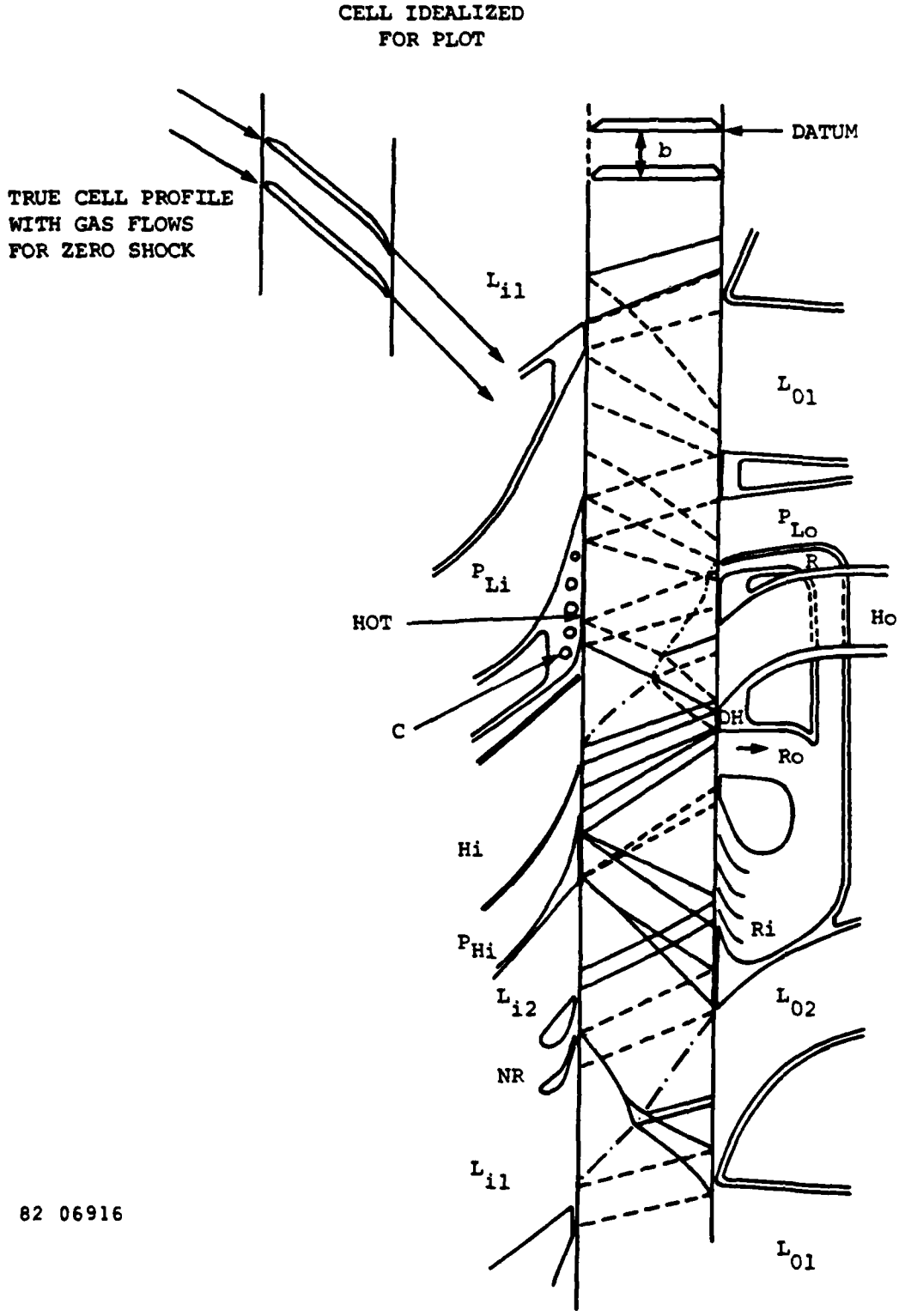

Figure 3-3. Ideal Wave Diagram for a Wave Rotor/Turbine Constructed from State, Pole, and Position Diagrams (Pearson/Horlock).

work transfer efficiency. The total cycle time τ_c can be obtained from this diagram once the peak sound speed a_{D3} (i.e., combustion inlet gas temperature) and rotor length have been prescribed. That is, each of the dimensionless times shown in Figure 3-1 will be scaled to dimensional values by the acoustic transit time L/a_{D3}. The rotor tip speed v_T is thus related to the rotor radius by

$$2\pi r = v_T \tau_c \left[L/a_{D3}\right] \qquad [3\text{-}1]$$

The next step is to choose the effective collection efficiency of one of the primary manifolds; for example, the driven gas outlet manifold. The collection efficiency η_{col} is a measure of how close the flow into a given manifold is to being continuous; an infinite number N of tubes opening onto a finite manifold results in a perfect collection efficiency. The actual relation is $\eta_{col} = (N-1)/N$. Thus, a prescription of the collection efficiency gives the number of tubes in the driven gas outlet manifold N_{d3}. From this quantity, the width of individual tubes may be computed:

$$d = \frac{\tau_{d3}}{\tau_c} \left[\frac{2\pi r}{N_{d3}}\right] \qquad [3\text{-}2]$$

Using the mass flow into the driver gas port m_{D3} and the accompanying flow velocity and density of that gas, one can solve the relation

$$m_{D3} = \rho_{D3} u_{D3} h d N_{D3}, \text{ where } N_{D3} = \frac{\tau_{D3}}{\tau_{d3}} N_{d3} \qquad [3\text{-}3]$$

for the height h of each tube. Each of the other port mass flows can be derived from m_{D3} since the flow velocities and densities and manifold sizes (e.g., in terms of the τ_i) are known from the wave diagram and are related to each other by

$$m_i = \rho_i u_i h d \left[\frac{\tau_i}{\tau_{d3}}\right] N_{d3} \qquad [3\text{-}4]$$

The flow angles of each port can be obtained by matching the tangential velocity of the rotor with the tangential flow speed in the manifold coordinate system, assuming the rotor tubes are parallel to the axis of the rotor (the more general case is discussed in Section 4.4.1). Thus, if u is the flow speed in the manifold coordinates and θ is the angle of the manifold flow relative to a vector normal rotor face, then $u \sin\theta = V_T$; therefore, the flow angle is

$$\theta = \sin^{-1}\left[\frac{V_T}{u}\right]$$

where the manifold flow speed is known from the wave diagram.

In summary, the unknowns are τ_i, r, N_{d3}, d, N, Ω, h, and m_i, and the basic equations are:

$$\tau_c = \sum \left[\tau_{i(\text{ports})} + \tau_{i(\text{end walls})}\right]$$

$$r = \frac{V_T \tau_c L}{2\pi a_{D3}} \qquad [3\text{-}7]$$

$$N_{d3} = \frac{1}{1-\eta_{col}} \qquad [3\text{-}8]$$

$$d = \frac{2\pi r \tau_{d3}}{\tau_c N_{d3}} \qquad [3\text{-}9]$$

$$N = \frac{2\pi r}{d} \qquad [3\text{-}10]$$

$$\Omega = \frac{V_T}{2\pi r} \qquad [3\text{-}11]$$

$$h = \frac{m_{D3}}{N_{d3} u_{D3} \rho_{D3} d}\left[\frac{\tau_{d3}}{\tau_{D3}}\right] \qquad [3\text{-}12]$$

$$m_i = \rho_i u_i hd \left[\tau_i / \tau_{d3}\right] N_{d3} \qquad [3\text{-}13]$$

$$\theta_i = \sin^{-1}\left[\frac{V_T}{u_i}\right] \qquad [3\text{-}14]$$

where L, ρ_i, u_i, τ_i, V_T, η_{col}, and m_{D3} are prescribed. For purposes of FLOW code calculations where a particular tube size (i.e., h and d) is desired, several different values of L will normally be investigated. Larger values of L produce larger radii r for a given tip speed and, hence, larger values of d and smaller values of h; the product of hd depends only on the mass flow m_{D3}, the wave diagram, and the collection efficiency. Similar variations can be obtained by varying V_T instead of L.

3.3 HEAT TRANSFER

The magnitude of heat transfer in the wave rotor has been estimated analytically to determine the magnitude of its effect on the work transfer efficiency and on the rotor design. These estimates are corroborated by FLOW code results that compare wave rotor cases with and without heat transfer. The analytic estimates assume that the effort is small on the wave diagram and use a perturbation approach. The FLOW code includes a self-consistent determination of the wave pattern with or without heat transfer, as the case may be.

The analysis proceeds by assuming that heat transfer in each tube follows the behavior for fully developed pipe flow with an entrance flow correction appropriate for large Reynolds numbers. No heat transfer is assumed to occur where the average flow velocity is nominally zero. Thus, the heat transfer equation is

$$\frac{dT}{dx} = \frac{0.16}{d_h \sqrt[4]{Re}} \left[1 + \left[\frac{d_h}{L}\right]^{2/3}\right] \left[T_w - T\right] \qquad [3\text{-}15]$$

where

$$d_h = \frac{2hd}{h+d}$$

is the hydraulic diameter of the tube, $Re = \rho u d_h/\mu$ is the Reynolds number, and T_w is the tube wall temperature. The solution to this equation is

$$\frac{T_w - T}{T_w - T_i} = e^{-\frac{0.16}{d_h Re^{1/4}}\left[1 + \left[\frac{d_h}{\ell}\right]^{2/3}\right] x}$$

where T_i is the inlet flow temperature and $T = T(x)$ is the flow temperature a distance x from the tube entrance.

Several changes occur across a wave system which requires a change in the value of T_i. Across a shock wave, for example, the temperature ratio of the gas will be greater than 1 and will depend on the shock strength (i.e., its pressure ratio). Using Figure 3-2 as an example, we can write the heat transfer solutions for the driven gas in regions d1 and d3 as follows:

$$\left[\frac{T_w - T}{T_w - T_i}\right]_{d1} = e^{-\frac{\beta x}{d_h}} \text{ or } T(x) = T_w - \left[T_w - T_{ia}\right]e^{-\frac{\beta x}{d_h}} \text{ for } 0 < x \leq x_o \quad [3\text{-}17]$$

and

$$\left[\frac{T_w - T}{T_w - T_i}\right]_{d3} = e^{-\frac{\beta y}{d_h}} \text{ or } T(y) = T_w - \left[T_w - T_{ib}\right]e^{-\frac{\beta y}{d_h}} \text{ for } 0 < y \leq y_o \quad [3\text{-}18]$$

where $y_o = L - x_o$. Using T_{d3}/T_{d1} as the ideal temperature ratio across both shock waves, we can define the entrance temperature T_{ib} for any slug of driven gas reaching the first shock wave at position x_o in the tube as

$$T_{ib} = \left[T_{d3}/T_{d1}\right] T(x)|_{x=x_o} = \frac{T_{d3}}{T_{d1}}\left[T_w - \left[T_w - T_{ia}\right]e^{-\frac{\beta x_o}{d_h}}\right]$$

Thus, the temperature of this gas slug at the driven gas exit manifold is

$$T_o[x_o] \equiv T(y)|_{y=y_o} = T_w - \left[T_w - \frac{T_{d3}}{T_{d1}}\left[T_w - [T_w - T_{ia}]e^{-\frac{\beta x_o}{d_h}}\right]\right]e^{-\frac{\beta y_o}{d_h}} \quad [3\text{-}20]$$

The average value of the exit driven gas temperature is therefore

$$\langle T\rangle_{d3} = \frac{\int_o^L T_o[x_o]dx_o}{L} = T_w - \left[\frac{T_{d3}}{T_{d1}}\right][T_w - T_{ia}]e^{-\frac{\beta L}{d_h}} + \quad [3\text{-}21]$$

$$- T_w\left[1 - \left[\frac{T_{d3}}{T_{d1}}\right]\right]\frac{\left[1 - e^{-\frac{\beta L}{d_h}}\right]}{\left[\frac{\beta L}{d_h}\right]}$$

A similar expression exists for the driver gas except that expansion waves are present instead of shocks. These are also modeled as discrete waves for purposes of analyzing the heat transfer. Again, the ideal temperature ratio across the wave is used to relate the exit temperature of a gas slug approaching the wave to the "entrance" temperature of the same slug of gas leaving the wave. The averaging process can again be carried out, noting that the entering driver gas at D3 actually leaves at two main exit ports, D5 and D1 (ignoring the tuning ports in this approximation), which makes the integrals somewhat more complex but still tractable.

At this point, the averaged exit port temperature with heat transfer can be compared to the wave diagram temperature computed without heat transfer to estimate the magnitude of the effect. By also calculating the amount of heat transferred to each stream, one may also determine whether or not the chosen wall temperature T_w also corresponds to an equilibrium wall temperature for that particular set of flow conditions; that is, at equilibrium, the heat transferred to the rotor from the hot gas must equal the heat transferred from the rotor to the cold gas.

While the heat transfer path is generally not known in detail, for the linearized (small perturbation) approximation used here, we can assume that the heat addition or extraction line in the T-s space is straight between the initial and final states, as shown in Figure 3-4. Thus, for example, the heat transferred out of the driver gas after a given expansion, say from state D3 to state D5, is given by

$$\delta Q_{35} \cong \left[S_{5s} - S_5\right]\left[T_5 + \frac{1}{2}\left[T_3 - T_5\right]\right] = \left[S_{5s} - S_5\right]\left[\frac{T_3+T_5}{2}\right] \quad \text{or [3-22]}$$

$$\delta Q_{35} = \dot{m}_{D5} C_p \left[\ell n\left[\frac{T_{5S}}{T_5}\right]\right]\left[\frac{T_3+T_5}{2}\right]$$

These estimates have been made for a variety of rotor configurations and flow conditions. An interesting effect emerges from the results which have been tabulated in Table 3-1. Comparing cases 2, 3, and 4, we see that the relative size of a tube (i.e., d, h, and L) has no noticeable effect on the equilibrium wall temperature of the wave rotor, even though the quantities of heat transferred may vary a lot with tube size. Also, it is clear that the equilibrium wall temperature in several interesting cases (e.g., 1 through 6), which correspond to cruise missile combustion temperatures of 3500°F, is rather high for the basic wave diagram shown in Figure 3-2. The rotor wall temperature ranges from 1970°F to 2060°F for these cases.

It is possible to run the fully compressed air stream through the wave rotor again for extra cooling of the rotor before passing that gas on to the combustor. Some pressure losses inevitably occur with an extra scavenge of this sort, but the rotor will act as a recuperator, reducing the amount of fuel needed to reach the peak combustion temperature and thereby enhancing the efficiency of the device. A somewhat larger rotor diameter will be needed to encompass the extra cooling part of the cycle but, if it is still within the engine envelope, then this approach has a large payoff in terms of reducing the metal temperatures still further.

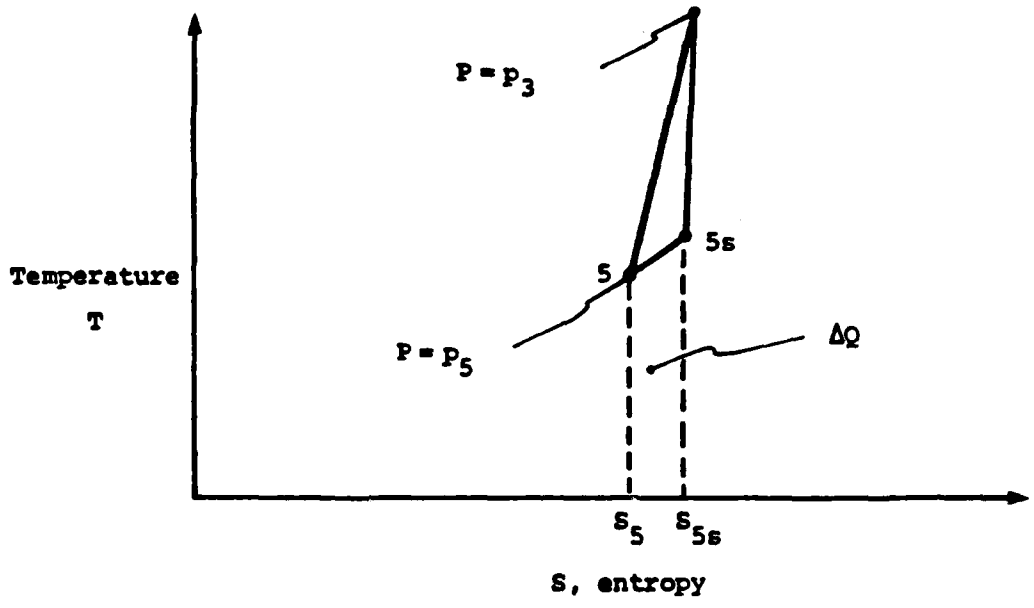

Figure 3-4. Heat Transfer from an Expanding Gas to the Wave Roto Walls

Table 3-1

EQUILIBRIUM WALL TEMPERATURES
AS A FUNCTION OF ROTOR DESIGN VARIABLES

Case	$(T_w)_{equilib}$	d (cm)	h (cm)	L (cm)	r (cm)	V_T (cm/s)	$\Delta Q_{13,driven}$ (erg/sec)
1	1400°K	.92	1.11	9.6	3.8	15,240	$4x10^{11}$
2	1350°K	.41	1.24	9.6	3.8	15,240	$6.0x10^{11}$
3	1350°K	.66	.77	9.6	7.6	12,192	$6.6x10^{11}$
4	1350°K	.92	.55	12.	7.6	12,192	$6.6x10^{11}$
5	1400°K	.92	1.11	8.0	3.8	18,288	$3.5x10^{11}$
6	1350°K	.71	.57	7.6	3.0	15,240	$2x10^{11}$
7	1250°K	.90	2.63	18.0	7.5	15,240	$3x10^{12}$
8	1100°K	.92	1.11	9.6	4.0	15,240	$2x10^{11}$
9	1400°K	.39	.81	9.6	3.7	15,240	$6.3x10^{11}$
10	1350°K	.53	1.19	9.6	4.2	15,240	$5.3x10^{11}$
11	1375°K	.34	1.30	9.6	3.6	15,240	$7.1x10^{11}$

NOTES

Each of these cases is for a 100 lb_f thrust engine flying at M=0.65, sea level conditions with a pressure ratio of 2.54, a peak pressure of 30.5 atm, an inlet air temperature of 757°K, and, with one exception (Case 6 @ 1 lb/sec), the inlet air flow is 2.5 lb/sec. CASE 1 is used as a guide, with 24 tubes, 1 wave cycle per revolution, and a combustion gas inlet temperature of 2200°K (3500°F). CASE 2 has 47 tubes. CASE 3 has 47 tubes and a lower tip speed. CASE 4 has 47 tubes, 2 wave cycles per revolution, and lower tip speed. CASE 5 has higher tip speed. CASE 6 has lower mass flow (1 lb/sec). CASE 7 has a lower combustion gas inlet temperature of 1922°K (3000°F), 46 tubes, and 14 lb/sec. CASE 8 has a lower combustion gas inlet temperature of 1644°K (2500°F). CASE 9 has higher peak pressure (51 atm), air inlet temperature (811°K). CASE 10 has lower pressure ratio (2.24), P_{max}=26.8 atm, inlet air flow = 2.4 lb/sec. CASE 11 has higher pressure ratio (2.82), P_{max}=33.8 atm, inlet air flow = 2.6 lb/sec.

The work transfer efficiency is affected by heat transfer, in this approximation, by increasing the available work in the driven exit gas stream. If no other effects were present, this would represent a net increase in the work transfer efficiency. However, in actuality and in the FLOW code results, the ability of the hot gas to do work on the cold gas is reduced by heat transfer, and the work required to compress the cold gas after it heats up somewhat is also increased. As long as the overall pressure ratio of this process is fixed, the slack must be taken up by requiring changes in the mass flows of the driver and driven gases. That is, a smaller flow of driven gas per unit flow of driver gas can be compressed when heat transfer via the rotor wall occurs. This is a greater effect than the increase in the available work of the driven gas, so that the net effect is to decrease the work transfer efficiency.

3.4 LEAKAGE

Several different types of leakage can occur in a wave rotor, with differing effects on its performance. There are inner and outer radial gaps at each face of the rotor, between the rotor and the manifolds, where most of the leakage may occur. If the manifold is connected to a shroud enclosing the rotor, then the radial leakage can be reduced by pressurizing the shroud to some intermediate level which is less than the peak manifold pressure but greater than the minimum manifold pressure. An equilibrium, intermediate level of pressure may be attained quite naturally, which depends on the balance of leakage from the high pressure manifolds to the plenum and from the plenum to the lower pressure manifolds; or it can be sustained at a nonequilibrium pressure from an outside source, such as bleed air from a compressor. Other sources of leakage include azimuthal flows from high pressure manifolds to adjacent low pressure manifolds.

Leakage has been identified as a problem area affecting performance in several key experiments in the past (see Appendix A) and has been measured indirectly in several cases. Using the MSNW energy exchanger

data for leakage and work transfer efficiency (see Figure 3-5), one can derive an approximate equation relating these two variables:

$$\eta = \eta_o - C_1 \left[\dot{m}_{leak}/\dot{m}_{total}\right] = 0.835 - 1.375 \left[\dot{m}_L/\dot{m}_T\right] \qquad [3\text{-}24]$$

where we have assumed that the loss in efficiency depends linearly on leakage. An additional adjustment has to be made to incorporate the fact that the MSNW experiment utilized only 40 percent of the periphery of the wave rotor; the remaining 60 percent was inactive but still contributed to the leakage. The corrected equation can be written as

$$\eta = \eta_o - 0.40\, C_1 \left[\dot{m}_{leak}/\dot{m}_T\right] = 0.835 - 0.55 \left[\dot{m}_L/\dot{m}_T\right] \quad . \qquad [3\text{-}25]$$

In order to apply this equation to situations where air is the working fluid and where the peak pressures and temperatures are different, the loss term dependence on these parameters must be modeled. To this end we assume that the leakage flow (radial) is choked since the gap height to length is very small and the gap length exceeds the critical value

$$L_{crit} = \frac{D_h}{f}\left[\frac{1-M_g^2}{\gamma M_g^2} + \frac{\gamma+1}{2\gamma}\ln\left[\frac{(\gamma+1)M_g^2}{2+(\gamma-1)M_g^2}\right]\right] \qquad [3\text{-}26]$$

M_g is obtained from the relation

$$\frac{P_o}{P_o^*} = \frac{1}{M_g}\left[\frac{2+(\gamma-1)M_g^2}{\gamma+1}\right]^{1/2}$$

where P_o/P_o^* is the pressure ratio across the gap. Under these circumstances, the leakage flow rate depends directly on the acoustic speed $(\gamma RT)^{1/2}$. Thus, the change in gas species and temperature are contained in the values of γ, R, and T.

For example, consider the peak temperature to be 3000°F (1922°K) and the gas is air. Using the same gap as in the MSNW experiment for the low

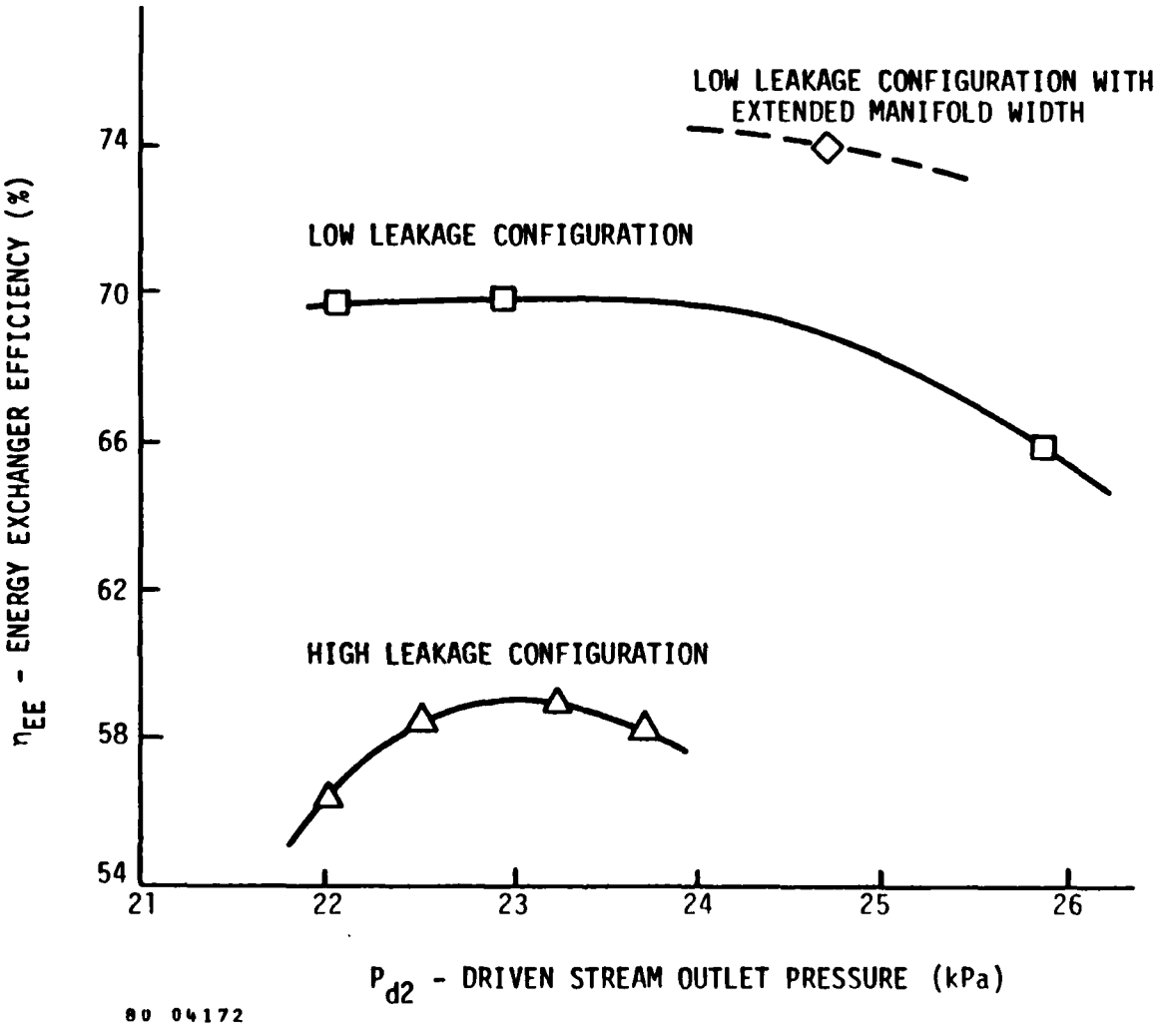

Figure 3-5. Experimental Data for Work Transfer Efficiency Variation with Outlet Port Pressure. Dashed line indicates experimental verification of FLOW code optimization (see Figure 4-3).

clearance case (i.e., 5 mils = 0.013 cm) and a rotor diameter of 15 cm, we can expect the leakage to be five times that experienced on the MSNW device or 20 percent of the inlet air flow to the rotor with a work transfer efficiency of

$$\eta = 0.835 - 0.55(.20) = 0.725$$

according to Equation [3-25].

Detailed FLOW code calculations are presented in Section 4 to support these initial estimates. The use of higher shroud pressures can be used to reduce the leakage considerably. Experiments at these elevated temperatures and pressures are clearly required to verify both these estimates as well as the more complete performance projections made with the FLOW code.

3.5 RE-ENTRANT DUCTS

Wave rotors may use outflow from one port as the inflow to another port. Two practical applications of this situation can arise: the flow of compressed air through an external combustor before re-entry on the wave rotor as the high temperature driver gas, and re-entry of a partially expanded outflow from one port to another so that the final stages of expansion may occur. Every case of interest in this study involves a re-entrant duct corresponding to the combustor flow example. In addition, wave rotors producing shaft work output may also require a second set of re-entrant ducts to complete the gas expansion and derive the final amounts of shaft work from the device.

To counter duct pressure losses, re-entrant duct flows require that the flow start out with a higher stagnation pressure than it has on exiting the duct. These losses are associated with wall friction and bends in the duct which can cause areas of flow separation. Similarly, abrupt changes in the duct cross section as well as bifurcation of the flow and rejoining the flow may lead to pressure-recovery losses. The

combustor also adds heat to the flow, and other parts of the duct may extract heat from the flow because of lower wall temperatures. We shall assume a fixed relative pressure loss of 6 percent for the combustor re-entrant duct case based on accepted values in the literature (see Reference Kerrebrock, p. 103 for example).

It is easy to show that the combustor flow case requires at least some level of pressure recovery in the compressed air exit manifold of the wave rotor. That is, the static pressure of the combustion gas entering the wave rotor is equal to the static pressure of the exiting compressed air by virtue of their intimate contact within the wave rotor. Thus, without pressure recovery, the compressed air stagnation pressure would equal its static pressure and would therefore be less than the stagnation pressure of the combustion gases; no flow through the combustor would result. The stagnation pressure of the compressed air exiting the wave rotor can ideally be larger than the combustor exit gas stagnation pressure according to the relation

$$\frac{P_{ao}}{P_{co}} = \left[\frac{2 + (\gamma-1)M_a^2}{2 + (\gamma-1)M_c}\right]^{\frac{\gamma}{\gamma-1}} > 1$$

where the important effect is due to the difference in temperatures of the two gases, each having the same velocity on the rotor (i.e., $M_{combustor} < M_{air}$). For conditions of interest, the ratio of stagnation pressures may be as large as 1.17. With a 75 percent recovery of the dynamic head in the exit flow manifold, this would yield a stagnation pressure ratio of 1.11. If the combustor pressure losses are limited to less than 6 percent (i.e., a stagnation pressure ratio of 94% in the combustor or better), then net flow through the combustor will occur.

An imbalance between the tangential flow speeds for gases entering the wave rotor and the tip speed of the rotor may also occur, which can lead to either higher or lower stagnation pressures of the compressed air

exiting the rotor. These may be used intentionally to increase the compressed air flow stagnation pressure to an acceptable level. The work for raising the stagnation pressure of that stream can be taken from combustion gas flow leaving the rotor by vectoring that flow to give some reactive force to the rotor or by supplying a small amount of shaft power input to the rotor (e.g., from an external drive motor).

From this discussion one can see that pressure recovery is critical to proper operation of the combustor re-entrant loop. Detailed measurements are strongly needed in order to confirm the estimates made above for a given level of combustor pressure loss.

The FLOW code calculations proceed on the basis that a particular wave pattern results in flow speed for the compressed air outlet which can be converted at 75 percent to stagnation pressure. That stagnation pressure is then reduced by the combustor losses to give the boundary condition for the combustor inlet gas pressure to the wave rotor. A surplus of flow generally exists at the compressed air outlet so that there is no difficulty in balancing the mass in and out of the rotor at each end of this duct.

The conditions applying to the second class of re-entrant ducts, namely those providing the second stage of expansion to a wave rotor/turbine, are not so simple to satisfy since there is no excess of mass flow and substantial stagnation pressure losses may occur when the rotor develops shaft work from the flow exiting the rotor and entering the duct. In fact, an additional expansion is generally required on the rotor so that the gas fill pressure in the rotor tubes is sufficiently below the gas pressure of the re-entrant duct flow. Then it will be possible for the duct flow to scavenge the fill gas before performing work on the rotor. The treatment of this case by the FLOW code also proceeds in a similar manner to the preceding case. The initial wave diagram is designed with certain external duct losses in mind so that the fill gas is

at a lower pressure than the duct flow entering the rotor after accounting for these losses.

Additional modifications must be made to the FLOW code in order for transient effects on the time scale of a single wave rotor cycle to be properly represented when a re-entrant duct is present. The code now calculates only equilibrium re-entrant duct flows which are established over several cycles. This is adequate for the type of investigation where the most important phenomena to be determined or estimated is the quasi-steady operation of the device. The fast transient response of the wave rotor will become of interest when the question of stability must be answered, especially when the system is being driven externally by forces on a short time scale. There is already good evidence from the Pearson rotor and the Brown-Boveri Comprex operation that these devices can be designed to be stable over a wide range of operating conditions when the external constraints are quasi-stationary on the time scale of a revolution. Therefore, the need to upgrade the FLOW code for fast transients becomes necessary only when details of compressor surge and fast changing throttle conditions and their interaction with a wave rotor need to be understood.

3.6 REFERENCE PRELIMINARY DESIGN

As an example, consider the case of a 1000 lb_f thrust, 12 inch intake diameter, bypass ratio of 2.2 flying at sea level at Mach 0.65. Total intake air will be 5 lbs/sec, and the core engine will ingest 2.5 lb/sec air. For the wave diagram shown in Figure 3-2 and for a wave rotor compression ratio of 2.5, following a compressor pressure ratio of 11 and a diffuser compression of 1.33, the peak pressure in the engine is 37 atm. If we consider a peak (combustor) temperature of 3000°F (1922°K), then the sound speed of a_{D3} will be 2870 ft/sec (87580 cm/sec). Assigning the values of L = 9.6 cm, v_T = 500 ft/sec (15240 cm/sec), η_{col} = 0.80, and m_{D3}, the wave diagram yields the port flow values of u_i, ρ_i, T_i,

etc. summarized in Table 3-2. The rotor design values for this case are

L = 18 cm	v_T = 15,240 cm/sec
r = 7.5 cm	Ω = 19,538 rpm
h = 2.5 cm	N = 46 tubes
d = .90 cm	

A 600 lb_f thrust engine with the same engine inlet diameter (e.g., 12 inches) will have a similar wave diagram. The main design differences will be a smaller core engine mass throughput (e.g., 5.8 lb/sec) and, therefore, a smaller wave rotor or at least smaller tubes. The port locations and intrinsic gas flow properties will be the same as in Table 3-2; absolute mass flows for each port will be reduced in the same proportion as the core engine mass flow. In this case,the only wave rotor parameter which needs to change is the tube height (e.g., from 2.6 to 1.1 cm).

3.7 RELATED PRELIMINARY DESIGNS

Several wave rotor preliminary designs related to the reference case described above have been developed to illustrate possible changes in the basic design parameters which cover the range of parameters considered in the FLOW code analysis of wave rotor performance. Table 3-1 includes the other illustrative design examples developed using the design equations presented in Section 3.2 above, such as cases 1 through 6, which correspond to higher combustion temperatures (i.e., T(peak)= 3500 F); lower combustion temperatures (case 8); higher peak pressures (i.e., case 9 at P(peak)= 50 atm); larger number of tubes (i.e., cases 2-4 at N=47 tubes); higher tip speed (i.e., case 3 at V_t=22,860 cm/s); lower and higher wave rotor pressure ratios (2.2 and 2.8, respectively, for cases 10 and 11); and shorter rotor lengths. These cases are simply points in a continuum of design possibilities. The most impressive feature is their overall similarity. There are very slight dimensional changes amongst these cases. The greatest differences are in the equilibrium wall

Table 3-2

Example of Ideal Wave Diagram Flow Parameters
for Pressure Exchanger Wave Rotor
(See Figure 3-1 for Nomenclature)

Port Designation	Velocity, U_i (cm/sec)	T^* (°K)	P^* (MPa)	Port Locations (°)	Density, ρ_i (mg/cm^3)	Port Size$^+$ τ_i (msec)	Mass Flow $\dot{m}_i$ (g/sec)	Port Flow Angles, θi (°)
Driven Gas Inlet, d1	18,589	752	1.51	0 to 157	7.07	1.34	6355	40
Driver Gas Inlet, D3	19,825	1922	3.77	157 to 244	6.80	0.74	3590	38
Driven Tuning Inlet, D5i	3,973	1728	2.57	295 to 298	5.14	0.03	21	76
Driver Tuning Inlet, D1i	9,295	742	1.81	350 to 360	5.90	0.08	118	59
Driven Gas Outlet, d3	19,825	960	3.77	187 to 264	13.6	0.66	6355	38
Driver Tuning Outlet, D4o	9,913	1841	3.26	264 to 269	6.09	0.05	97	57
Driver Gas Outlet, D5	7,946	1696	2.40	269 to 321	4.90	0.44	619	63
Driver Tuning Outlet, D5o	3,973	1665	2.25	321 to 321	4.67	0.02	15	76
Driver Gas Outlet, D1	18,589	1494	1.51	321 to 114	3.51	1.28	2997	40

* Static Values

$^+$ Total Cycle Time = 3.07 msec

NB: These values correspond to Case #7 in Table 3-1.

temperatures amongst those cases (e.g., cases 1-6 and 8) where the inlet combustion temperatures are different compared to the reference case 7.

In summary, the designer can change the tip speed, rotor length and radius, and tube height and width to accommodate a variety of flow and combustion conditions. The rotor wall temperature is within present day materials capabilities, except possibly at the highest combustor temperatures considered (i.e., $T_{comb} \approx 3500°F$). At the upper limit of T_{comb}, an extra cooling flow of the compressed air can be used to keep the rotor wall temperature within bounds. The cooling flow also allows the rotor to act as a recuperator to help increase the cycle efficiency.

Section 4
WAVE ROTOR ANALYSIS

4.1 INTRODUCTION

The performance of several wave rotor designs has been evaluated in terms of the wave rotor component efficiency for on-design and off-design operation. The designs include pressure exchanger wave rotors and wave rotor/turbines. Gas stream properties are computed for each of the inlet and outlet ports; details of the unsteady on-rotor flows are used to illustrate the underlying phenomena which produce the port flows. A range of key design variables has been used to determine the sensitivity of wave rotor performance to these variables. Work transfer efficiencies in the range of 70 to 75 percent appear feasible for wave rotors designed for the 600 lb_f to 1000 lb_f thrust engine class. Off-design performance for single variable design parameter variations is very dependent on the particular parameter being varied. However, off-design performance corresponding to actual off-design engine operation appears to be very good since some control can be exerted over rotor tip speed to accommodate the wave rotor operation to the off-design changes occurring in engine-supplied flow parameters (e.g., mass flow, pressure, and temperature). Wave rotor wall temperatures also appear to be quite acceptable (i.e., in the range of 1700 to 1950°F) for combustion temperatures in the range of 2500 to 3500°F.

The chief tool for analyzing the wave rotor component is a one-dimensional, unsteady gasdynamic computer code, called the FLOW code, which was developed previously by Mathematical Sciences Northwest, Inc. (MSNW) specifically for wave rotor analysis. The FLOW code has been upgraded as part of this research to model flow losses more accurately and to compute shaft work output. The results of FLOW code calculations are presented in this section for wave rotors which are pure pressure exchange wave rotors. Analytic estimates are provided for wave rotor/turbines

which produce shaft power. The requirements for steady flow in the inlet and outlet to the wave rotor are formulated and used to define realistic classes of wave rotor designs. Specific examples are chosen from this family of acceptable wave rotor designs for detailed evaluation. These examples include several historical designs including wave rotor/turbines such as the Pearson rotor and the GPC wave rotor, pressure exchange wave rotors such as the Rolls-Royce wave rotor, and also a modern pressure exchange wave rotor designed by MSNW for high component efficiency.

The examples chosen for analysis illustrate why some of the earlier efforts were unsuccessful (and still have problems) in obtaining good performance and why other designs were successful. The modern pressure exchange wave rotor example is explored in depth to determine the sensitivity of a high efficiency design to variations in design and operating parameters. These variations correspond to either design or operating tolerances and to off-design engine operation (see Section 3.4 for a definition of these wave rotor flow conditions).

The flow code used for these calculations has been validated by detailed experimental data from MSNW's wave rotor experiments. The code is described in more detail below, but it should be pointed out here that the extension of this code to higher temperature and higher pressure conditions still requires additional validation in order to certify its predictive capabilities for the cases examined in this report. The FLOW code needs to be compared to the results of well-instrumented, carefully controlled hot wave rotor tests. This is a high priority need in order to proceed with confidence to an engine development program.

Results from the code calculations include gas flow conditions for all of the inlet and outlet ports on the rotor, a discussion of the main wave phenomena responsible for these flows, the wave rotor work transfer and shaft work efficiencies, depending on the type of rotor, and presentation of preliminary sizing and operating data for rotors which could be integrated with the turbofan engines discussed in Section 2. The

sensitivity of wave rotor performance to tip speed, port placement and size, gas inlet and outlet conditions, tube size, number of tubes, leakage, and heat transfer has been analyzed for on-design conditions. Wave rotor response to off-design engine conditions for lower and higher flight speeds also has been investigated. The effects of heat transfer, viscosity, impedance mismatching, and gas leakage are included in all of the computations. These results also have been corroborated with analytic estimates to provide a more intuitive interpretation of the results.

4.2 THE FLOW CODE

The FLOW code uses the flux-corrected transport algorithm developed by Boris and Book to integrate the following one-dimensional Euler equations of unsteady, compressible gas flow:

$$\frac{\delta \rho}{\delta t} = \frac{\delta}{\delta x}(\rho u) \qquad [4\text{-}1]$$

$$\frac{\delta \rho u}{\delta t} = -\frac{\delta}{\delta x}(\rho u^2) + \frac{\delta p}{\delta x} - 0.5\,\pi\, C_D \mathrm{sgn}(u)\rho u^2 \qquad [4\text{-}2]$$

$$\frac{\delta E}{\delta t} = -\frac{\delta}{\delta x}(uE) - \frac{\delta}{\delta x}(uP) + \pi\, C_H \left[\frac{\gamma R}{\gamma - 1}\right] \rho |u| \left[T'_w - T\right] \qquad [4\text{-}3]$$

$$\text{where } E = \frac{p}{\gamma - 1} + \frac{1}{2}\rho u^2$$

As Equations [4-2] and [4-3] show, the heat transfer and viscous drag terms are based on a developed pipe flow analysis where a friction factor f of approximately 2×10^{-5} has been used. These calculated unstady tube flows are driven by the flow conditions prescribed at the inlet and outlet manifolds. These port conditions are supplied as boundary values to the FLOW code for each successive time step. The flow pattern in a single tube is computed as a function of time for several successive complete revolutions of the rotor until the solution repeats each previous cycle to within a desired level of accuracy. This periodic flow constraint is typically achieved within three complete cycles at which point the flow

conditions in each manifold are accumulated to give the total mass and enthalpy flows for each manifold and to determine averaged flow properties such as the pressure, temperature, density, and velocity. In cases where shaft power is being produced, the rotor tube angles, flow velocity direction, and manifold flow angles are used to compute the tangential momentum of the gas flowing onto and off of the rotor in each port: the sum of these terms multiplied by the rotor tip speed gives the net shaft work output from the rotor. The work transfer efficiency, which measures the efficiency of pressure exchange operation, is also computed from the ratio of manifold flow conditions. These efficiencies are defined in Section 4.4.

The original FLOW code was developed under DOE contract and was subsequently modified for the calculations presented here in order to upgrade the treatment of manifold boundary conditions and losses and also to incorporate the calculation of shaft work terms. Figure 4-1 compares the output of the original flow code to the trace of a pressure transducer mounted near the end of one of the tubes on the MSNW wave rotor. The correspondence between the code and the experimental data is remarkably good for a wide variety of experimental conditions. The code also predicted the measured work transfer efficiency reasonably well, as shown in Figure 4-2. Subsequently, the code was used for a preliminary optimization of the MSNW rotor design according to the variation in port width shown in Figure 4-3. As a result of these code calculations, some single port width modifications were made in the test rotor which led to an improvement very close to that predicted by the codes. That is, the peak of 74 percent achieved by the experiment shown in Figure 4-4 was a direct result of the code prediction of 75 percent shown at $A_{d2}/A_{D1} = 1.05$ in Figure 4-3. The ease and speed of predicting design modifications of this sort with the FLOW code has established it as a superior tool for wave rotor analysis and design.

The upgraded FLOW code is capable of treating the finite tube width opening and closing transients which create their own class of wave

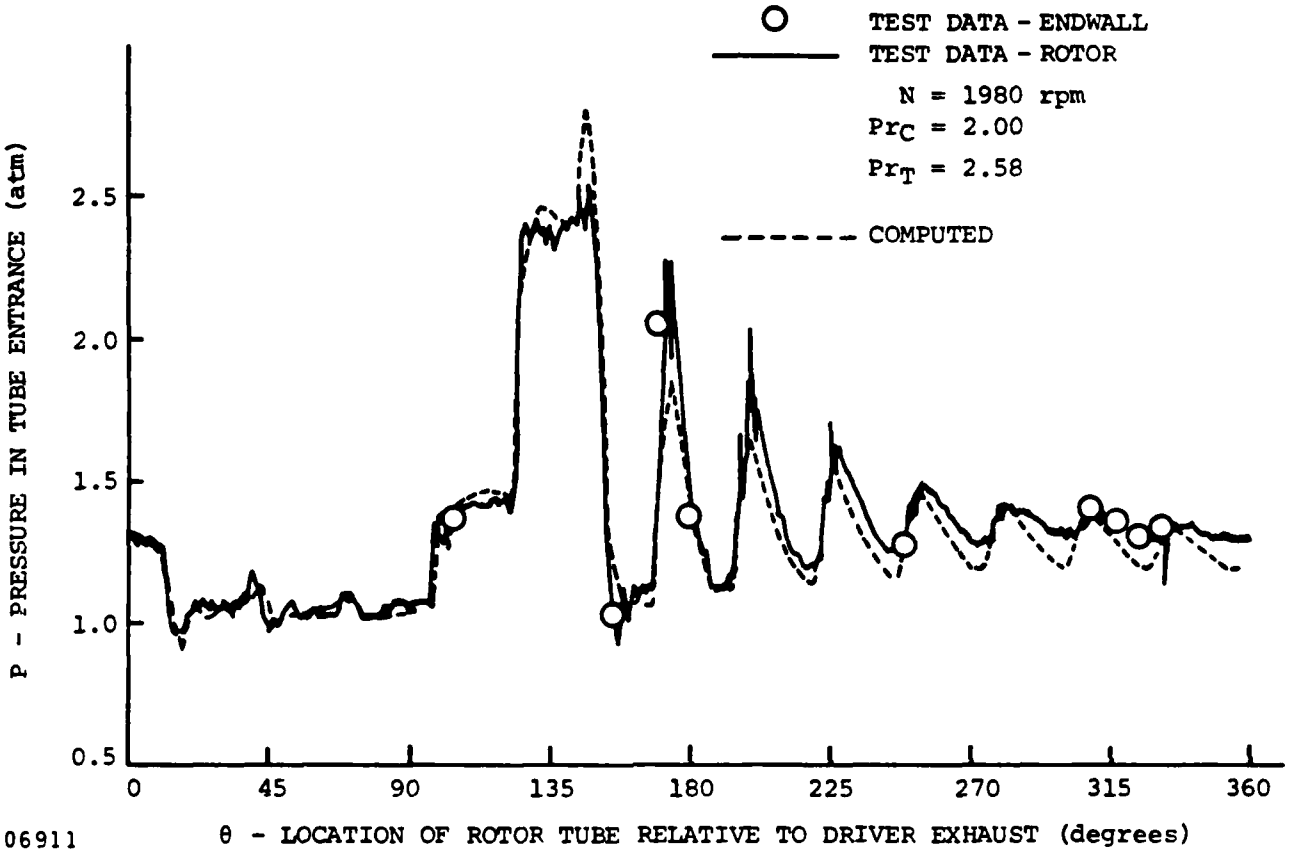

Figure 4-1. Measured and Computed Pressure History for One Wave Rotor Cycle with Wave Management for $\theta > 145°$

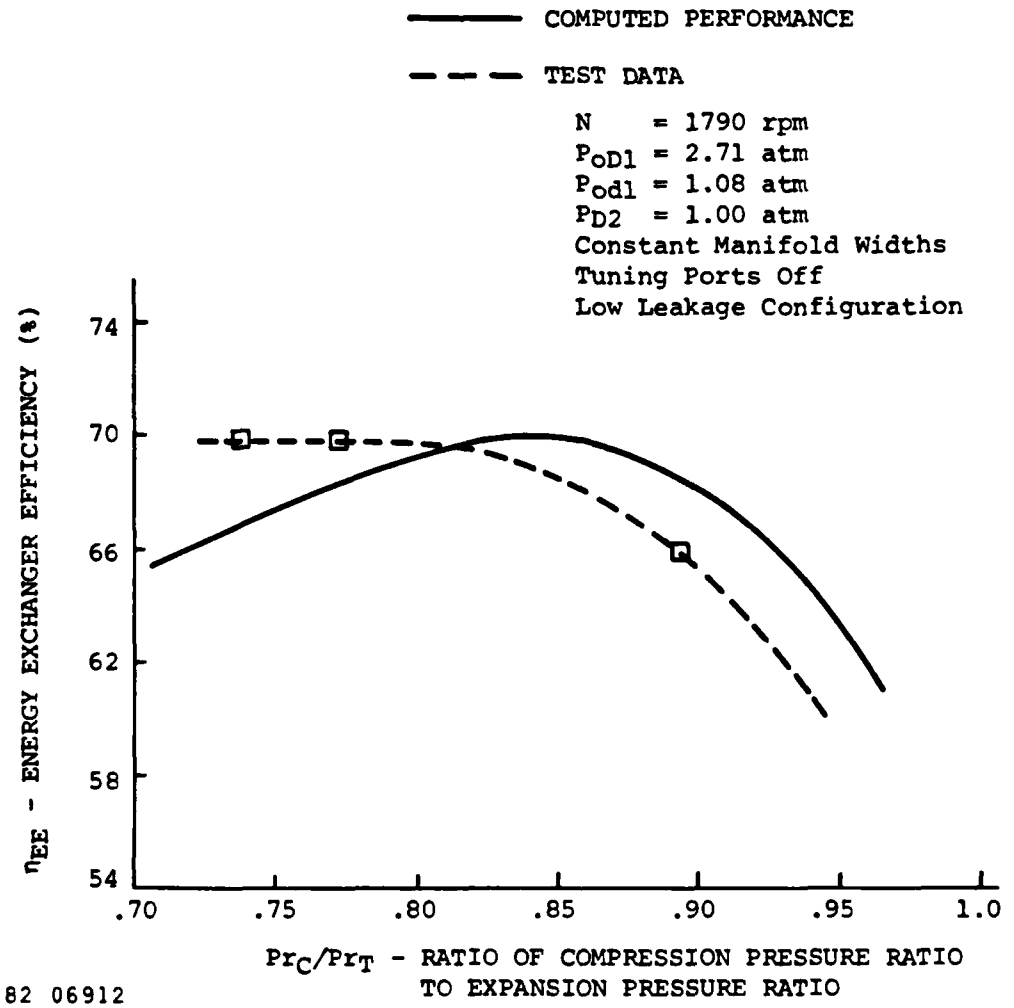

Figure 4-2. Computed and Measured Wave Rotor Efficiency

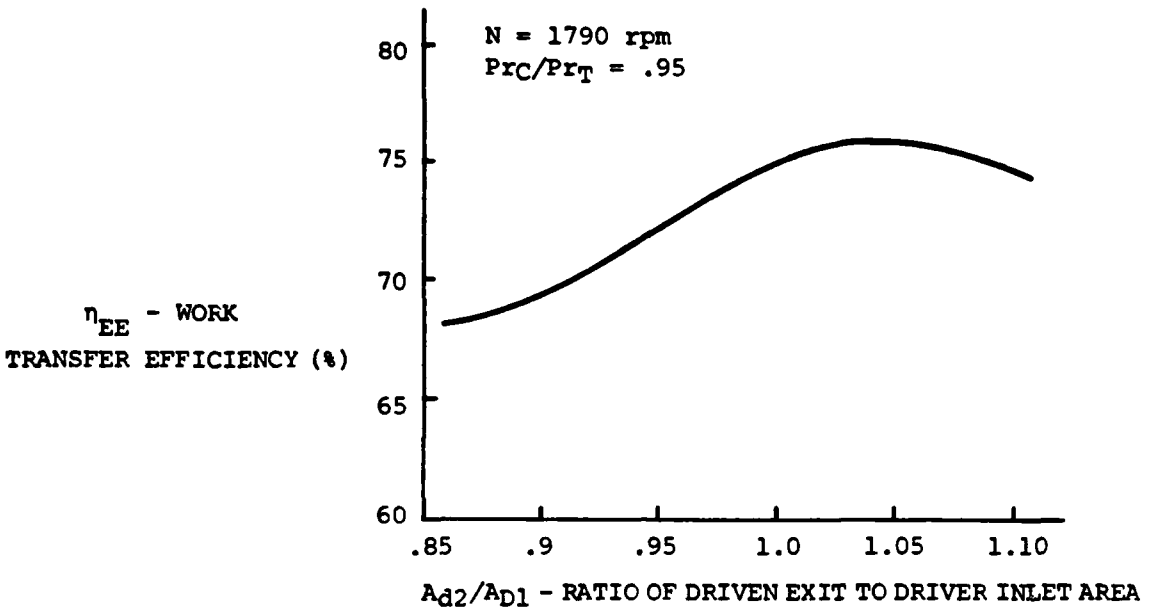

Figure 4-3. FLOW Code Optimization of Work Transfer Efficiency as a function of port widths.

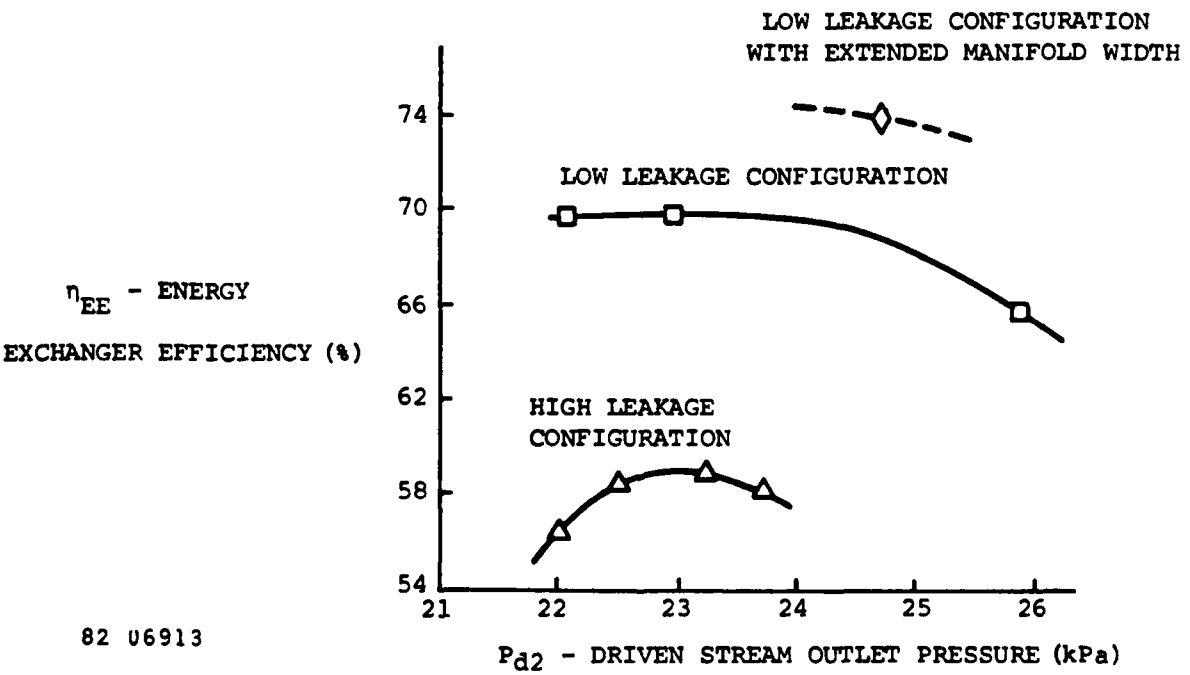

Figure 4-4. Experimental Data for Work Transfer Efficiency Variation with Outlet Port Pressure. Dashed line indicates experimental verification of FLOW code optimization.

disturbances in the wave rotor. These transients may involve sonic flow conditions when the end of the tube is partially open. The losses associated with partially open tubes are also incorporated as pressure recovery losses in order to prescribe the tube boundary conditions properly. We follow an earlier treatment by Spaulding for these losses. Equations for the partially open tube analysis are presented in Appendix D. The finite wall thickness of each tube also contributes to an area change in the stream tube dimension; we assume that the area change is gradual enough due to streamlining the ends of each tube wall so that the flow transition is isentropic. It does result in flow acceleration (deceleration) at the tube ends for inflow (outflow) and a corresponding change in the pressure boundary values computed in the flow code. Incorporation of these changes is estimated to contribute to as much as a 14% change in the computed work transfer efficiency of the wave rotors considered for the turbofan engine.

The upgraded *FLOW* code also incorporates a finite stagger angle for the tubes which allows it to represent helical wave rotor tube arrays. An additional modification permits the user to assign two stagger angles for each tube - one on the left and one on the right - with a sharp turn in the tube angle located near the right hand end of the tube. This option was developed specifically to allow reaction forces to be modeled for wave rotor/turbines (e.g., the GPC and Pearson rotors). The modeling associated with this option is discussed in Section 4.5. To complete the upgrade, we included manifold flow angles so that impulsive loading of the rotor can also be calculated; that is, the flow angle of gas incident on the rotor may result in tangential gas velocities which are different than the rotor tip speed resulting in work transfer to or from the rotor. The combination of impulsive and reactive (i.e., mismatched tangential inflow and outflow) effects gives a complete characterization of the shaft power being produced by such a rotor.

Inputs to the *FLOW* code are summarized in Table 4-1. The user must prescribe whether or not the heat transfer and viscous drag are to be

Table 4-1

INPUT DATA FILE FOR FLOW CODE

DESCRIPTION OF VARIABLES

GM	ratio of specific heats (gamma)
NFR	=0 no wall friction, =1 assume wall friction
CD	friction coefficient
NHT	=0 no heat transfer to wall, =1 assume heat transfer
CH	heat transfer coefficient
THDRAG	multiply CD and CH by DRAGM for θ > THDRAG
DRAGM	see THDRAG
ATUB	cross-sectional area of tube (cm^2)
NTUB	number of tubes
TOP	angular width of tube (degrees)
ANGL	tube angle on left boundary relative to rotor axis
ANGR	tube angle on right boundary relative to rotor axis
W1	atomic weight of species 1
W2	atomic weight of species 2
NSPECI	species in tube at t=0
DELTAT	timestep size (δt, seconds)
THT	rotational speed (degrees per second)
VT	tip speed (cm/sec)
MAXSTP	number of timesteps to take
IPRINT	printer output frequency
IPLT1	output frequency to be used for P vs t and V vs t plots
IPLT2	output frequency to be used for contour plots
NX	number of spatial cells
DELTAX	grid spacing (δx)
THETAI	initial value of θ (usually 0)
TW	wall temperature (°K)
PINIT	initial pressure (atm)
TINIT	initial temperature (°K)
VINIT	initial velocity (cm/sec)

AM	dead space leakage flow Mach number
INDX(4)	index of 1) driven inlet, 2) driver inlet, 3) driven outlet, and 4) driver outlet ports

PORT PARAMETERS

NLPORT	number of ports on the left hand side
NRPORT	number of ports on the right hand side
THST	starting angle location of port (degrees)
THEND	closing angle location of port (degrees)
PRESS	pressure (atm) of port (stagnation pressure for inflow, static pressure for outflow)
INOUT	=0 for input ports, =1 for outflow ports
TEMP	temperature (stagnation temperature °K) [only used for inflow ports]
NSPEC	species number (see W1 and W2) of gas at inflow ports
PORTA	port flow angle (degrees) relative to vector normal to rotor end plane

PARAMETERS NEEDED FOR LEAKAGE CALCULATIONS

XLIP	lip thickness - channel length for leakage gas (cm)
PSHROUD	shroud pressure (atm)
D1	inner diameter of rotor (cm)
D2	outer diameter of rotor (cm)

For each of driven inlet, driven outlet, and driver inlet ports give:

DELT	gap width (cm)
XMACH	Mach number of gas in port

calculated. That is, cases with and without heat transfer can be computed in order to determine the magnitude of that effect. Similarly, the tube wall temperature can be prescribed so that the amount of heat transferred to the rotor from the hot gases can be compared to the amount transferred from the rotor to the cold gases; equilibrium wall temperatures require these two quantities to be equal, which suggests a quick trial and error technique for arriving at the equilibrium wall temperature. Clearances and shroud pressures are also set by the user in order to control the amount of leakage associated with a given calculation. Tip speed, number and cross-sectional area of tubes, and angular tube width determine the basic rotor dimensions. The angular rotor speed then embodies the rotor radius once the tip speed is given. The stagger angle(s) of the tubes can be set equal to zero for the pure pressure exchange applications.

Outputs from the FLOW code include the density, pressure, flow velocity, temperature, enthalpy, and species at each grid point (typically 20 points) along the length of the tube at each instant in time. This data is integrated across each port for each cycle to determine the flow conditions in or out of the port. The grid point data is printed out for preselected angular positions throughout one cycle. At the end of a cycle, the port data is printed out; this data includes the mass flow, enthalpy flow, and averaged temperature and pressure of the port flow, the amount of heat transferred to or from the flow if it is an exhaust port, and the net angular momentum associated with the flow in the direction of the rotor tip speed.

The more detailed, point-by-point information for a complete cycle is displayed in a series of contour plots of the temperature, pressure, density, and velocity. The contact surfaces are also tracked and displayed in a similar plot showing the location of each of the ports and end walls; for example, see Figure 4-5. Finally, the pressure and velocity are plotted along the left and right hand boundaries of the wave rotor for one complete cycle to indicate the magnitude and, in the case of velocity, the direction of these variables. Such plots reveal the

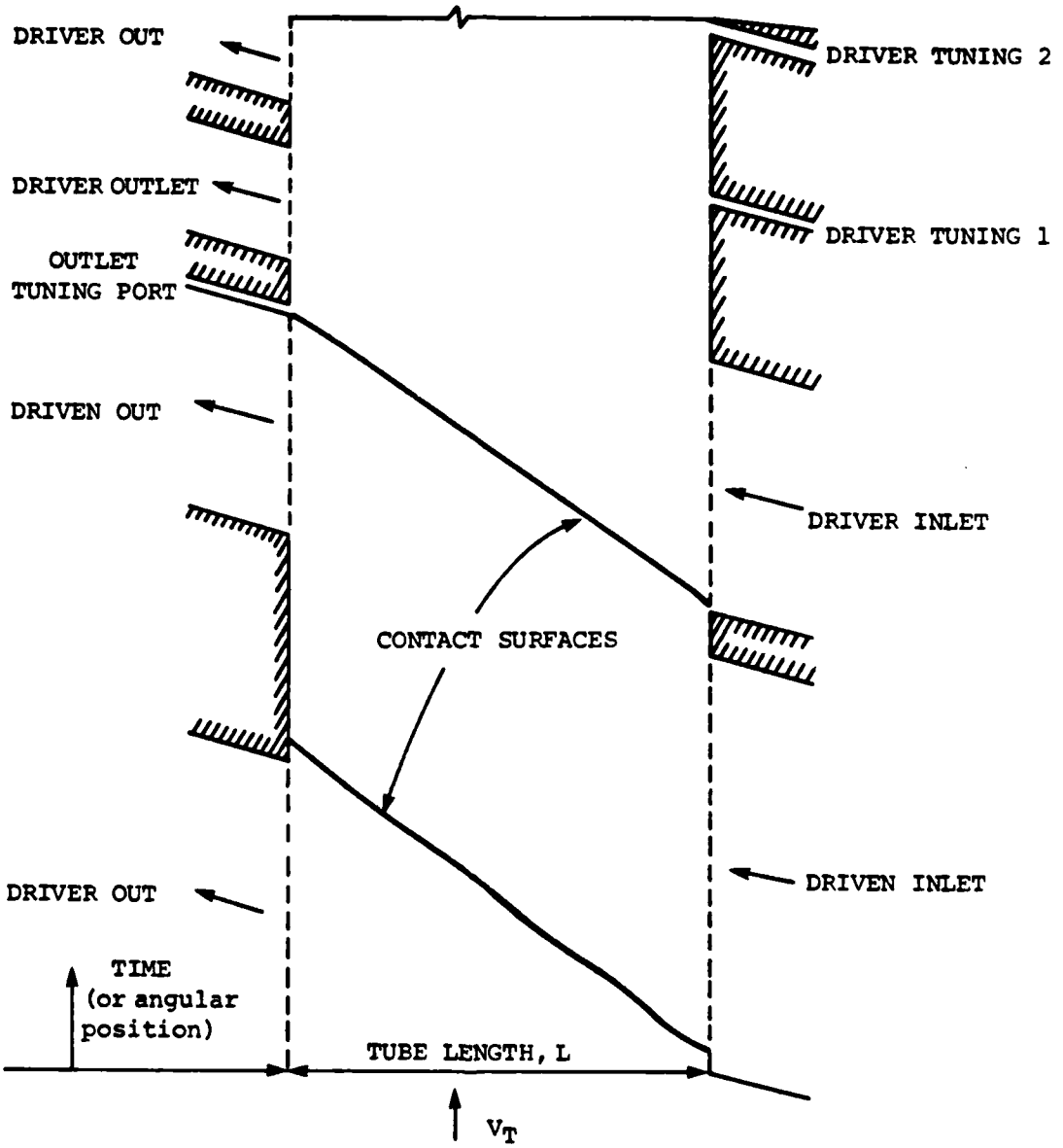

82 06914

Figure 4-5. Contact Surfaces and Port Locations for Pressure Exchanger Wave Rotor

location of reversed flows and pressure peaks in the manifolds. As many as fifteen contact surfaces can be tracked independently in the current version of the code, and the number of separate ports can be as great as twenty.

4.3 FLUX CORRECTED TRANSPORT ALGORITHM

One of the key virtues of the FLOW code is its accuracy and speed. The Flux Corrected Transport (FCT) algorithm used in this code has the advantage of high accuracy compared to other finite difference techniques used in the past for integrating the fluid equations of motion. The FCT technique was originally developed by Boris and Book at the Naval Research Laboratory. It has subsequently been improved upon; the version used here is called the SHASTA FCT. It has the property of suppressing the effects of numerical viscosity and numerical dispersion. Other finite difference schemes often require the use of an artificially large viscosity to suppress numerical instabilities near discontinuities such as shock waves and contact surfaces. These instabilities result from the numerical approximation to the exact differential equations; the second order error terms persist as viscous effects spreading the width of compression waves well beyond their actual widths. In other cases, third order error terms act as an amplifying force for small amplitude, high frequency waves in the vicinity of larger compression waves, producing wave trains up and downstream from the main disturbance which are pure numerical anomalies with no corresponding physical effects in the actual flows.

Figure 4-6 compares several numerical various approaches for the case of a square wave disturbance. Clearly, the FCT algorithm preserves the shape of this wave the best; therefore, it reproduces the actual solution with the least distortion. We have tested our version of the FCT algorithm against known analytic solutions of the fluid equations; for example, for shock waves with pressure ratios of 2.5, for rarefaction waves, and for wave reflection at a stationary wall for both kinds of

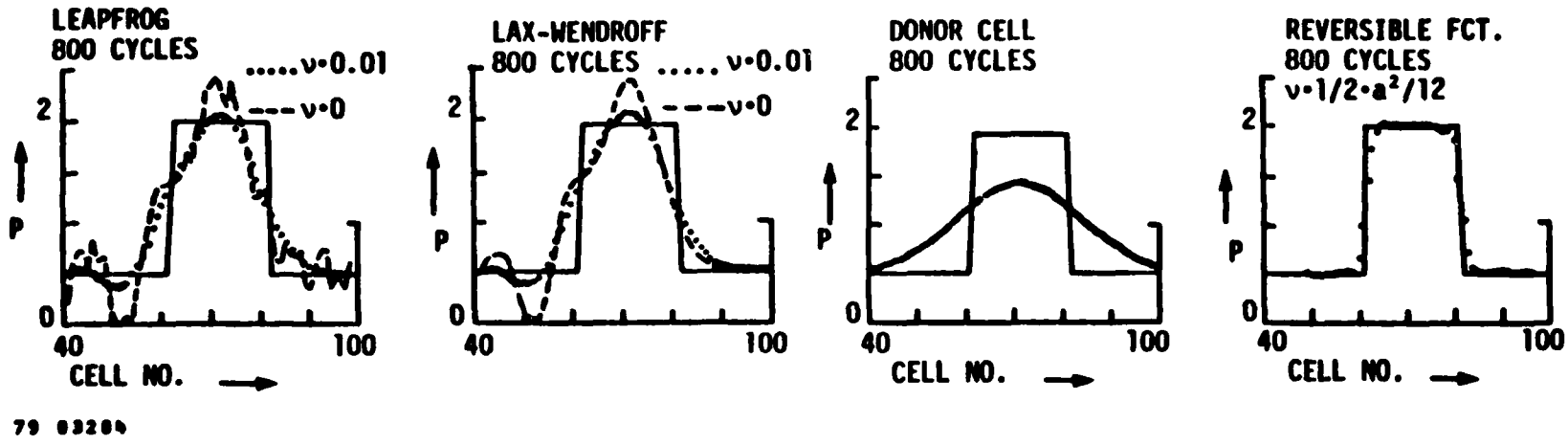

Figure 4-6. Comparison of Gasdynamic Numerical Schemes

waves. In all cases, we observed very close agreement with the analytic solutions.

There is some concern that the FCT algorithm may not track very small disturbances for many transit times in a single tube. This would have the effect of an artificially large dissipation rate which damps small disturbances. However, we have found that 20 spatial steps is sufficient to simulate rather small disturbances found in the traces taken from the MSNW wave rotor experiment. If there is any inaccuracy of the sort described, it may have more to do with waves trapped within a closed volume rather than waves which are driven by strongly changing boundary conditions, as in the actual experiment and in all wave rotors of interest for propulsion.

4.4 BOUNDARY CONDITIONS AND EFFICIENCIES

A basic analytic calculation is usually carried out to determine the approximate location and width of each of the ports and flow boundary conditions before the FLOW codes can be run. This initial wave rotor configuration may later be modified to improve performance on the basis of full FLOW code calculation results. Several techniques have been developed for specifying the initial configuration, ranging from the use of a simplified wave diagram where all waves have zero width, to the use of relatively complete characteristic calculations which include wave reflections and interactions with the tube-manifold boundaries. Two of these techniques are described below.

The work transfer efficiency and the shaft work efficiency each depend on the values of the flow parameters as calculated at particular ports of the wave rotor. Therefore, it is essential that these port flow parameters be calculated in as self-consistent and accurate a manner as possible. The basic analytic calculation gives only a first approximation to these efficiencies. Yet that information is useful since it provides an upper bound to the actual efficiencies; that is, only a few of the

losses are included. More accurate values of the efficiencies are obtained from the FLOW code, which includes a wide variety of losses with a self-consistent computation of the gas dynamics. These efficiencies are defined here and related to more conventional expansion and compression efficiencies found in the gas turbine literature.

4.4.1 FLOW Code Boundary Values

Flow properties at each of the wave rotor ports are supplied to the FLOW code as boundary conditions to the unsteady tube flow. These boundary conditions represent compressor outlet, combustor inlet, combustor outlet, and turbine inlet conditions for the engine cycle. Port locations and widths are derived from the wave diagram described in Section 3.2. Generally, the stagnation pressure and temperature are prescribed at each inlet port and the static pressure is given at the outlet ports. At each step in the calculation, the code determines whether the anticipated value of the pressure at the end of the tube is greater or less than the static pressure in the manifold. This comparison actually determines whether the flow must go in or out of the tube. Conditions at the tube mesh points corresponding to the ends of the tubes are calculated iteratively by using the projection of the forward or backward facing characteristic originating on the previous time step from the tube mesh points located one spatial point in from the ends. An iterative process is then required to solve for the boundary mesh point conditions using a technique described by Spaulding for wave rotor calculations.

This technique can be applied to partially open tubes as well as fully open tubes and to tubes with finite tube wall thickness. Flow in or out of partially open tubes can reach sonic conditions when the opening is very small. In those cases where the sonic condition is detected, the sonic flow equations replace the subsonic equations in the calculations. Finite tube wall widths are treated as isentropic converging or diverging area changes in a quasi-steady flow approximation which leads to slight

increases or decreases in the flow velocities, and related flow variables also change.

As an example, consider the flow equations for fully open outflow. Figure 4-7 shows a rotor tube on the left, with wall thickness δ and interior width d. Three flow stations are distinguished: the position w inside the tube, the position th in the throat (i.e., at the very end of the tube), and the position e corresponding to the external manifold flow. As the figure shows, the flow area changes from A_w in the tube to A_e, the equivalent cross-sectional area of the stream tube in the manifold; the ratio of these two quantities, Φ, is

$$\Phi = \frac{A_e}{A_w} = \frac{(d + \delta)}{d} \frac{\cos \theta}{\cos \beta}$$

The equations governing the flow from the tube to the manifold are

CONTINUITY $$\rho_w A_w u_w = \rho_e A_e u_e \qquad [4-4]$$

IDEAL GAS LAW $$P_w = \frac{\rho_w A_w^2}{\gamma}, \quad P_e = \frac{\rho_e A_e^2}{\gamma} \qquad [4-5]$$

ENERGY CONSERVATION $$\frac{\gamma-1}{2} u_w^2 + a_w^2 = \frac{\gamma-1}{2} u_e^2 + a_e^2 \qquad [4-6]$$

RIEMANN INVARIANT $$QQ = u_w + \frac{2}{\gamma-1} a_w \qquad [4-7]$$

ISENTROPIC CONDITIONS $$a_w = sP_w^{\frac{\gamma-1}{2\gamma}}, \quad a_e = sP_e^{\frac{\gamma-1}{2\gamma}} \qquad [4-8]$$

where QQ, the invariant, is known from the previous time step. The unknowns are u_w, u_e, a_w, a_e, ρ_w, ρ_e, and P_w. These seven equations may be reduced to the single equation for the variable P_w:

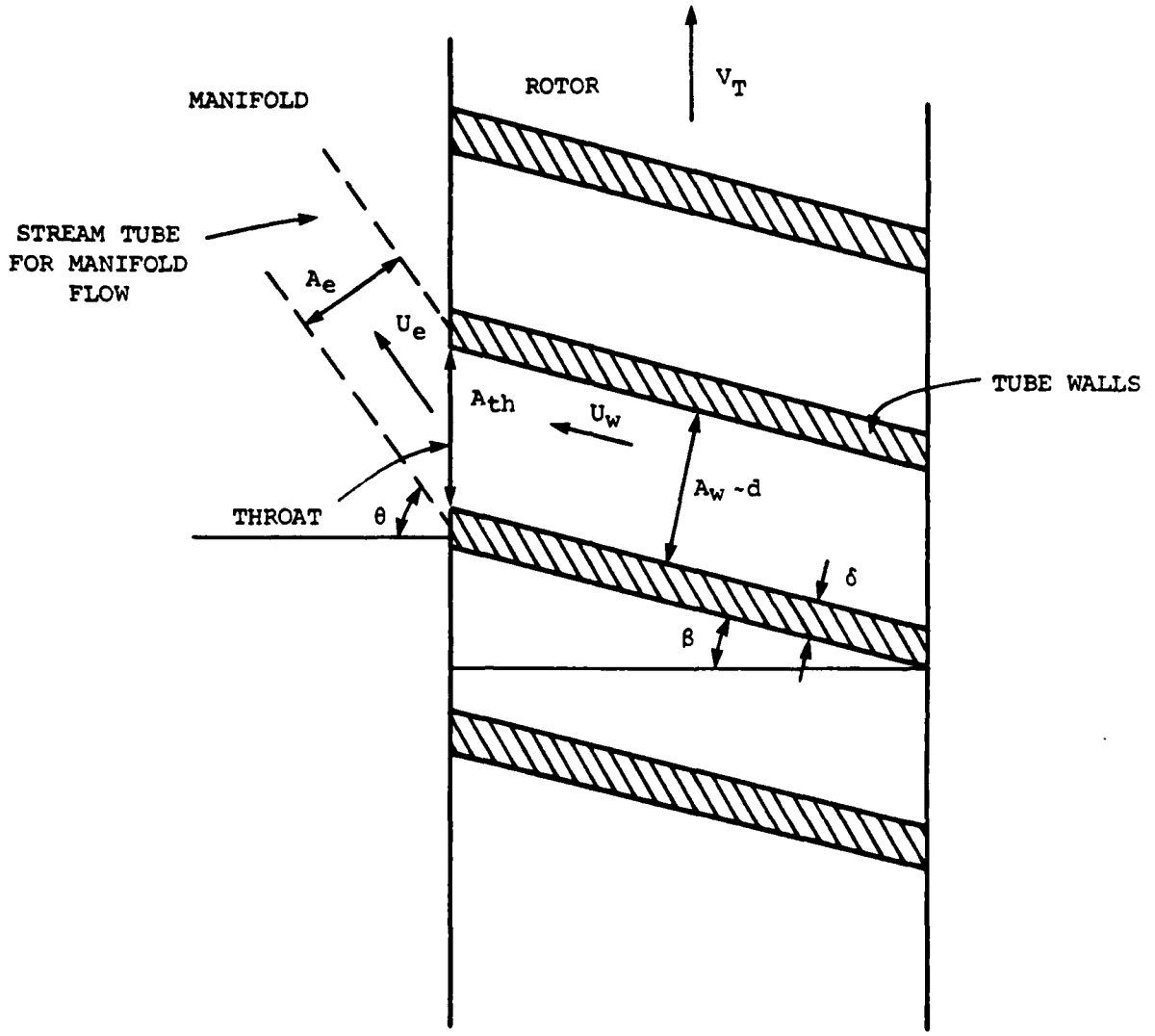

Figure 4-7. Fully Open Outflow Condition Showing Rotor Tube Geometry and stream tube for flow in the exhaust manifold.

$$P_w = P_e \left[\Phi^2 \left[1 + \frac{2s^2 \left[P_w^{\frac{\gamma-1}{\gamma}} - P_e^{\frac{\gamma-1}{\gamma}} \right]}{(\gamma-1)\left[QQ - \frac{2}{\gamma-1} sP_w^{\frac{\gamma-1}{\gamma}} \right]^2} \right] \right]^{\frac{\gamma}{2}} \qquad [4\text{-}9]$$

This equation can be solved iteratively in the form given with the initial guess of $P_w = P_e$. Implicit in this formulation is the assumption that the transformation of coordinates from the rotor frame to the laboratory frame does not affect the static pressure P_e, which has been assigned as the external boundary condition.

4.4.2 Definition of Efficiencies

Two efficiencies are used to describe the performance of a wave rotor. These are the work transfer efficiency η_w, and the shaft power output efficiency or shaft work efficiency, η_s. These are defined as

$$\eta_w = \frac{W_{d(out)} - W_{d(in)}}{W_{D(in)}} \qquad [4\text{-}10]$$

$$\eta_s = \frac{W_s}{W_{D(in)}} \qquad [4\text{-}11]$$

where $W_{Din} = mc_pT_{Din}\,[1 - (P_{ref}/P_{Din})^{\alpha}]$, $W_{dout} = mc_pT_{dout}\,[1 - (P_{ref}/P_{dout})^{\alpha}]$, and $W_{din} = mc_pT_{din}\,[1 - (P_{ref}/P_{din})^{\alpha}]$ represent the available work in the inlet driver gas, the outlet driven gas, and the inlet driven gas, respectively, and W_s is the shaft power output of the wave rotor; $\alpha \equiv (\gamma-1)/\gamma$. The available work terms are given in terms of a reference state pressure; that is, these terms represent the work that could be obtained by an isentropic expansion to that pressure. The work transfer efficiency represents the change in the driven gas available work compared to the available work in the driver inlet stream. The shaft work efficiency represents the shaft work derived from the rotor compared to the same driver gas available work. Therefore, each of these efficiencies

is a component efficiency which equals one in an ideal system but which is modified by loss terms which irreversibly use up the available energy in the driver gas inlet stream.

Losses which reduce the work transfer include entropy production in shock waves, friction losses and heat transfer at the walls of the tubes, and pressure recovery losses. Pressure recovery losses occur for partially open tube inflow where an abrupt area change exists between the external manifold stream tube dimensions and the interior tube dimensions. It also occurs, although to a lesser extent, for the reverse situation of a partially open tube with an abrupt area change and outflow conditions. The greatest losses are assumed to occur in all of the outflow manifolds where zero pressure recovery is assumed. This assumption is very conservative since it should be possible to design the manifolds with finite subsonic diffusers and finite, but not perfect, pressure recovery. Thus, the FLOW calculations presented in this document are strictly conservative in this respect.

The work transfer efficiency is related to the more conventional expansion (turbine) and compression (compressor) adiabatic efficiencies used by engine designers. Figure 4-8 shows a diagram of a wave rotor and a turbine inside a dashed box. The enthalpy-entropy states corresponding to the inlet and outlet flows of the wave rotor and the turbine accompany this diagram. The net work output from the dashed box divided by the available work of expansion of the inlet gas stream to this box is equal to the work transfer efficiency of the wave rotor when the turbine inside the box has an efficiency equal to 1. The general expression for the box efficiency is given by

$$\eta_{box} = \frac{w_T}{\dot{m}_1 (h_1 - h_{2s})}$$

In terms of the thermodynamic states shown in Figure 4-8, this expression can be rewritten as

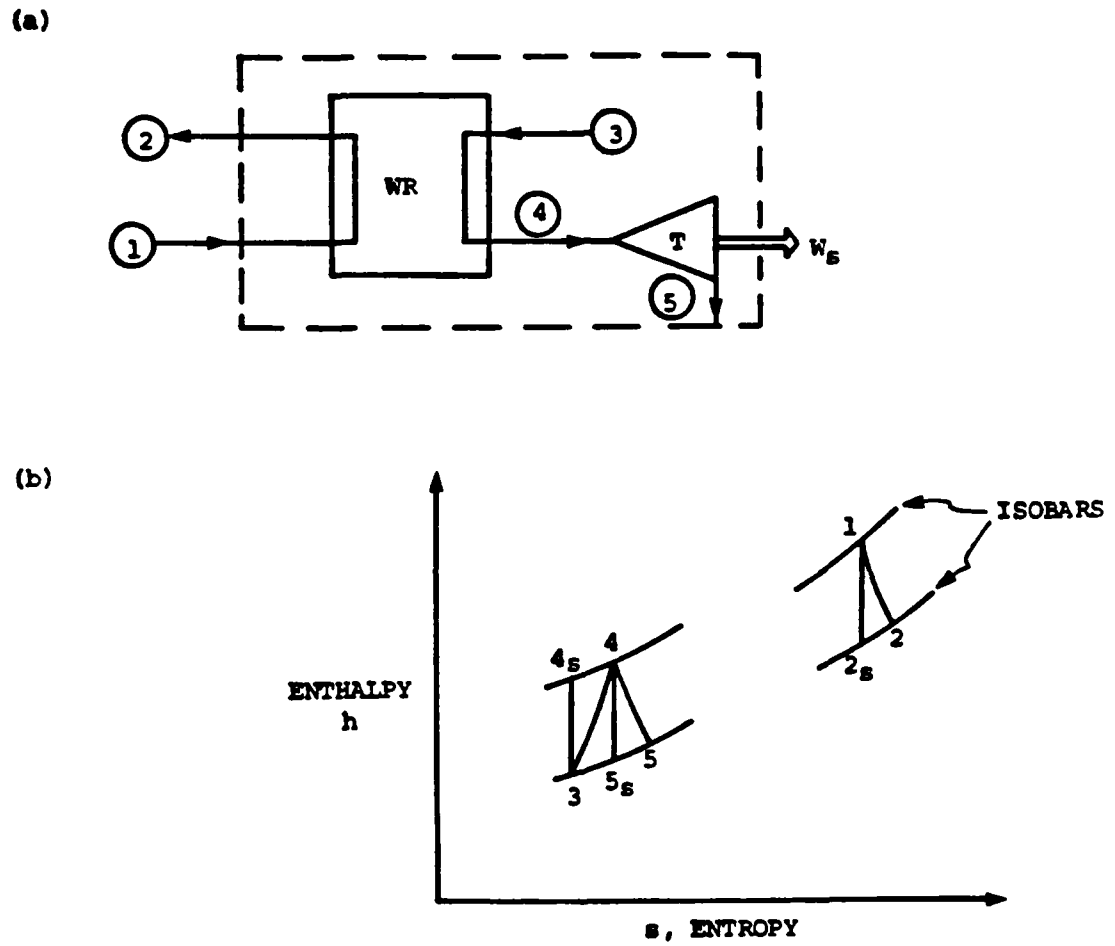

Figure 4-8. (a) Wave Rotor and Turbine Combination

(b) Equivalent Thermodynamic States. Subscript s denotes isentropic compression or expansion.

$$\eta_{box} = \frac{\dot{m}_4\left[h_4-h_5\right]}{\dot{m}_1\left[h_1-h_{2s}\right]} = \frac{\dot{m}_4\left[h_4-h_{5s}\right]}{\dot{m}_1\left[h_1-h_{2s}\right]}\ \eta_T \qquad [4\text{-}13]$$

Using the standard definitions for adiabatic expansion and compression efficiencies

$$\eta_{TE} = \frac{h_1-h_2}{h_1-h_{2s}} \qquad [4\text{-}14]$$

$$\eta_{CE} = \frac{h_{4s}-h_3}{h_4-h_3} \qquad [4\text{-}15]$$

and the condition that the rotor is adiabatic

$$\dot{m}_1\left[h_1-h_2\right] = \dot{m}_3\left[h_4-h_3\right] \ , \qquad [4\text{-}16]$$

we can write the combination of these equations as

$$\eta_{box} = \frac{\dot{m}_4}{\dot{m}_3}\ \eta_{CE}\ \eta_{TE}\ \eta_T\ \frac{h_4-h_{5s}}{h_{4s}-h_3} \ . \qquad [4\text{-}17]$$

If there is no leakage (i.e., $\dot{m}_3 = \dot{m}_4$), the pressure ratios $P_5/P_4 = P_3/P_4$, and the gases are perfect with constant specific heat (i.e., $h = c_pT$), then

$$\eta_{box} = \eta_{CE}\ \eta_{TE}\ \frac{T_4}{T_{4s}}\ \eta_T \qquad [4\text{-}18]$$

which tends to

$$\eta_W = \eta_{CE}\ \eta_{TE}\ \frac{T_4}{T_{4s}} \qquad [4\text{-}19]$$

for the case of a perfect turbine; that is, η_W represents the component efficiency of the wave rotor alone.

The shaft work efficiency η_s can also be written in terms of more

conventional component efficiencies by recognizing that the work extracted from the shaft is supplied by turning the gas on the rotor in the same way that a turbine does. Detailed calculations of the change in momentum of the gas as it enters and leaves the rotor requires all of the rotor manifold flow conditions (i.e., speed, direction, and amount of mass flow) to be known. The thermodynamic expression of this work is similar to Equation [4-16] with a shaft work term added:

$$\dot{m}_1\left[h_1-h_2\right] = W_s + \dot{m}_3\left[h_4-h_3\right]$$

In this case, internal work is also being transferred to compress the incoming air. Unfortunately, it is not possible to give a completely independent measure of the partition of work between shaft power and internal work transfer without specifying the ratio T_4/T_1. That is, the fraction of the work available in the driver gas which is needed to compress the driven gas is proportional to T_4/T_1; a portion of the rest of the driver gas available work produces shaft work output.

Using the definition of an equivalent adiabatic turbine efficiency, we can write

$$\eta_s = \frac{W_s}{\dot{m}_1\left[h_1-h_{2s}\right]} = \frac{\dot{m}_1\left[h_1-h_2\right] - \dot{m}_3\left[h_4-h_3\right]}{\dot{m}_1\left[h_1-h_{2s}\right]} \qquad [4\text{-}21]$$

$$= \frac{\eta_{TE}\left[h_1-h_{2s}\right] - \frac{1}{\eta_{CE}}\left[h_{4s}-h_3\right]}{\left[h_1-h_{2s}\right]}$$

$$\eta_s = \eta_{TE} - \left[\frac{T_{4s}}{T_4}\,\frac{1}{\eta_{CE}}\right]\frac{T_4}{T_1}$$

If we consider $\eta_w^{\bullet} = \eta_{CE}\eta_{TE}\,T_4/T_{4s}$ to be an equivalent work transfer efficiency under these conditions, then η_s and $\eta_w^{\bullet}$ are related by

$$\eta_s = \eta_{TE} \left[1 - \frac{1}{\eta_w^{\circ}} \frac{T_4}{T_1} \right] \qquad [4\text{-}23]$$

For very high driver gas temperatures (i.e., $T_1 >> T_4$), η_s tends to η_{TE}, as one would expect.

4.5 PRESSURE EXCHANGER WAVE ROTOR ANALYSIS

4.5.1 Scope

Several wave rotor configurations for a pressure exchanger are possible including the traditional four port machines tried in the mid-fifties by Klapproth, Brown-Boveri, and others as well as the nine port machine concept developed more recently at MSNW. These earlier versions of the pressure exchanger suffered from poor scavenge and very nonuniform flows in the manifolds. The nine port machine specifically addresses the question of nonuniform port flows and scavenging by requiring that there be no waves incident on any port other than the relatively small tuning ports which are used to suppress wave reflections in the tubes. Both four and nine port machines are examined here in order to illustrate their differences and to quantify the advantages of the nine port machine. The nine port machine also serves as a reference case against which to measure the sensitivity of the pressure exchanger performance to variations in its design and operating parameters.

4.5.2 Nine Port Pressure Exchanger

The reference case nine port pressure exchanger design corresponds to the component which will serve as the topping stage in a 600 lb_f thrust turbofan engine flying at Mach 0.65 at sea level. This engine has a bypass ratio of 5.0; since the total mass flow of air through the engine is 30 lb_m/sec, the core engine ingests approximately 6 lb_m/sec of this flow. The wave rotor provides the final factor of 2.5 in pressure, raising the compressor output flow from 15 atm to its peak value of 37.5 atm before the air enters the combustor. Seventy-five percent of the air

flow through the wave rotor must be heated and reinjected onto the rotor in order to provide the factor of 2.5 compression; the rest of the compressed air can be heated up to a reasonable turbine inlet temperature (e.g., by cooling the outside of the combustor can) and used in the high pressure turbine to extract shaft work. This flow is then recombined after expansion through the turbine, with the combustion exhaust gases from the wave rotor to provide the input gases to the low pressure turbine (refer to Figure 2.16 for an illustration of this cycle). The nine port wave diagram has already been discussed in Section 3 (see Figure 3-2). The rotor tip speed is 15,240 cm/s (500 ft/s), the rotor diameter is 14.8 cm, and its length is 14.3 cm. The reference case design and operating values are summarized in Table 4-2. Figure 4-9 illustrates the relative port locations and size, contact surfaces, and flow code contour plots for pressure for this case. The reference case involves both heat transfer and wall friction, plus all of the pressure recovery losses discussed earlier.

The reference case work transfer efficiency is 70 percent. A variety of related designs (i.e., port widths, port positions, rotor diameter, rotor speed) and operating conditions (i.e., driver and driven gas flow velocities, pressures, etc.) have been considered in order to find ways of improving the operation of this case. These alternative designs would require a more detailed evaluation in order to assess all of their merits, but they do serve to point the way to better designs. Improvements of 3 efficiency points to 73% appear easily obtainable through minor modifications of the reference conditions and additional optimization may be possible through further design changes. Such changes should be distinguished from the more arbitrary design and operating variations discussed below, which are used to quantify the sensitivity of the reference case performance to its constituent parameters.

Table 4-2

Design and Operating Parameters for Reference Nine Port Pressure Exchanger Wave Rotor

ROTOR DESIGN	FLOW RESULTS
Diameter (cm)	14.8
Length (cm)	14.3
Tube Width (cm)	1.7
Tube Wall Thickness (mm)	0.7
Tube Height (cm)	1.1
Tube Hydraulic Diameter (cm)	1.4
Number of Tubes	26
Number of Cycles/Revolutions	1
Tip Speed (cm/sec)	15,240
RPM	19,689
Clearance (mm)	0.13
OPERATING CONDITIONS	
Peak Temperature [$T_{D3,o}$ °K]	2240
Peak Pressure [$P_{D3,o}$ MPa]	3.57
Pressure Ratio	2.3
Air Inlet Mass Flow (g/s[lb/s])	2400 (5.3)
Combustor Mass Flow (g/s[lb/s])	1800 (4.0)
Driven Gas Exhaust Temperature [T_{d3} °K]	1077
Driver Gas Exhaust Temperature [T_{D1} °K]	1666
Driven Gas Inlet Temperature [T_{d1} °K]	728
Driver Gas Inlet Temperature [T_{D3} °K]	2209
Wall Temperature [T_W °K]	1260
Work Transfer Efficiency (%)	70

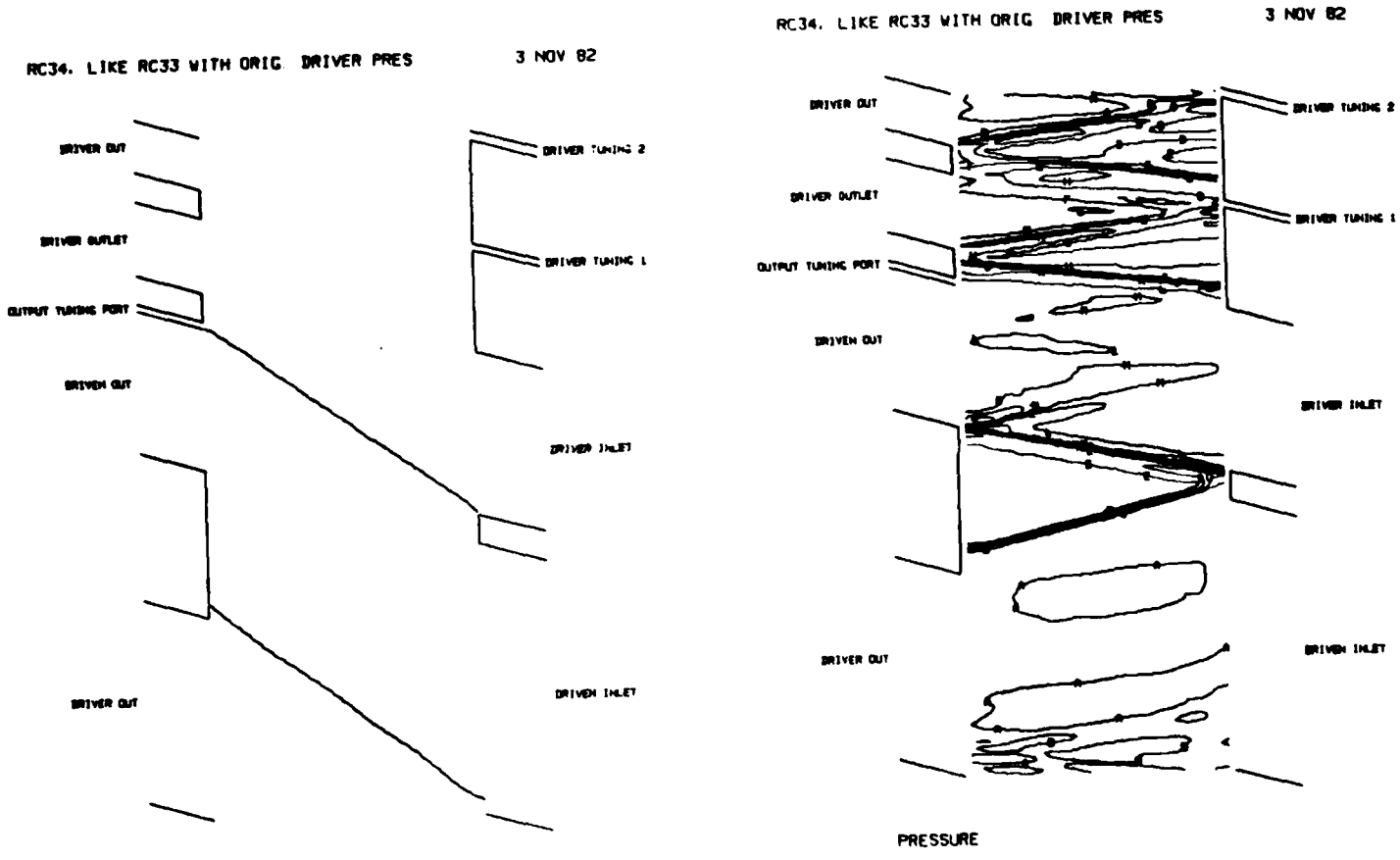

Figure 4-9. FLOW Code Results for Nine Port Pressure Exchanger Wave Rotor: Reference Case showing contact surfaces (left), port locations and relative sizes, and pressure contours (right).

4.5.3 Performance Sensitivity for a 9 Port Pressure Exchanger

The driver gas pressure, heat transfer coefficient, and clearance were varied in order to determine the wave rotor performance sensitivity to these parameters in its operation and design. These variables are related to external duct pressure variations, to heat transfer losses, and to leakage. Each of these effects has been judged to be critical by earlier researchers as well as in our own preliminary estimates of wave rotor performance. The results of these FLOW code calculations are shown in Figure 4-10, where the vertical axis measures the percentage change in work transfer efficiency and the horizontal axis indicates the fractional variation below or above the reference value for each of these three variables.

The strongest effects occur when the pressure at the inlet port for the combustion gas is artificially depressed below the design value. Under these conditions, the driven gas is not removed completely from the rotor by the time a tube passes by the exit port for this gas. Because of this poor scavenging, the driver gas cannot expand fully in the time allotted for it on the rotor, and less work is transferred to the driven gas than is desired. At the other extreme when the inlet driver gas pressure is higher than design, overscavenging occurs, which results in excess driver gas escaping from the driven gas exit port. This has the immediate effect of raising the work transfer efficiency somewhat at the expense of also raising the temperature of the gas mixture now exiting from the driven gas port. The temperature of the gas leaving the driver gas ports is necessarily lower. Generally speaking, the most uniform performance of the wave rotor is achieved for on-design or slightly overscavenged conditions, a design strategy that is relatively easy to follow.

In actual engine operation, independent driver gas pressure variations would not occur because the driver gas inlet flow is linked

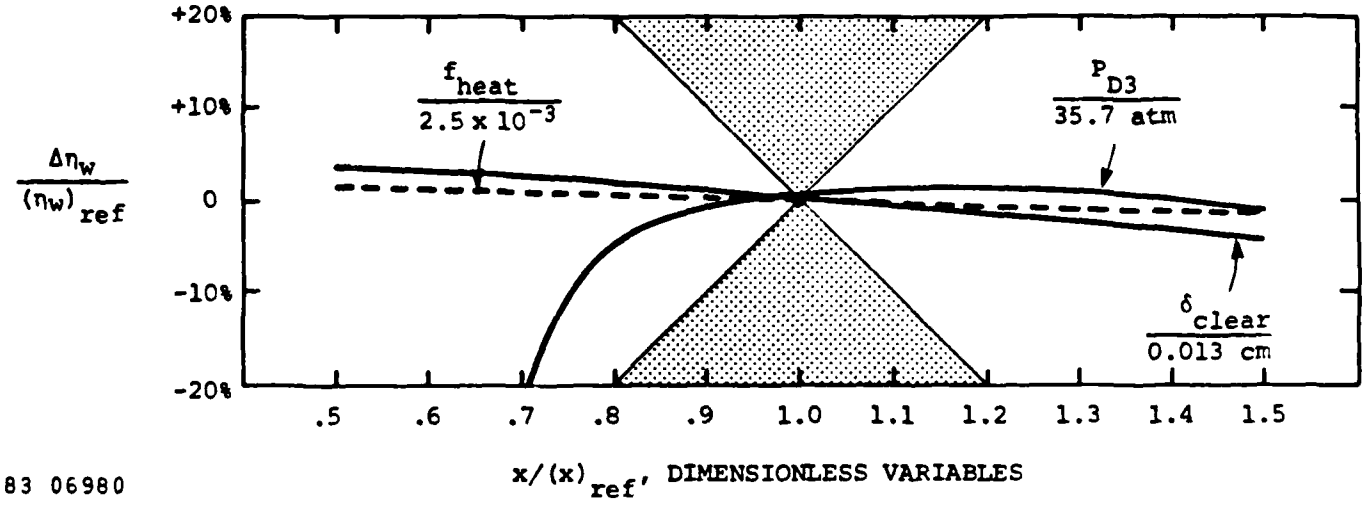

Figure 4-10. Sensitivity of Wave Rotor Work Transfer Efficiency η_w to:

Driver Gas Inlet Pressure, P_{D3}

Heat Transfer Coefficient, f_{heat}

Leakage (Clearance), δ_{clear}

Shaded regions indicate unacceptably high sensitivity.
(Reference case from Table 4-2)

through the combustor to the driveng as outlet port pressure and flow conditions. Therefore, actual off-design engine operation will impose a mixture of off-design wave rotor parameter values that vary in a very structured way compared to the single parameter design sensitivities being discussed here. Off-design engine conditions result in off-design wave rotor performance which is much closer to its on-design performance, as will be shown in Section 4.5.5. Additional adjustments in off-design wave rotor operating conditions, which can be controlled by flight speed and combustor temperature sensors, can be made to provide nearly uniform performance over the entire range of off-design engine conditions.

Variations in the work transfer efficiency also occur when the heat transfer coefficient and the seal clearance controlling gas leakage are changed. Figure 4-10 shows a mild effect due to enhanced heat transfer. The reference value used for the heat transfer coefficient corresponds to the Reynolds number for the mean flow velocities in the tube. Clearly, for slower velocities the Reynolds number will also be smaller, implying a larger friction factor; however, the total heat transfer term also depends on the velocity to the first power, so that the variations in friction factor are countered by this velocity factor. Perhaps the most plausible way that the heat transfer might be much larger than in the reference case would be if a background turbulence exists in the tube during parts of the cycle where the mean flow velocity is zero. At heat transfer levels smaller than the reference value, the effects of heat transfer are negligible compared to other stronger losses related to leakage, pressure recovery, etc. Leakage, long recognized as a key problem for efficient wave rotor operation, has a slightly nonlinear effect on the work transfer efficiency in the vicinity of the reference case. At very low leakage levels, the work transfer efficiency increases by 4% and, at higher leakage levels, the efficiency declines approximately 7%. Clearly, the leakage must be controlled, and the next series of rotor designs and tests must address this problem directly with a constructive solution.

4.5.4 Performance Optimization Techniques for a 9 Port Pressure Exchanger

Wave rotor design parameters can be varied purposely to improve the reference case performance. The first method uses mismatches between wave and contact surface arrival times and port locations to suggest the direction of design adjustments. The wave arrival times can be adjusted to some degree by varying the rotor tip speed, since the wave speeds and rotor speeds are keyed to each other once the length of the rotor has been chosen. This approach affects all of the waves in the same way and is a useful solution if the entire wave system is not yet periodic.

Another way of adjusting the design is to move one port relative to the others to better intercept the flow of a particular gas stream. Such adjustments also affect all of the other waves in the system, but not in the same way; hence, the results of such changes are much more difficult to predict without first analyzing the results of a few such changes. Port widths can be changed for similar effects. It is possible to adjust the air inlet and driver gas outlet pressures (without necessarily interfering with engine applications) to help speed or retard certain waves and thereby redirect the flows throughout the rotor cycle. These techniques represent gross adjustments.

A finer scale of modifications relate to the behavior of the tuning ports; the tube height, width, length, and number of tubes; and rotor radius. Tuning ports play an important role in cancelling unwanted waves and in allowing a broad performance range; in this sense, they are important for maintaining performance during off-design engine operation, which is discussed in more detail below. The number of tubes and tube size can be adjusted to control the amount of heat transfer by changing the wall surface area exposed to a given mass flow. The heat transfer also affects the wave pattern and efficiency of the device, as treated in Section 3. Lastly, the angular speed can be varied for a given tip speed

AD-A131 167 INVESTIGATION OF WAVE ROTOR TURBOFANS FOR CRUISE MISSILE ENGINES VOLUME 1.. (U) MATHEMATICAL SCIENCES NORTHWEST INC BELLEVUE WA R TAUSSIG ET AL. APR 83 2/2

UNCLASSIFIED MSNW-13.213.01.70-VOL-1 N00140-82-C-9729 F/G 21/5 NL

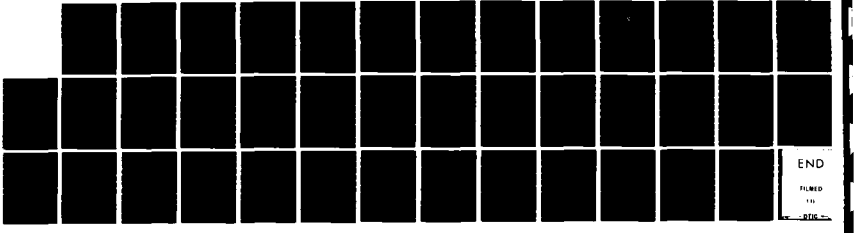

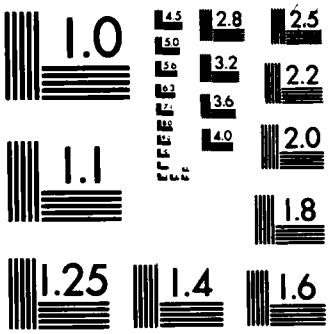

by changing the rotor radius; for a given number of tubes, this also varies the tube wall area exposed for heat transfer as well as the hydraulic diameter of the tubes.

Without making an exhaustive appraisal of these design modifications, a few cases are illustrated in Figures 4-11 through 4-14 to show some of the possible benefits of these techniques. In some cases, such as Figure 4-11, the effect of the change is to increase the amount of overscavenge relative to the reference case and in that way improve its work transfer efficiency. In Figure 4-12, the effect of decreasing the number of tubes and decreasing the heat transfer area is countered by a decrease in the collection efficiency, so that the net effect is only a small increment in performance as measured by the work transfer efficiency.

The conclusion of this set of FLOW calculations is that some very direct techniques for rotor design optimization are available via the FLOW code. These can be systemized in order to obtain the greatest design payoffs first and then the second order increments once the first echelon have been put into effect. Also, because several different approaches can have similar effects benefiting the rotor performance, there is considerable choice as to how this is done. Therefore, other more pressing design considerations can be factored into the optimization to give some priority to the design modifications.

4.5.5 Off-Design Rotor Performance

Off-design rotor performance has been computed from the FLOW code by assuming that the flight Mach number has been changed by changing the fuel flow conditions to the engine in such a way as to keep the combustant temperature constant. Changes in flight speed are interpreted as percentages above or below the reference case Mach II. These changes are accompanied by increases or decreases in the wave rotor port mass flows, pressures, and temperatures with resulting modifications in fuel consumption and output thrust of the engine. We have considered

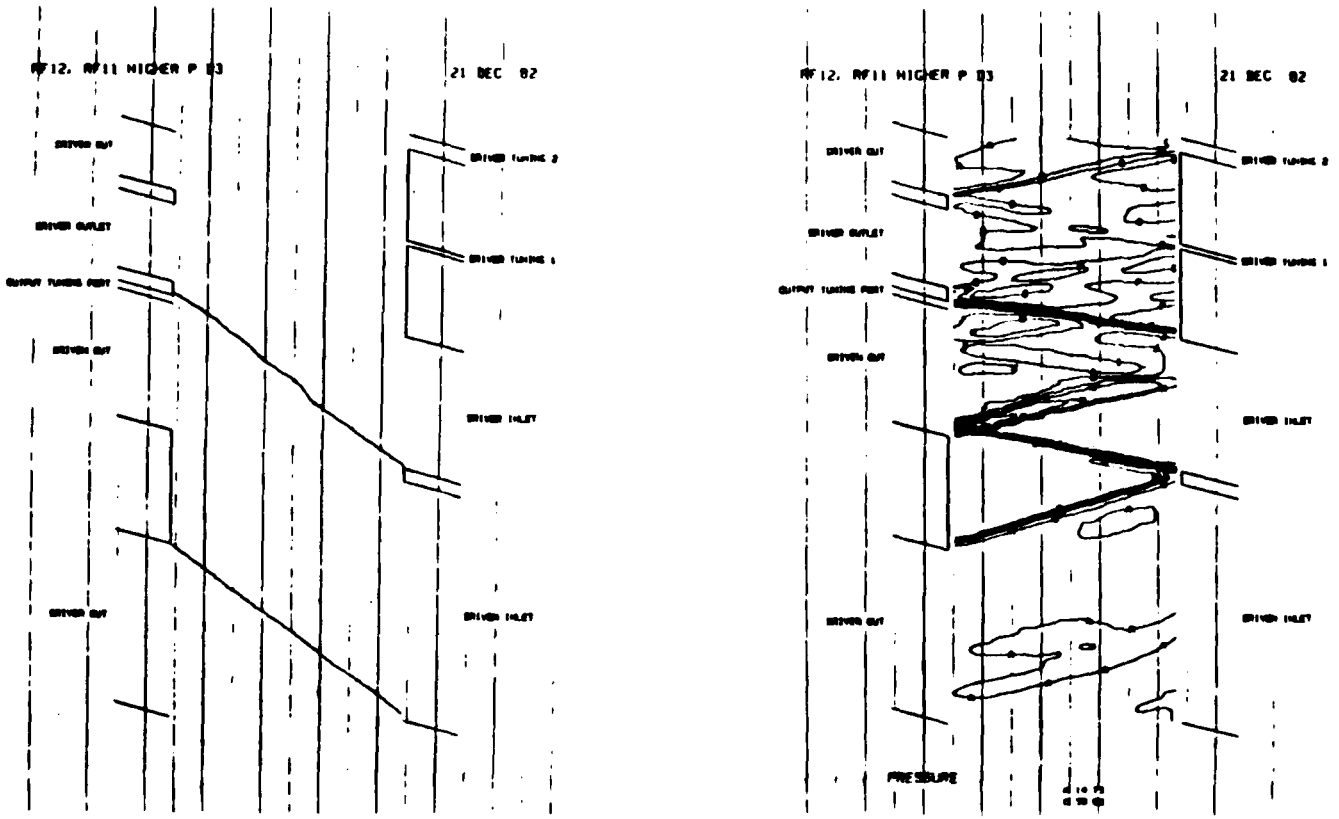

Figure 4-11. Nine Port Pressure Exchanger Wave Rotor with Overscavenged Driven Gas Flow: Contact surfaces (left) and pressure contours (right).

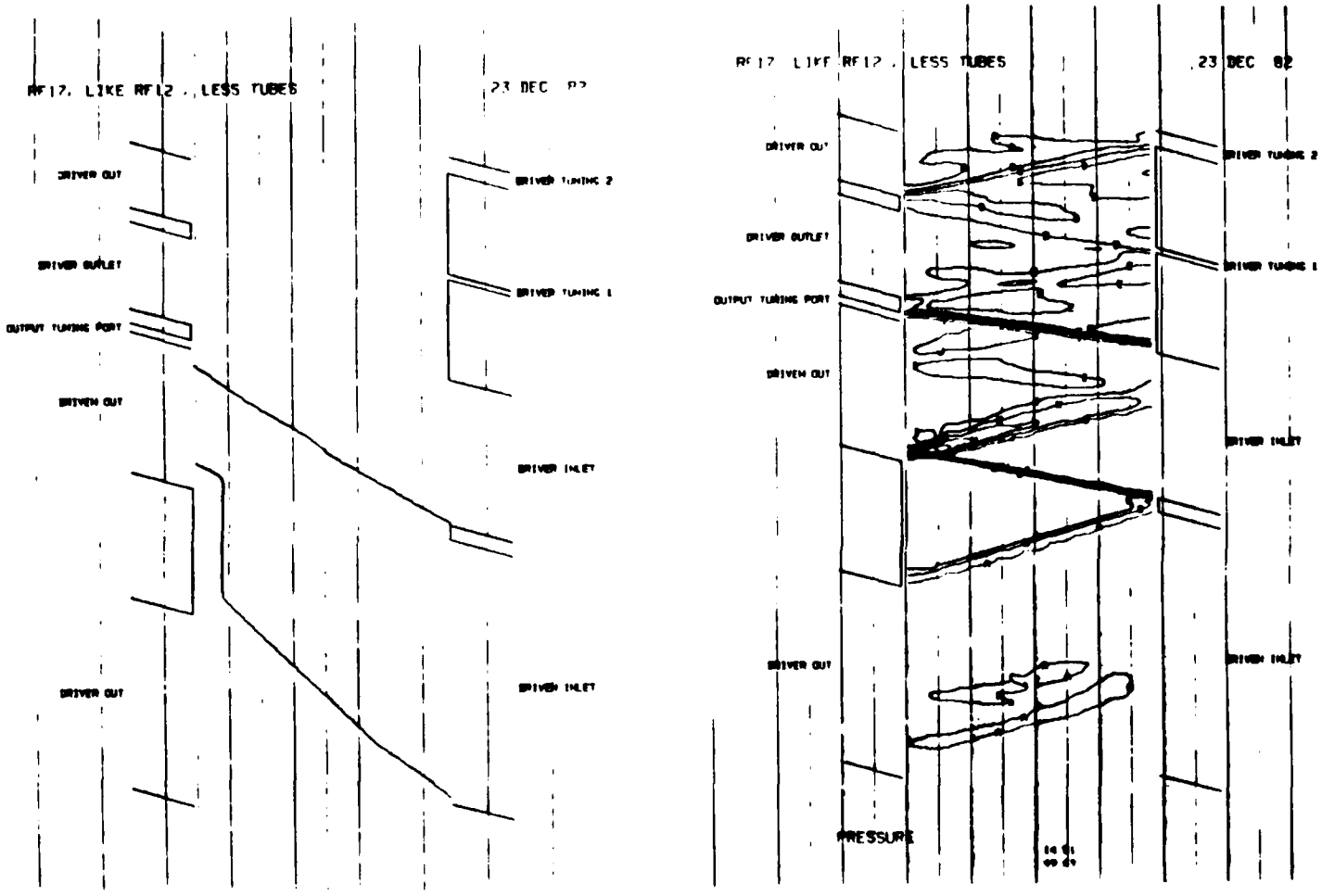

Figure 4-12. Nine Port Pressure Exchanger Wave Rotor with Decreased Number of Tubes: Contact Surfaces (left) and pressure contours (right).

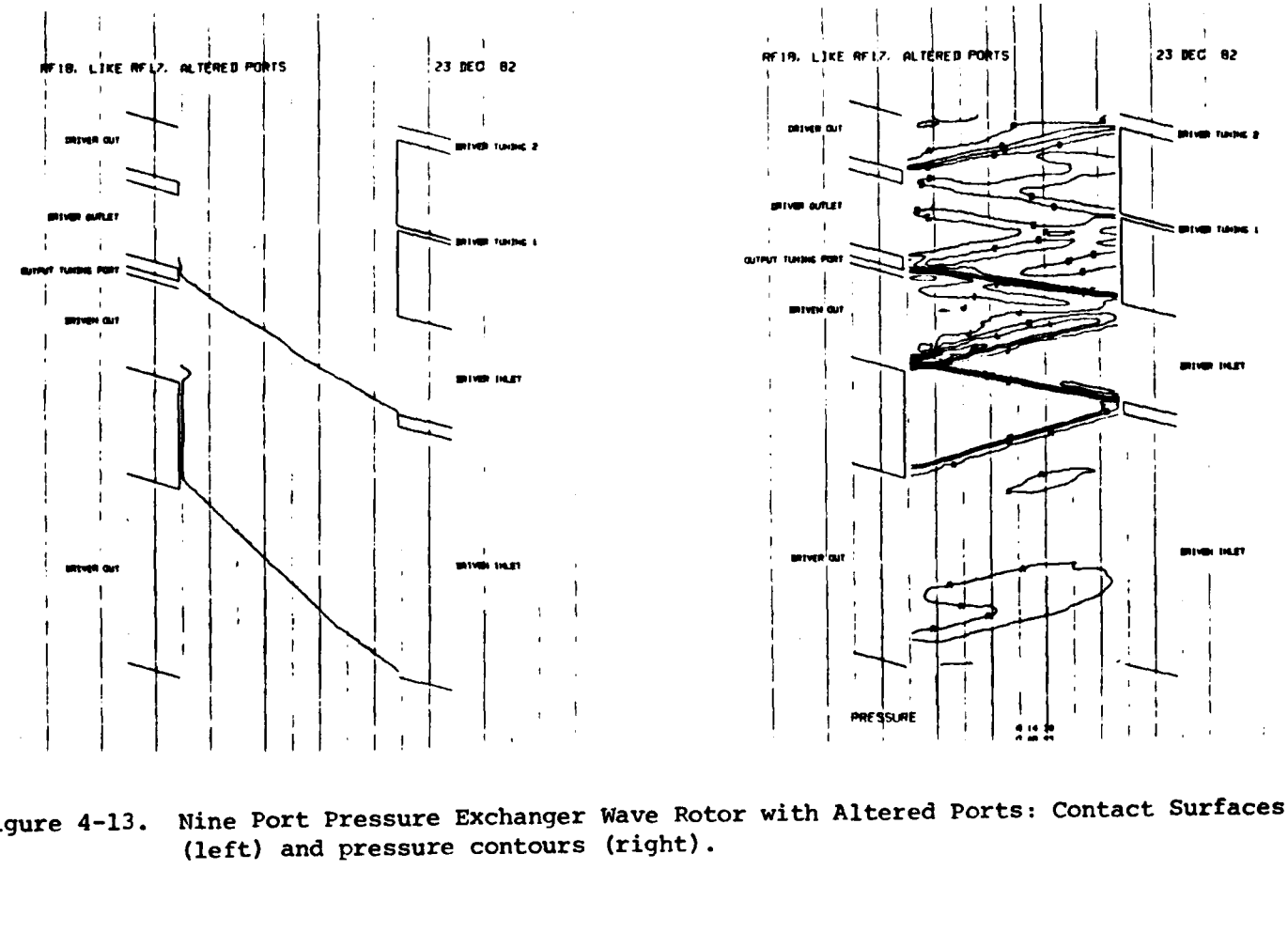

Figure 4-13. Nine Port Pressure Exchanger Wave Rotor with Altered Ports: Contact Surfaces (left) and pressure contours (right).

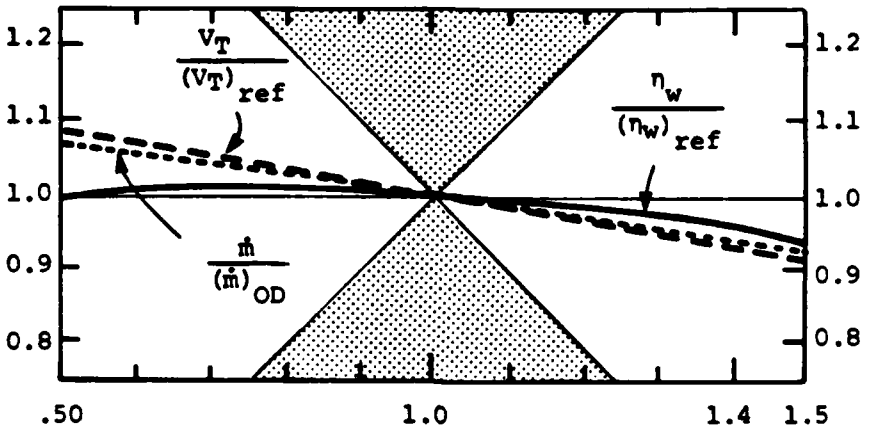

83 06985

Figure 4-14. Off-Design Performance η_w of a wave rotor corresponding to off-design wave rotor turbofan engine operation at various flight speeds. The wave rotor tip speed V_T is varied as shown, relative to the reference value, to compensate for higher or lower mass flows. The actual wave rotor mass flow compared to the mass flow required by the off-design engine operation is indicated by $\dot{m}/(\dot{m})_{OD}$.

off-design performance ranging from 50 to 150 percent of the reference flight Mach number. The flow conditions required of the rotor and the combustor have been derived from the cycle code calculations discussed in Section 2. The rotor flow conditions have been recalculated with the FLOW code using the off-design port temperatures and pressures required by the cycle code. The off-design FLOW calculations were made first with the same design as the reference wave rotor (i.e., same port locations and sizes) and same tip speed. The resulting mass flows were close to the off-design requirements but, with a linear change in rotor tip speed proportional to the flight Mach number, a much better match was obtained as illustrated by the example shown in Figure 4-14. The results show high performance maintained (i.e., $\eta_w/(\eta_w)_{ref} \cong 1$) for the wave rotor over quite a wide range of flight conditions and never varying by more than 6% from the reference case.

Changes in rotor tip speed and fraction of compressed air routed through the combustor are up to the designer's discretion and, therefore, comprise the chief avenues for maintaining high performance at off-design conditions. One might also consider variable port sizes by having movable port closure devices or by altering the flow through tuning ports at the leading and trailing edges of the main ports. The former technique has numerous sealing and mechanical problems associated with it, but the latter approach seems more practical for the lower temperature flows where simple valves are manageable. For this discussion, we have restricted the rotor adjustments to just the first method (rotor tip speed).

Similar off-design calculations were made in which the combustor temperature is varied and the Mach number is held constant. As the combustion temperature is decreased from design conditions, the acoustic speed and, hence, the typical wave speeds on the rotor are also reduced after the inlet air hammer shock (first shock in Figure 3-2) has traversed the tube. Thus, the rotor tip speed should be reduced accordingly to allow for the longer wave transit time in the tube. However, the driver gas pressure has also been reduced at the same time, so that less gas

actually passes through the driver gas port and less work of expansion is available in this gas for compressing the inlet air. This decrease in available work must match the corresponding change in inlet air flow and decreased pressure rise requirements of that flow. As a result of these coupled effects, the change in rotor tip speed is not completely effective in matching the resulting wave pattern to the manifold configuration for the on-design rotor; the amount of inlet air passed on through the combustor is varied in order to help compensate for these effects and to increase the rotor performance. Again, the performance of the wave rotor remains high over a ±50% variation in combustor temperature when the simple wave rotor control strategy just described is applied.

The off-design FLOW code results illustrate an important feature of wave rotors; namely, that they can be operated off-design with good performance and that this can be achieved via an active control system which is programmable in advance via a mechanical or electronic system which senses flight speed and combustor temperature and adjusts the rotor accordingly.

Alternative passive control approaches also exist which include the plateau nozzle approach used by Pearson in his rotor; the end-wall "pockets" utilized by Brown-Boveri in their Comprex; and, as mentioned above, variable tuning port flows. Each of these approaches merits a more careful evaluation before deciding on the best design approach. The purpose of the particular calculations which have been discussed above was to establish that at least one attractive approach exists for operating the rotor off-design and that its performance is calculable over the whole range of desirable operating conditions.

4.5.6 Four Port Energy Exchanger

A moment of consideration shows that a four port pressure exchanger automatically involves nonuniform inlet and outlet flows with mixing (i.e., pressure recovery) losses in the manifolds with no "pockets" or

other wave cancelling devices; that is, waves traverse the tubes and reach the ends of the tubes while the tube is still in the middle of a port. The main reason for this is that the gas flows cannot be matched with simple wave regions to make the cycle periodic. The existence of non-simple wave regions in the flow guarantees that waves will impinge on the port openings.

The consequence of nonuniform manifold flows is a mixing loss in the kinetic energy available at the outlet ports and, hence, a loss of stagnation pressure. This is manifested as a drop in the work transfer efficiency of this class of rotors relative to the efficiency of the nine port devices. A sample wave pattern taken from a FLOW code calculation for a configuration similar to those tested by Rolls-Royce is shown in Figure 4-15. A sketch of the rotor plus manifolds is shown in Figure 4-16. In this case, three cycles of waves were designed for one revolution of the rotor and, hence, the wave system is triply periodic; each part of this triplet is identical for the subgroup of four ports shown. This particular set of flow conditions resulted in a rather strongly underscavenged situation, as shown by the location of the contact surfaces in Figure 4-15, and a work transfer efficiency of approximately 40 percent, representing one of the lower values of efficiency for this particular design. Other FLOW calculations corresponding to very small changes in outlet driver gas pressure resulted in large motions of the contact surface, changing the scavenging but not improving the wave rotor efficiency very much (only a few percent). Experimental data for this case is rather scant, but it appears that a related version of this rotor achieved a measured product of compression and expansion efficiencies of 61 percent for the flow temperatures and velocities used in Figure 4-15.

In the simple configuration for the four port cycle shown in Figure 4-16, it would appear that the off-design performance would not be very good since the predicted on-design efficiency is so low. The use of the remedies discussed for the off-design performance of the nine port machine could also be applied here. No detailed calculations have been made to

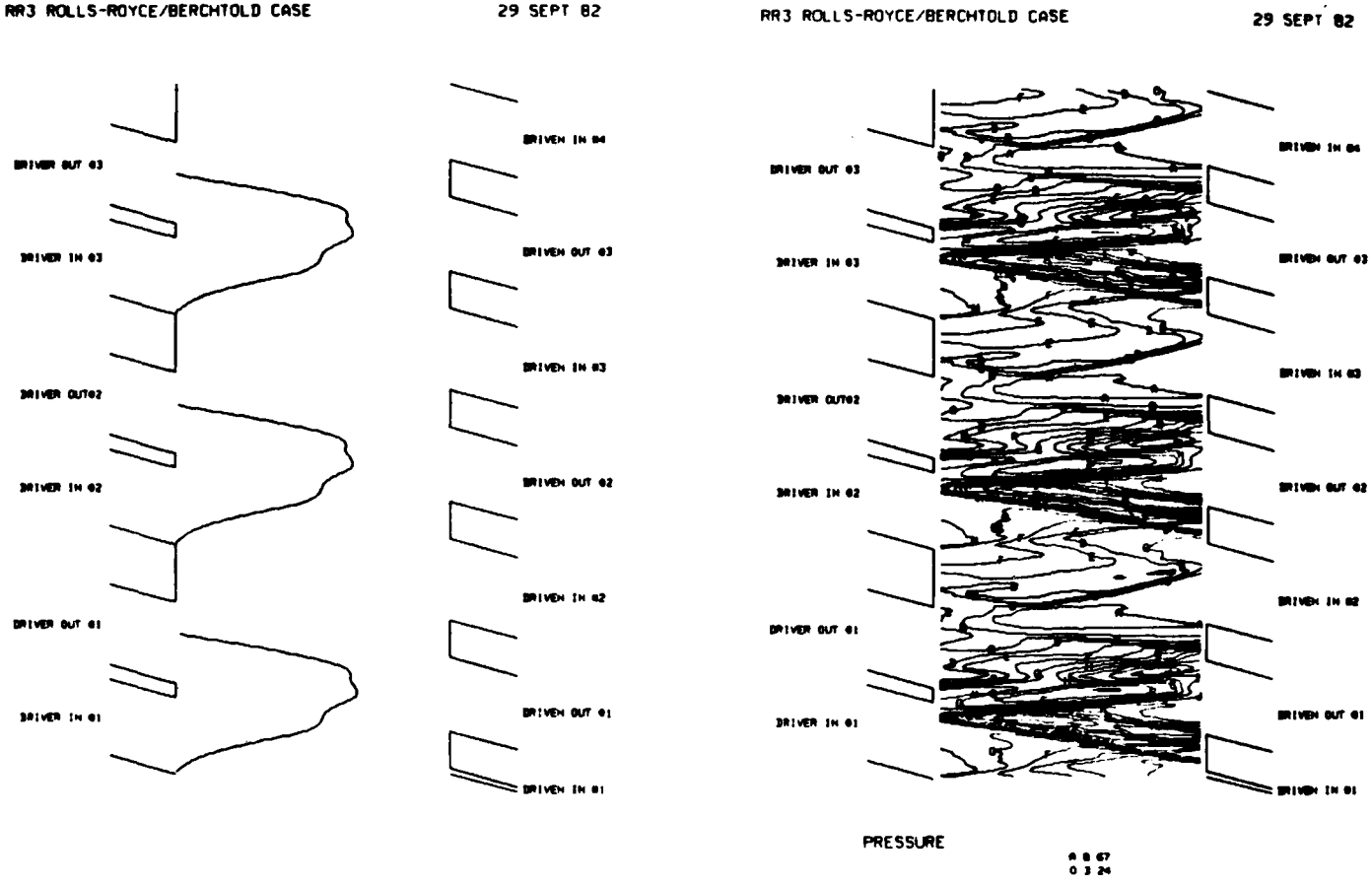

Figure 4-15. FLOW Code Contact Surfaces (left), Ports, and Pressure Contours for a Three Cycle, Four Port/Cycle Pressure Exchanger Wave Rotor.

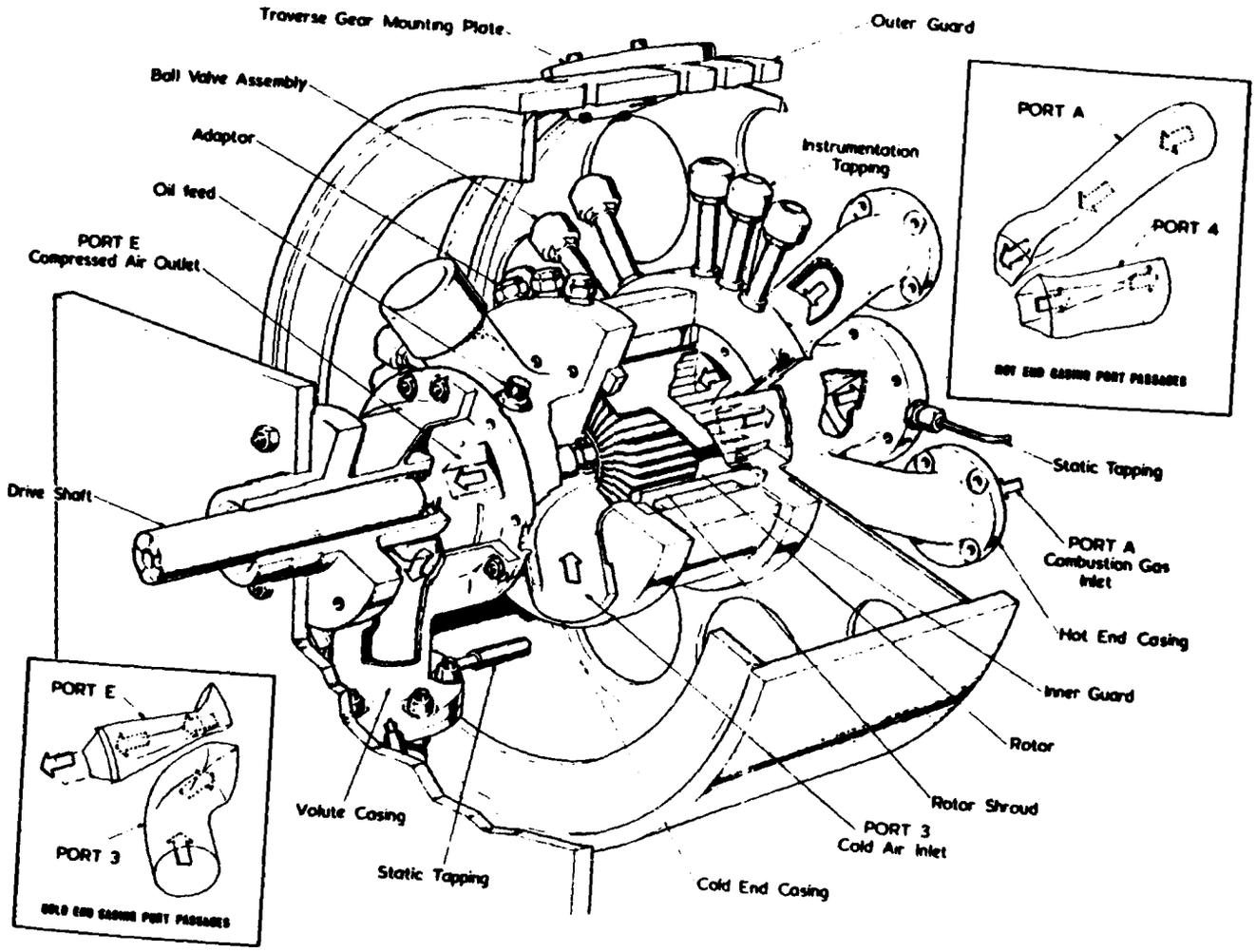

Figure 4-16. Sketch of Three Cycle, Four Port/Cycle Pressure Exchanger Wave Rotor Used in Rolls-Royce Tests.

confirm their effectiveness for this wave rotor configuration, and one would need to do that before drawing more definite conclusions for this case. The four port cycles discussed here would not be appropriate for use as a topping cycle for the peak temperatures and pressure ratios (i.e., 2.5) being considered in this study since the backwork ratio approaches 1 for a wave rotor component efficiency on the order of 60% or lower. These initial code predictions are sufficiently low that other wave rotor configurations offer more long-term potential than the four port machine.

4.6 WAVE ROTOR/TURBINE ANALYSIS

4.6.1 Scope

Wave rotor/turbines (those wave rotors which are intended to produce shaft work in addition to pressure exchange) have been investigated previously by such companies as General Electric, Ruston-Hornsby, and the General Power Corporation. This type of wave rotor is generally characterized by helical tubes and may derive shaft work from both reactive and impulsive loading of the rotor tube walls, in very much the same way as an ordinary turbine blade. Most of these devices have produced a disappointingly small amount of power output, with the notable exception of the Pearson rotor built and tested for many hundreds of hours by the Ruston-Hornsby Turbine Company. A more detailed account of that work is given in Appendix A. Both the Pearson rotor and the GPC rotor are examined here in order to contrast the two approaches to wave rotor/turbines and to extract those design elements which contribute to the success of the Pearson rotor.

The FLOW code has been modified to calculate shaft work output from wave rotor/turbines. At the time of this writing, only a few preliminary cases have been run with this version of the FLOW code; it has been judged not yet sufficiently reliable to report those results. However, the bulk of the work to modify the code is complete, and it would take only a

modest additional effort to verify its reliability and use it to project the performance of wave rotor/turbines.

As a result of progress on the FLOW code, only analytic results are presented here for wave rotor/turbines. These consist of a treatment of a simplified model of wave rotor turbines as applied to the GPC rotor using an ideal wave diagram as a starting point. The Pearson rotor is considerably more complex and has already been discussed in some depth by Pearson in a forthcoming chapter of a text on advanced turbomachinery. We have synopsized the relevant sections of his discussion. The wave diagram for a Pearson rotor is shown in Figure 3-3. There is a strong need to carry out additional analysis to determine the performance of the Pearson rotor and to evaluate its sensitivity to design and operating parameters at the same level of treatment given to the pressure exchanger wave rotor, in order to compare the two devices fairly.

4.6.2 Wave Rotor/Turbine Principles

The wave rotor/turbine acts as a combined compressor and turbine which produces net shaft power output. The compression is accomplished by wave action on the rotor in much the same way as the pressure exchanger wave rotor. The work of compression is taken from the high temperature, high pressure combustion gases as they expand down to the lowest pressure on the device. The combustion gases also supply the energy to produce shaft work. In some designs, the thrust is provided directly as the combustion gases leave the rotor; that is, as a reactive force on the rotor. In other cases the compressed air leaving the rotor may provide a similar reactive thrust, or the combustion gases may be vectored impulsively onto the rotor. In more complex systems, some of the gases exit and are re-injected back onto the rotor at a different place in the cycle without any external reprocessing; the angle of injection provides impulsive thrust to the rotor.

Shaft work extraction from a wave rotor/turbine is only efficient if it is taken from gas streams not required for scavenging or pressure exchange on the rotor. Since the low pressure scavenge is being driven by the compressor, it makes little sense to extract shaft power from the gas taken off of the rotor during this transition; that would only increase the work which must be provided by the compressor. As we discussed above, work cannot realistically be extracted from that fraction of the compressed air leaving the rotor on the way to the combustor or from the combustion gases as they enter the rotor; the former stream needs all of the pressure it can retain to flow through the combustor, and the latter stream must retain its available work to compress the inlet air. Therefore, the most effective way to produce shaft work relies on the fact that more compressed air is produced than is actually needed as combustion gases to drive the compression processes. The extra compressed air can be re-injected onto the rotor to produce impulsive forces if the point of re-injection occurs at a part of the wave cycle where the tube pressures are lower than the compressed air pressure. This third process involves a re-entrant flow and is one of the principal reasons for the success of the Pearson wave rotor/turbine design, as shown in Figure 3-3.

It also is clear that wave rotors with substantial changes in the tube stagger angle from one side of the rotor to the other will produce large reactive forces. This implies that all of the exhaust flows from such a rotor suffer substantial stagnation pressure losses just as that fraction of shaft work is being extracted from the flow. From the foregoing discussion, this approach appears to be doomed to failure since it causes an increase in the compressor work required to complete the low pressure scavenge and depletes the stagnation pressure rise needed to force the compressed air through the combustor and back onto the rotor. Therefore, the most efficient production of shaft work on wave rotor/turbines appears to be from impulsive loading, as described above.

4.6.3 The Pearson Wave Rotor/Turbine

Several features of the Pearson wave rotor/turbine are unique to the process of shaft work production. Additional techniques have also been developed to make this rotor perform well over a broad range of operating conditions. When gas is exhausted from a cambered tube and reactive shaft work is produced, the gas cannot be re-introduced onto the rotor until the gas remaining in the tube has undergone sufficient additional expansion to reduce the tube pressure to the pressure in the re-entrant loop. Thus, an extra exhaust expansion is needed; that is, the exhaust port is divided in two with the higher pressure portion re-injected after the lower pressure exhaust has brought the tube pressure down to the appropriate level. This explains the presence of ports P_{LO} and L_{O1} on the right side of Figure 3-3, where the flow from P_{LO} re-enters the rotor through port P_{Li}.

Features which improve the rotor's off-design performance include the use of tuning ports much like those used in the pressure exchanger, which are placed at the leading edge of an inlet port to help suppress the production of tube opening losses which occur from tube exposure to a sudden increase of pressure. Pearson has also introduced injection nozzles across the opening of entrance manifolds in order to exactly cancel the compression wave which reflects back through the tube to the entrance manifold. Normally this wave can be designed to reach the end of the tube just as the tube reaches the trailing edge of the manifold and is closed off. But, during off-design operation, the reflected wave may reach the manifold before this time and cause a serious disruption of the incoming flow. This nozzle design employs a "half-wave" plateau technique of pressurization where the tube pressure is raised in two equal segments as a result of the flow acceleration through the nozzles. The final pressure rise just equals the stagnation pressure in the nozzle flow so that no wave is reflected at the tube-manifold interface.

Pockets along the end wall of the rotor also help to suppress wave reflection for a variety of operating conditions for a single rotor

design. The gas leaving the end of a tube as it moves into confluence with one of these pockets is accelerated by the shape of the pocket and re-enters the tube at a higher velocity and at a different angle as the tube reaches the trailing edge of the pocket. If a rarefaction wave is also incident on the same end of the tube as it moves from the beginning to the end of the pocket, this wave will not be reflected with full strength because of the re-entering flow from the pocket. Thus, the pockets can manage waves over the full range of operating conditions for which the wave is incident on the pocket.

4.6.4 GPC Wave Rotor/Turbine

The General Power Corporation (GPC) wave rotor turbine differs in several significant respects from the Pearson rotor. The GPC rotor employs a sharp bend in the tube which constricts the flow area considerably and acts like a nozzle to accelerate the flow at a sharp angle as it leaves the rotor. In their approach, all of the shaft power appears to be extracted from reaction forces. In contrast, the Pearson rotor uses only a mild bend in the tubes to extract a small amount of reactive power; most of the shaft power is extracted through imulsive loading of the rotor blades. Also, the GPC rotor does not appear to use any technique to cancel or control reflected waves required to make the wave system periodic in one revolution of the rotor.

The wave diagram shown in Figure 4-17 incorporates the main wave phenomena found on the GPC rotor. The rotor tubes have a stagger angle of 45° relative to the rotor axis. The sharp bend in the rotor angle occurs on the right hand side in Figure 4-17; the bent portion of the tube is so short that it is not shown in this figure. Insteady, the bend manifests itself in the wave diagram by rflecting incident waves and by altering the angle and velocity of gas leaving the rotor on the right. Waves separating regions 1, 2, 3, 4, 5, and 6 and denoted by double lines are compression waves. These waves compress the incoming air and prepare it for entering the combustion chamber at station 4. The combustion gas

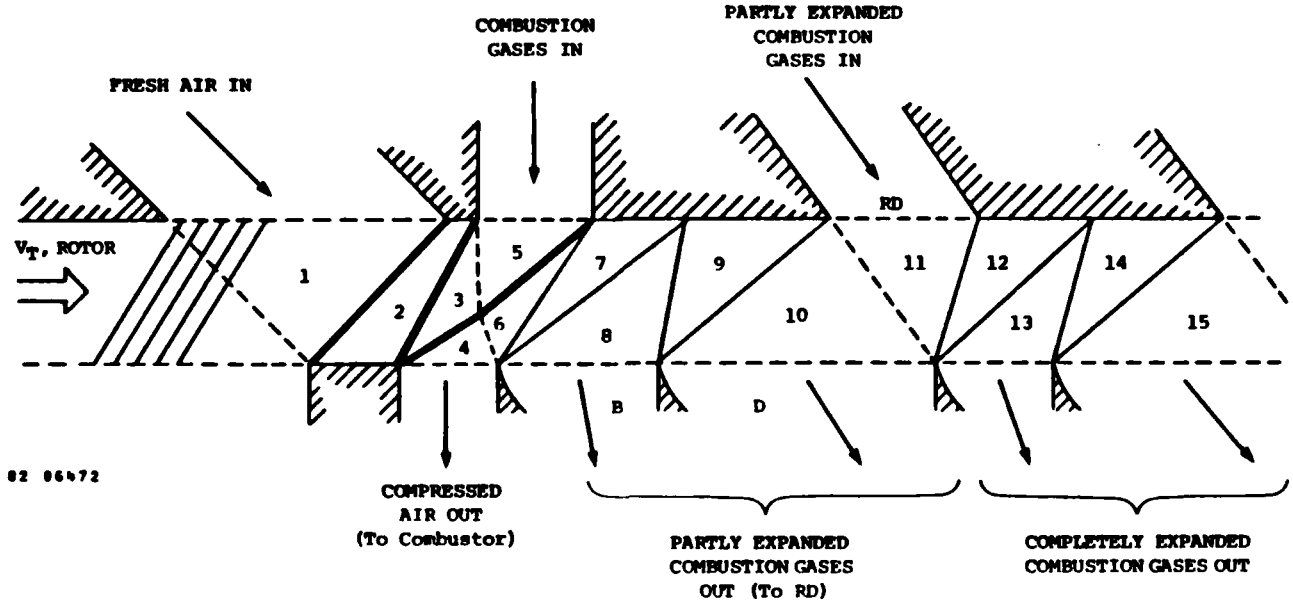

Figure 4-17. Wave Diagram for a Wave Rotor/Turbine Resembling the GPC Machine (RD = Re-entry Duct)

entering at 5 completes the compression, but only releases part of their available work; the remainder is extracted, in theory, from the series of expansions occurring from state 7 through state 15. The GPC re-injects flow leaving from regions 8 and 10 onto the rotor at station 11 to complete the expansion process.

In trying to reconstruct a plausible wave diagram for the GPC machine, several problems were encountered. Gas leaving the rotor at stations 8 and 10 to drive the re-entrant duct flow exits the rotor at two different gas pressures. In the actual GPC device, these flows are not separated so that considerable mixing losses are expected to occur as their pressures equilibrate. Reaction work is also extracted so that further pressure drop occurs, making it difficult to re-inject this flow unless the secondary expansion from 8 to 10 on the rotor is rather large. The combination of these processes is inefficient. A second problem area was not treated in this analytic approach but clearly exists, as mentioned above, which concerns the presence of reflected waves in the cycle which may prevent it from being truly periodic. The magnitude of the influence of the internally reflected waves needs to be determined numerically; with the FLOW code, for example. The absence of wave control mechanisms in the GPC design may also contribute to poor off-design behavior for this particular rotor.

Any one of these difficulties would be sufficient to prevent proper operation of the GPC rotor. It would be absolutely essential to obtain detailed measurements from such a device if it were not for the fact that the Pearson wave rotor/turbine has already operated successfully.

4.6.5 Wave Rotor/Turbine Performance

Analytical estimates as well as actual experimental data on wave rotor/turbine performance are available. The analytic estimates can be carried out on the basis of Pearson's or GPC's wave diagrams, and the

empirical data comes from the tests carried out by Ruston-Hornsby on the Pearson rotor in the 1950s.

It is possible to consider the shaft work efficiency of the wave rotor/turbine as if it were a conventional turbine and a conventional compressor working in tandem. Thus, we may substitute adiabatic turbine and compressor efficiencies for the values of η_{TE} and η_{CE} in the expression for η_S taken from Equation [4-22]. That is,

$$\eta_S = .892 - \frac{T_{4,s}}{T_4} \frac{1}{.85} \left[\frac{T_4}{T_1}\right] = .892 - 1.06 \left[\frac{T_4}{T_1}\right] \qquad [4\text{-}24]$$

where the ratio T_4/T_1 is a variable parameter and a pressure ratio of 3.0 has been assumed. Thus, for values of T_1 = 3000°F (1922°K) and air inlet temperatures T_4 = 1100°F (870°K), the shaft work efficiency may be as high as η_S = 41%. The virtue of using data calculated from the wave diagram is that better estimates of η_{TE} and η_{CE} are obtained. For values corresponding to Pearson's experiments, an overall cycle pressure ratio of 12.2 is appropriate to the peak temperature case of 1250°K and the value projected for η_S is 63%.

The thermal cycle efficiency of Pearson's rotor is given in Figure 4-18 as a function of shaft horsepower output. Using the conventional definition of Brayton thermal cycle efficiency with the usual adiabatic definition of turbine efficiency η_T, we can write

$$\eta_{TH} \cong \eta_T \left[1 - \frac{1}{P_r^{\alpha}}\right] \qquad [4\text{-}25]$$

$$\text{where } P_r^{\alpha} \approx \frac{T_3}{T_1}$$

for a maximum work cycle and where the compression work is not shown because it is accomplished by internal work transfer. Substituting the temperature ratio 1250°K/300°K = 4.167 for the ratio T_3/T_1 in the above

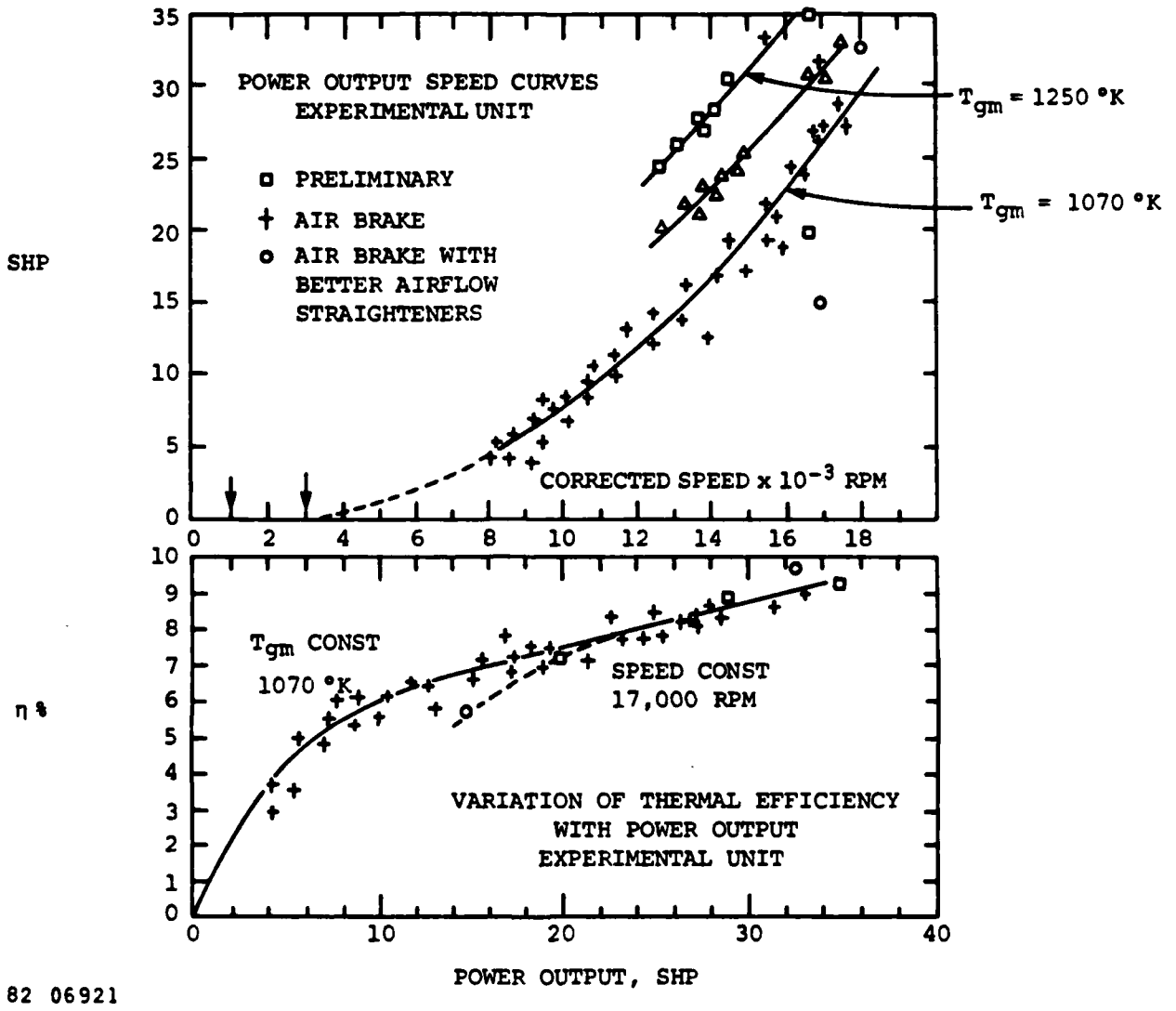

Figure 4-18. Experimental Data from the Ruston-Hornsby Tests on the Pearson Wave Rotor/Turbine. (SHP = shaft horse power, η = thermal cycle efficiency)

expression for the points corresponding to 35 shp, and noting that the thermal cycle efficiency was 9.4% for that case, we can solve for η_T = 18%. Carrying out the same steps at the peak temperature of 1070°K and 33 shp where the thermal cycle efficiency is 9.0% gives a second solution for η_T = 19%.

From this comparison, we can see that the empirical value for η_T is substantially less than the theoretically predicted value of 63%. Pearson has discussed several sources of loss in the Ruston-Hornsby experiments, which suggest that leakage and heat transfer are two of the main contributors to this poor component efficiency. It would be very useful to apply the FLOW code to this case to evaluate the possible losses in more detail.

The data in Figure 4-18 also illustrates that the wave rotor/turbine operates successfully for conditions which are considerably off-design, considering that the span of shaft horsepower was from 3 to 35 and the rotor speed varied from 8,000 to 18,000 rpm over this range. This represents a surprising capability when one understands that the wave rotor depends on the relative timing of waves relative to port opening and closing events. Further, the data supports the contention that the shaft work efficiency of the device is maintained to a large degree over this range so that the component performance is not seriously degraded. That leads to the conclusion that the rotor performance is not particularly sensitive to operating conditions once the proper design has been arrived at.

Relatively little is known at this point as to the sensitivity of the rotor performance to design features. However, from historical evidence it appears that it is very easy to design a poorly performing wave rotor turbine since the majority of them have not produced net shaft power output. Once the proper design principles are recognized, as, for example, in the Pearson rotor, then it is no longer a hit-or-miss process to design a good wave rotor/turbine. The use of the upgraded FLOW code

will also speed that design refinement procedure several orders of magnitude compared to earlier efforts and will allow a quick appraisal of the effect of design modifications on the rotor performance. Therefore, completion of FLOW code testing for this purpose is a high priority item in order to determine the peak wave rotor/turbine performance one may expect.

Section 5
RISK EVALUATION

5.1 SCOPE

Technical risks associated with the development of a wave rotor for a turbofan propulsion system have been identified on the basis of historical experience and from the analysis presented in this report. A potentially high-risk area in wave rotor development is defined as one which will have a large effect on the wave rotor turbofan engine performance. In the analysis presented in Sections 2 through 4 of this report, wave engine design and operating parameters have been varied over a range of values in order to bracket the projected performance of the wave engine turbofan. The risk assessment discussed here is based on the projected range of turbofan performance, its sensitivity to wave rotor performance, and on estimates of the relative ease or difficulty in attaining wave rotor parameters which yield good performance.

The scope of this risk assessment is exploratory. There are additional risk areas which can only be assessed after a conceptual engine design evaluation has been carried out and after a more detailed design of the wave rotor itself has been completed. The technical risks addressed in this study concern primarily the projected performance of the wave rotor and not the interplay of the design of this component with the design of the rest of the engine. These other areas of risk do need to be evaluated before proceeding with engine development, and a recommendation is made to that effect for the next phase of research.

5.2 IDENTIFICATION OF HIGH RISK AREAS

High risk areas in wave rotor development are those which will have a large impact on a wave rotor turbofan engine performance. The main way in which the wave rotor affects the overall engine performance is through the

peak temperatures and pressures it can withstand, its work transfer efficiency, and the associated inlet and exhaust flow properties of this component. The wave rotor may also affect the engine performance through its specific design, since these features must meet overall envelope and weight constraints and influence the work transfer efficiency. For example, engine performance may be adversely affected if the engine weight becomes excessive because the ultimate range of the device will be diminished dispite any gains in the TSFC. A more complete evaluation would have to consider specific missions and their required range. Similarly, an outsized engine encounters increased aerodynamic drag in proportion to the increase in cross-sectional area, which requires an increase in engine thrust in order to maintain a given set of flight conditions. For a fixed thrust, the flight speed is lowered and the range may be reduced despite possible gains in the TSFC. However, an increase in inlet diameter means that higher bypass ratios are feasible, which can lead to a considerable increase in TSFC under certain conditions.

The principal quantitative measures used here to describe the way in which the preliminary rotor design variables affect the turbofan engine performance are the rotor component efficiency and creep strength. The two main areas of risk presently identified with the rotor component efficiency are leakage and heat transfer. Each of these two effects depends strongly on the wave rotor design and the peak temperature involved, and each was addressed in a preliminary way in Sections 3 and 4, from the design point of view and as a part of the wave rotor performance analysis. The main variables affecting the rotor creep strength are the rotor wall temperature and the tip speed. These also depend on the rotor design and peak cycle temperature.

The most sensitive areas of risk for operating variables are associated with pressure control and the design steps taken to insure good off-design performance of the rotor (e.g., see Section 4.5.5).

5.3 RISK ANALYSIS

A general technique has been used here to help quantify the areas of high risk. First, the potential high risk areas identified above are associated with one or more of the design or operating variables. The ranges of variation of those variables for the 600 to 1000 lb. thrust engines are considered using the analytical results presented in Sections 3 and 4. The turbofan engine performance variations, in terms of TSFC, corresponding to the design or operating parameter ranges identified for the wave rotor are determined from the cycle analysis presented in Section 2. If the TSFC fractional variations are on the same order or exceed the fractional variations in the wave rotor parameters, then the area is judged to be high risk. If not, then the area is considered to be moderate to low risk.

The second step in risk assessment involves a judgment as to the relative difficulty or ease in achieving the design and operating parameters corresponding to the reference case preliminary design for the wave rotor. Historical experience as well as MSNW's own experience in wave rotor design and testing enters into this judgment. Specific intervals may be placed about the wave rotor turbofan engine performance which measure the potential increase in TSFC relative to a particular goal; for example, a TSFC of .70. These intervals will include any wave rotor design and/or operating parameters which yield a TSFC 10% higher than the goals, and a TSFC 20% higher than this same goal. The problems in meeting these goals are discussed below for the highest risk areas.

Figure 5-1 shows the thrust-specific fuel consumption as a function of specific thrust or engine size. The solid line indicates the performance expected if the wave rotor work transfer efficiency η_w = 70%. The two dashed lines indicate the values of TSFC if η_w = 60% and 50%, respectively. These results are presented again in Figure 5-2 where TSFC has been normalized by the value of TSFC for η_w = 70% as the reference

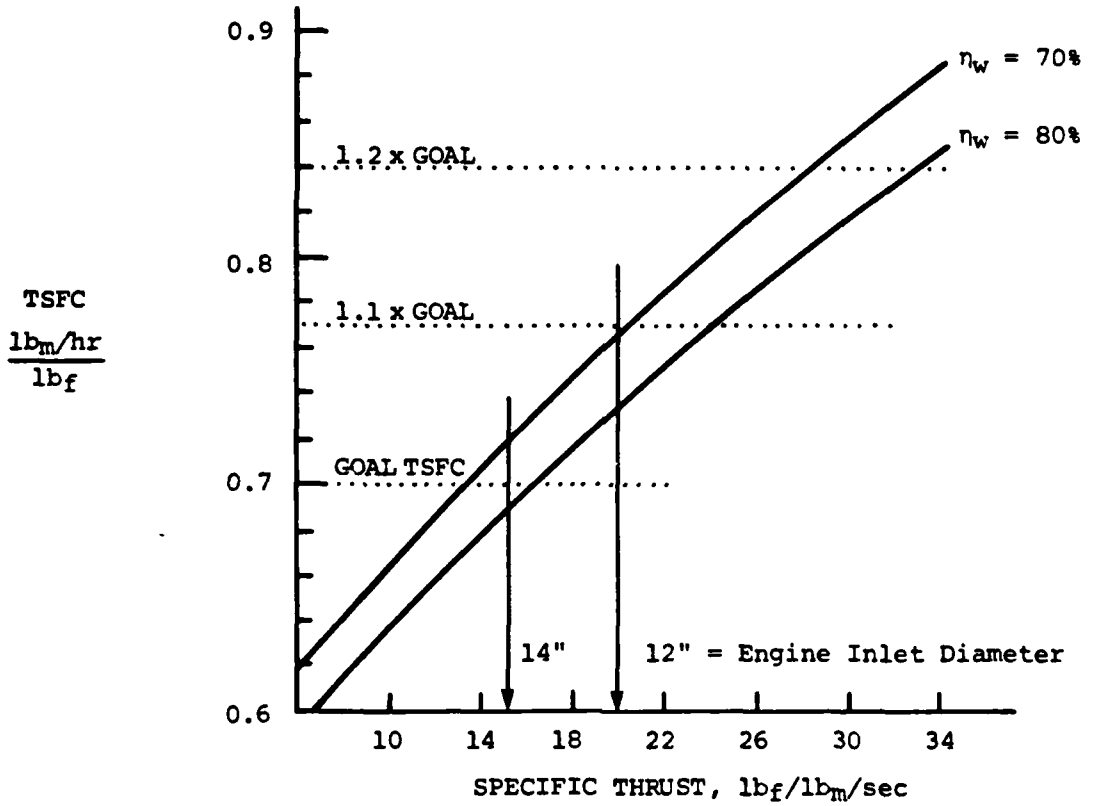

Figure 5-1. Minimum Thrust Specific Fuel Consumption (e.g., see Figure 2-4) vs. Specific Thrust for Two Wave Rotor Work Transfer Efficiencies η_w: 600 lb_f thrust engines, Mach 0.65 at sea level.

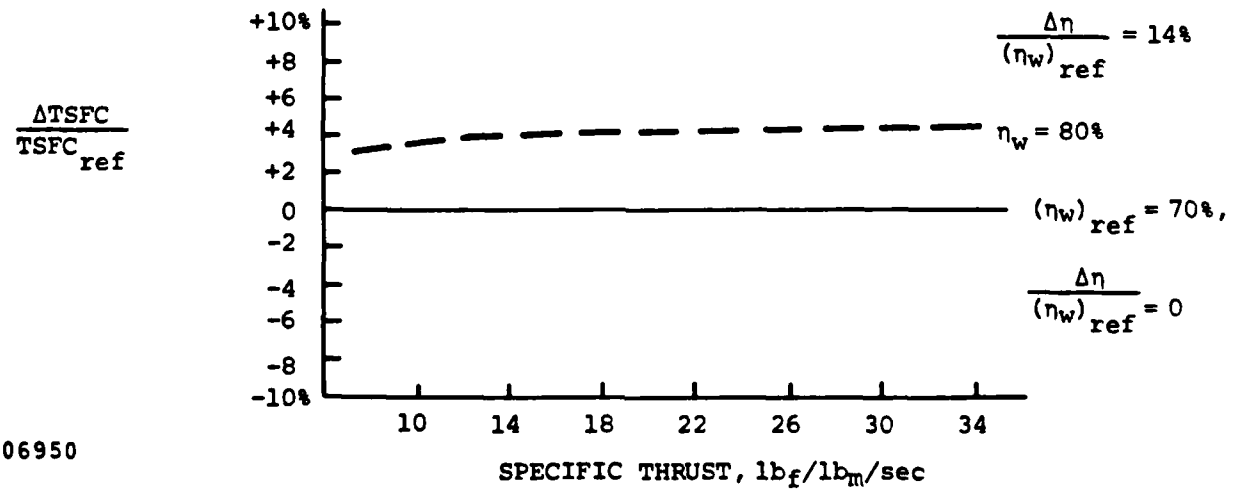

83 06950

Figure 5-2. Percent Change in TSFC vs. Specific Thrust as a function of η_w.

value. Since the percentage change in TSFC is considerably less than the percentage change in η_w, also shown in Figure 5-2, we may consider the work transfer efficiency, and all of those rotor design and operating variables which affect it, as being a low risk area. Figure 5-1 also indicates that a 12 inch diameter engine requires a rotor component efficiency of at least 70% (total engine pressure ratio = 48, peak temperature = 2500°F) to be within the 10% interval, while increasing the engine diameter to 14" relaxes the constraint on rotor component efficiency to values less than 70%, which may be relatively easy to achieve.

The second measure of performance depends more on the absolute value of the peak cycle temperature and, hence, on the ability of the wave rotor to withstand those temperatures. Figure 5-3 shows the stress required of various high temperature materials to produce 1% creep after 10,000 hours of operation. While the missions considered here do not require that lifetime, Figure 5-3 does give a measure of the material strength for creep resistance. The actual stresses producing creep depend directly on the material density and on the tip speed squared. Lines of constant stress are also shown in Figure 5-3 for various tip speeds. Rotor wall temperatures are on the bottom horizontal axis and ranges of peak cycle temperatures yielding these wall temperatures are on the top horizontal axis. We can compute from this figure approximately which materials are good candidates for the rotor at various peak cycle temperatures. Therefore, the key variables in this figure are the rotor wall temperature expected from a given peak cycle temperature and the rotor tip speed.

In Figure 5-4 we have plotted the percentage change in TSFC versus engine pressure ratio, where the reference line (i.e., abscissa) is for 3000 F peak combustion cycle temperature. Two values of η_w have been used which approximately bracket the range of work transfer efficiencies expected for the wave rotor. Also, the influence of peak cycle temperature relative to the reference temperature of 3000°F is indicated in terms of the percentage change in this variable. Several results may

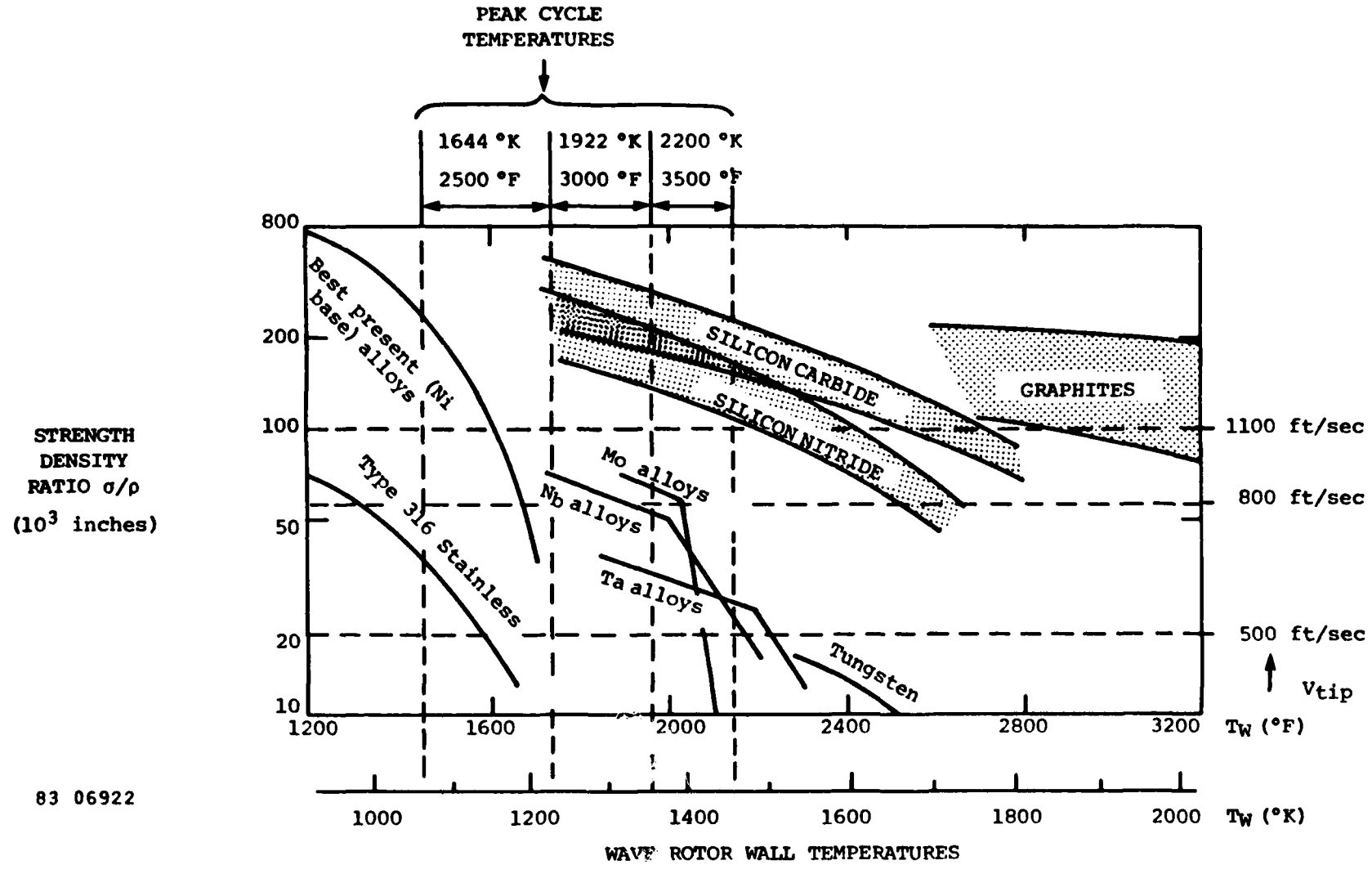

Figure 5-3. Cross Plot of Creep Strength (1% in 10,000 hours) of Candidate Wave Rotor Materials vs. Rotor Tip Speed (V_{tip}) and Rotor Wall Temperatures (T_W). Peak cycle temperatures corresponding to a range of rotor wall temperatures are shown at the top of the figure.

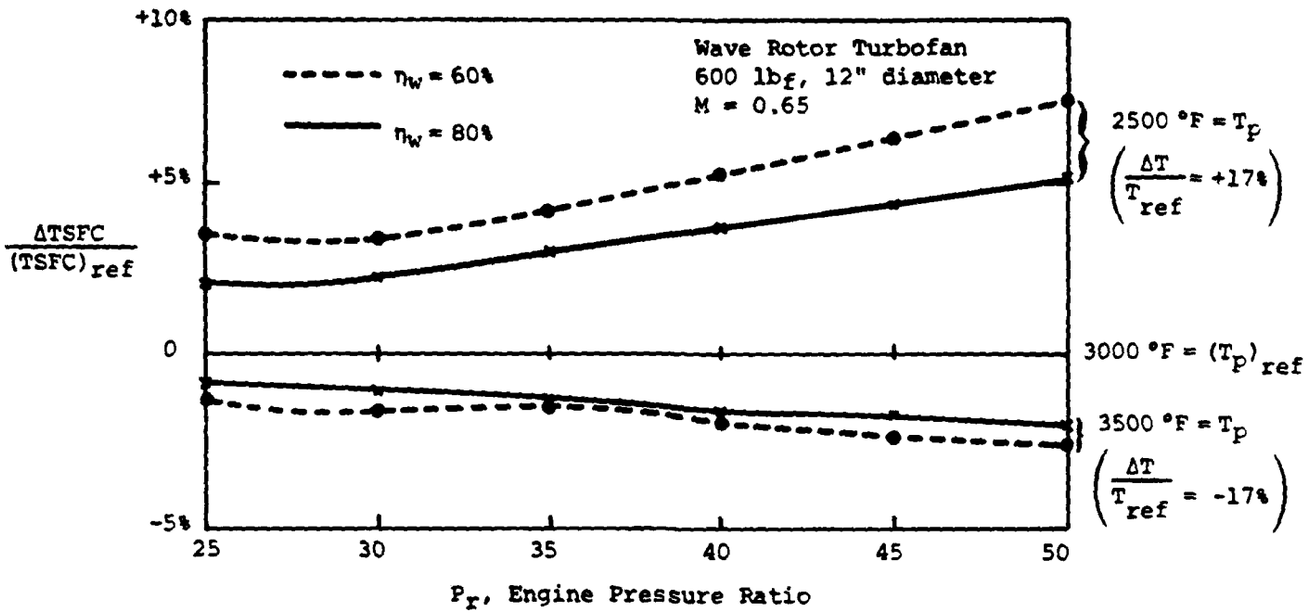

Figure 5-4. Percentage Variation in Thrust-Specific Fuel Consumption vs. Engine Pressure Ratio P_r for two values of work transfer efficiency η_w and two values of peak cycle temperature T_p (compared to the reference temperature of 3000 °F; data taken from Figure 2-2). The reference TSFC values for both η_w = 60% and 80% are plotted along the ΔTSFC = 0 axis.

be extracted from this figure by itself and in conjunction with the materials data in Figure 5-3. First, the sensitivity of TSFC to changes in the peak cycle temperature is least at lower pressure ratios and highest at P_r = 50; in any case, the percentage change in TSFC is always much less (by a factor of 2.5 up to 17) than the percenage change in peak cycle temperature for a fixed pressure ratio. Second, the TSFC increment gained by increasing the peak cycle temperature from 2500°F to 3000°F is greather than for the next 500°F increase in T_p to 3500°F by a factor of 3. Considering this data together with Figure 5-3, one sees that the jump from 2500°F to 3000°F may entail a shift from nickel-base alloys to either additional cooling or to more exotic refractories or ceramics for the wave rotor. In this sense, the wave rotor is sensitive to peak cycle temperatures. If one may operate with the lowest possible wall temperatures (e.g., 1750°F) for T_p = 3000°F, then a wave rotor made of nickel-base alloys may still be feasible if the tip speed is kept below 500 ft/sec. This appears to be likely since these conditions correspond to reference case 7 in Table 3-1.

Additional rotor cooling is also feasible. As we saw earlier, increasing the heat transfer coefficient affected the work transfer efficiency and the amount of heat transferred but did not make any significant changes in the wall temperature of the rotor. Any substantive decrease in the rotor wall temperature for a given thermal cycle will be associated primarily with changes in the overall wave pattern, in order to affect the amounts of time the hot and cold gases stay on the rotor. For example, additional scavenging with compressed air will cool the rotor and, through recuperative action, increase the thermal cycle efficiency. In the hot stage experiments, one of the key measurements must be a determination of the location of the hot and cold gas streams in each port. Deviation from the predicted flow patterns would indicate the need for rotor design motification to improve scavenging and the proper operation of the device. Such changes could have a significant impact on the wave pattern and would fall into this category of risk assessment.

To conclude, neither component efficiency nor peak temperature constraints appear to be high-risk areas in terms of the desired engine TSFC. A 12" wave rotor turbofan engine would permit at TSFC = 0.70 goal to be met if the wave rotor work transfer efficiency lies in the range of 70 to 80%; a 14" engine would meet this goal if the wave rotor efficiency lies in the range of 65 to 80%. At higher combustion temperatures (i.e., T_p > 2500°F), this goal is met more easily and, hence, the risk associated with achieving high η_w is reduced; however, the risks associated with rotor materials increases. A peak cycle temperature of 3000°F still appears to be feasible since the wave rotor wall temperature is still within reasonable creep stress limits at the design tip speed of 500 ft/sec. The predicted wave rotor efficiency for these conditions is 70%, well within the 10% interval around the desired TSFC value of 0.70. Off-design rotor performance corresponding to off-design engine conditions is also limited to TSFC excursions less than 10% about the design value of TSFC.

5.4 WAVE ROTOR TECHNOLOGY STATUS

It is important in the context of this preliminary risk analysis to acknowledge the relatively mature aspects of wave rotor technology and to point out those areas of uncertainty for the particular applications being considered. A commercial wave rotor has been developed over the past 20 to 30 years by the Brown-Boveri Company (see Appendix A). This rotor is used as a supercharger for Diesel engines and has been developed into several different size ranges and load ranges, the smallest being approximately the same size as the larger of the pressure exchanger wave rotors considered in this study and the largest being approximately 10 inches (25 cm) in diameter. The rotors are made of a low thermal expansion coefficient material and are cast using the lost wax method. Ceramic rotors have also been cast in a mock-up of a production line to determine the costs and technical problems in forming large numbers of them with reliable quality. Experimental rotors are also produced by this group using a sophisticated EDM technique to cut the tubes in stock metal,

including refractory metals. Bearings, shrouds, seals, external ducting, speed control, and external gas flow control are all problems which have been resolved by Brown-Boveri for their particular application.

Similar techniques have been employed in the fabrication and design of many of the experimental wave rotors tested over the years. Several of these rotors were operated at significantly higher temperatures than the supercharging application would require. For example, the Pearson rotor encountered peak gas temperatures of 1250 K (1800 F). These experimentalists met their particular challenges with modifications in the basic technologies which were appropriate to a laboratory experiment but which would undoubtably have to be modified for a production item. The point is that there is a substantial technology base which can be used as a starting point for many of the design requirements of the small wave rotor. The chief difficulties appear to lie in extending upwards the rotor wall temperatures, presumably at the expense of a shorter mission lifetime, but possibly also at the expense of additional technical problems such as seals, and the attendant problems of thermal distortion in the rotor and retaining structures(ducts, shaft shroud, and bearing case).

While encouraging because of its existence, the actual use of the Brown Boveri technology base poses some potential problems. First, we must find a way to access that data. This might be accomplished through an inter-industry arrangement as part of a project team. If that is not possible or desirable, then an inter-governmental exchange might be arranged, if the Brown-Boveri Company was willing. In preliminary discussions, they have indicated an interest in fabricating an experimental rotor. That would be a good start, and it would let them understand the potential for this particular application. If their interest were stimulated by this information, they might be persuaded to become more deeply involved in a technology exchange.

A most important aspect of the next stage of research is to establish the specific problem areas in the design and fabrication of the wave rotor which are not covered by the present development of the Brown-Boveri devices. That assessment is properly part of a conceptual engine design evaluation, recommended for the next phase of research.

Section 6

RECOMMENDATIONS FOR FURTHER RESEARCH

6.1 SUMMARY OF CONCLUSIONS

The conclusions of this study indicate a favorable outlook for the use of wave rotors to improve the performance of small turbofan aircraft engines. Analysis of the details of wave rotor performance both for on-design and off-design conditions supports the original estimates of relatively high work transfer efficiency - on the order of 70% for the reference case considered. The overall turbofan engine performance measured in terms of thrust-specific fuel consumption is remarkably insensitive to the wave rotor efficiency for variations about the reference value, so that this appears to be a particularly robust application for wave rotor technology. A reduction of 25% to 30% in the thrust-specific fuel consumption for the 600 to 1000 lb_f thrust class of turbofan engine is expected from the use of the wave rotor as a high temperature topping stage.

There is a general lack of detailed empirical data on wave rotor performance, especially at the temperature and pressures desired for the turbofans considered in this study. A limited data base at lower temperatures and pressures has been developed by MSNW and used to validate the FLOW design code for wave rotors. Somewhat scantier data at higher temperature also exists for the Pearson wave rotor/turbine. However, additional data is required to demonstrate the projected performance of a hot stage wave rotor and to validate the rotor design codes at those conditions.

A preliminary evaluation of technical risk showed that none of the areas investigated could rightfully be considered high risk areas in terms of their potential effect on the turbofan engine performance. It was also concluded that a more detailed design evaluation of the wave rotor

combined with a conceptual engine design evaluation would be needed in order to establish the level of risk in various design features of the wave rotor related to its integration with a turbofan engine. The present risk analysis was limited to just those aspects of rotor design needed to carry out FLOW code and cycle analysis.

The cycle analysis covered a broad range of possible engine operating conditions in terms of pressure ratio, peak temperature, and component efficiencies for both wave rotor/turbine based engines and pressure exchanger based engines. These results have established the best range of performance for these types of engines and have indicated areas for possible improvement. There are a number of other potentially attractive engine configurations, such as hybridized versions of wave rotor turbofans where the wave rotor produces both shaft work and compresses the inlet air. Also, recuperated versions of the wave rotor need to be considered to determine their impact on the engine thrust-specific fuel consumption. Other parameter variations, including the flight conditions, deserve a deeper investigation to locate possible regimes beyond those considered in the context of this study which may be particularly efficient; for example, at much lower subsonic conditions or near trans-sonic conditions and at different altitudes. When a specific engine concept has been selected for detailed study, the present cycle code needs to be upgraded to include a more complete model of duct losses, combustor losses, and real gas effects. The present format for this code is satisfactory for general evaluation but is not yet sufficiently detailed for actual engine design without these modifications.

The FLOW code analysis of the wave rotor demonstrated that the efficiency of this device is projected to lie within bounds which will reduce the engine thrust-specific fuel consumption a significant amount depending on the cycle pressure ratio, temperature, and other component efficiencies. This analysis was limited to the two primary types of wave rotor discussed above with an emphasis on the pressure exchanger rotor since the most is known about its design and performance from an empirical

point of view. While the FLOW code represents the gasdynamics as a one-dimensional phenomenon in a rotor compression tube, the results indicate that nonuniform two-dimensional flows will occur at times in the inlet and outlet manifolds to the rotor, and the rotor flow itself must be multi-dimensional due to boundary layer effects, possible large-scale turbulence, and boundary layer separation near the tube entrance. Therefore, the present FLOW code results must be viewed as averaged properties of the tube flows. Many of the multi-dimensional flow effects and their losses have been modeled into the FLOW code. These include pressure recovery losses as the tube flow exits to a manifold; similar losses which occur when the tube is partially open and the gas must funnel through a narrow throat; pipe flow models of heat transfer and momentum transfer with the tube walls; and separation at the tube entrance due to a mismatch between incident manifold gas velocity and rotor tip speed. Some of these higher dimensional effects have been validated in an averaged sense with the low temperature MSNW wave rotor experimental data. In order to have full confidence in the results of the present study, additional experimental data for wave rotor performance at the conditions considered here needs to be acquired.

6.2 RECOMMENDATIONS

The foregoing discussion of the results of this study suggests that a combined program of analysis, modeling, and experimental testing needs to be carried out. Specific recommendations for Phase 2 are prioritized by the order in which the data is needed to increase the level of confidence at each stage with the least cost to the total program. These recommendations address the immediate need to obtain experimental data as well as the companion requirement to understand the design problems and compatibility of the wave rotor component with the rest of a turbofan engine. Each of these areas must be carried another step forward in order to decide whether a full engine development program is warranted. A second step beyond these immediate needs concerns the testing of breadboard and brassboard versions of an engine to gain the hands-on data

needed for the final development program go-ahead. Particular problems that may be show-stoppers are highlighted in the following recommendations since they become the milestones for future decisions.

1. WAVE ROTOR DEMONSTRATION

There is a particularly strong need to test a wave rotor at or near engine design conditions in order to demonstrate projected wave rotor component performance and to validate the ability of the design and performance codes to predict performance in detail.

The precise design of the wave rotor for testing needs to be established along with the particular objectives of those tests. A working list of objectives should include the need to measure each inlet and outlet port temperature, pressure, and mass flow in order to verify the work transfer efficiency of the device. The gas leakage should also be determined; the more detailed this measurement can be, the better. For example, the shroud pressure should be measured and gas flow into the shroud may also be measured. If leakage from individual ports is measurable, that would be ideal. Similarly, the equilibrium temperature of the rotor should be measured in order to determine the amount of heat transfer between the rotor and the gases.

Design objectives will also need to be scrutinized as an essential part of choosing a particular design for the test. Design objectives may include the need to harness the wave rotor in a test rig which imposes stresses on the device similar to, or which can be easily related to, those stresses encountered by the rotor in an actual engine configuration. Then the leakage and heat transfer tests will take on additional meaning since they will be made in a realistic engine environment.

Two levels of tests need to be considered. During the first tests, the wave rotor should run close to or at design conditions without

particular consideration as to how well it performs. That test will demonstrate a fundamental, important capability of the device: that it will operate at the design high temperature and pressure conditions. Previous wave rotors have been run under engine conditions but not at as high a temperature and pressure as we have considered in this study. Thus, successful completion of these basic run tests will constitute a milestone in the wave rotor R&D program.

The second level of testing will focus on a detailed evaluation of the rotor performance to measure its values, to determine the best areas of operation, and to correlate this performance with the analytic and numerical predictions. Performance goals can be set as a function of variable levels of success. These success levels have already been discussed in the section on risk evaluation and can be used to help decide what to do next if a particular level of success in a test is or is not met. It is important to establish these various performance goals at the outset so that a clear standard of success can be agreed upon.

The results of such tests will provide essential evidence as to the utility of the design codes for predicting wave rotor performance as well as for the absolute performance levels which can be expected from this device. Without this data, it would be a much higher-risk task to attempt engine tests directly. With this data, one may proceed with confidence to the engine test phase of the program.

2. DESIGN EVALUATION

A conceptual engine design evaluation is needed to determine the design of the wave rotor for a first generation wave rotor turbofan engine and to use that design to specify the wave rotor test design. The design evaluation should include turbofan engines based on both pressure exchanger wave rotors and wave rotor/turbines. This will require the FLOW code calculations, especially of the wave rotor/turbine, to project the performance of the wave rotor for specific engine configurations. The

best wave rotor design for the demonstration experiments will be selected as a result of this design evaluation. The major design problems anticipated concern the control of leakage and the attendant problems of thermal distortion of the rotor and connective ducts as the engine achieves full temperature operation.

The requirements for sealing the rotor are significantly different than for turbines and compressors where there is a uniform temperature and pressure distribution about the periphery. The contrary is true for wave rotors and, as a result, the usual design rules developed for conventional axial or radial flow machines may not apply. While these problems are not anticipated to be insurmountable, they may be difficult to resolve and costly to put into practice. These issues should be addressed as an essential part of the conceptual engine design evaluation.

3. *WAVE ROTOR MODELING*

Two distinct needs have been identified. These are, first, to improve the heat transfer modeling for the unsteady flow conditions occurring on the wave rotor, incorporating that model into an upgraded version of the FLOW code. The second need is to improve the model of nonuniform flows in the manifold in order to get better estimates of the pressure recovery losses there as well as gaining a more accurate boundary condition for the FLOW code calculations.

The present estimates of heat transfer lack modeling the influence of unsteady boundary layers and turbulence which are expected to occur in the wave rotors. These effects can be modeled and applied to the current one-dimensional version of the FLOW code. The current study indicated that an order of magnitude increase in the heat transfer coefficient would significantly decrease the wave rotor efficiency. While this has not been judged a high-risk area using the present definition of risk, clearly a better understanding of these phenomena would allow design improvements in the rotor performance and, possibly, a cooler rotor, which would have a

substantial impact on the materials and peak cycle temperatures which one could use.

The present analysis has assumed a total loss of dynamic head for gas leaving the rotor. That is clearly a conservative assumption since, at least in the combustor loop, there is a distinct benefit in retrieving some of the dynamic head in order to move the gas through the combustor and back onto the rotor. The level of pressure recovery is, therefore, an essential datum; this can be modeled by considering individual tubes simultaneously exhausting flow to a manifold and then mixing these flows to a uniform downstream state. The pressure of the downstream state should ideally form the boundary condition for the tube flows, requiring an iterative process that the present FLOW code is not set up to perform. The implementation of this process into the FLOW code would lend greater confidence to the manifold loss predictions and allow more precise design predictions to be made.

At a later date, when more experimental data has been obtained, it would also be worthwhile considering the development of two- or three-dimensional flow codes to treat the entrance conditions and radial and boundary layer effects more precisely. This would be warranted only if later calculations of engine performance are shown to depend more sensitively on the rotor parameters than is now believed to be the case. As such, higher dimensional code development is given a lower priority than the heat transfer and manifold modeling discussed above.

END

FILMED

9-83

DTIC